ATMOSPHERIC RESPONSES TO ARCTIC CLIMATE WARMING: PRECIPITATION, CYCLONE, AND SYNOPTIC PATTERNS

by

TOMOKO KOYAMA

B.S., Meteorological College, l992

M.S., Colorado State University, 2002

A thesis submitted to the

Faculty of the Graduate School of the

University of Colorado in partial fulfillment

of the requirement for the degree of

Doctor of Philosophy

Department of Atmospheric and Oceanic Sciences

2018

This thesis entitled:

Atmospheric responses to Arctic climate warming: precipitation, cyclone, and synoptic patterns

written by Tomoko Koyama

has been approved for the Department of Atmospheric and Oceanic Sciences

_____

John J. Cassano

_____

Jennifer E. Kay

Date_____

The final copy of this thesis has been examined by the signatories, and we find that both the content and the form meet acceptable presentation standards of scholarly work in the above mentioned discipline.

Abstract

Koyama, Tomoko (Ph.D., Department of Atmospheric and Oceanic Sciences)

Atmospheric responses to Arctic climate warming: precipitation, cyclone, and synoptic patterns

Thesis directed by Dr. Julienne Stroeve and Associate Professor John J. Cassano

In recent decades, a rapidly warming lower atmosphere has been observed in the Arctic. Consequently, we wish to address a fundamental question: how do weather patterns in the northern hemisphere respond to these significant changes in the Arctic, especially sea ice loss? To gain insight about the possible linkage between warming Arctic conditions and the resultant atmospheric responses, changes in cyclone activity and synoptic weather patterns were investigated in this study. Given that precipitation can also affect weather patterns, a newly developed reanalysis precipitation was evaluated over Greenland for future hydrological cycle research in the Arctic.

First, the Arctic System Reanalysis version 1 precipitation generally showed good agreement with gauge-based precipitation measured in coastal areas. However, precipitation at Summit, Greenland, a higher continental environment, indicated overestimated amounts with respect to Doppler radar measurements.

Secondly, no robust changes in cyclone activity were observed, despite the changes in moisture availability, regional baroclinicity, and vertical stability.

Lastly, we confirmed that persistent warm surface signals can generate a ridge at 500 hPa and a surface high-pressure system downstream of the ridge. When the Arctic surface forcing has a sufficiently long persistence over a moderately large area, it can induce mid-latitude cold-air advection.

Acknowledgements

As much as anything else, I'm grateful to my academic advisor and a committee member, John Cassano, and his wife Liz Cassano for their guidance to complete this dissertation. While my pursuit of a Ph.D. degree was the biggest challenge of my life, I couldn't accomplish the goal without their help. They always gave me the right amount of advice in a timely manner. I also would like to thank my research advisor, Julienne Stroeve, and my committee members, Mark Serreze, Jen Kay, and Matthew Shupe for their input and feedback to work on the series of research. They're not only excellent polar researchers but their enthusiasm helped me to re-discover both the joy and significance of polar science. I'm thankful to my former research advisors, Tomi Vukicevic, Dan Birkenheuer, and Bill Emery, who introduced me to different disciplines: data assimilation, radiative transfer modelling, and remote sensing. The work with them isn't included in my dissertation, but what I learned from them expanded my perspective as a scientist. I also appreciate many colleagues from different groups sharing various things with me.

In the graduate school, there were major obstacles that made me feel hopeless and I still need to fight back my tears when I recall those memories. However, I'm lucky to have a supportive network of mentors, family, and friends. A cute monster, Mike Wazowski, from a film titled *Monsters University*, is a fictitious character, of course, but his devoted effort to accomplish his goal made an

impression. I could get my energy back when I looked at the stuffed doll wearing a cap with the MU logo and will keep it by my side as one of my mentors. My husband, Brian DeVandry, who was more committed to complete the program than I was, kept telling me that I would earn the degree. I appreciate that he didn't let me skip a workout even when I was overloaded with assignments. Our late cats, Misha and Kokichi, who had often occupied a large part of my desk, were my special office mates from day one. Their unconditional love had emotionally helped me a lot. I hope our other cats, Makiko, Joji, and Tomekichi, are happier now as they can be on my desk longer without my supervision. My other family members and friends in the U.S. and Japan are more than an asset. I appreciate their continuous support for years and am so happy that I can tell my accomplishment to them!

TABLE OF CONTENTS

Contents

CHAPTER 1 ..... **17**

INTRODUCTION **17**

CHAPTER 2 ..... **23**

GREENLAND PRECIPITATION ANALYSIS FROM THE ARCTIC SYSTEM REANALYSIS (ASR): 2000-2012 ..... **23**

2.1. Introduction 23

2.2 Datasets and Methodology 28

2.3 Results 32

2.3.1 Comparison of monthly precipitation 32

2.3.2 The Northern Atlantic Oscillation (NAO) and precipitation 38

2.4. Summary and concluding remarks 41

CHAPTER 3 ..... **63**

SEA ICE LOSS AND ARCTIC CYCLONE ACTIVITY FROM 1979 TO 2014 ..... **63**

3.1. Introduction 63

3.2 Methodology 67

3.2.1 Data 68

3.2.2. Eady growth rate 69

3.2.3. Cyclone detection 71

3.2.4. Extreme cyclones 72

3.3. Atmospheric impacts of summer sea ice loss 74

3.4. Changes in vertical temperature difference 77

3.5. Changes in baroclinic instability 78

3.6. Changes in cyclone activity 79

3.6.1. Interannual variability and trend analysis 79

3.6.2. Cyclone deepening rates 80

3.6.3. Spatial pattern of cyclone activity 81

3.7. Changes in extreme cyclone activity 85

3.8. Summary and discussion 86

CHAPTER 4 108

MID-LATITUDE ATMOSPHERIC RESPONSES TO AUTUMN ARCTIC NEAR-SURFACE TEMPERATURE ANOMALIES IN CMIP5 MODELS 108

4.1. Introduction 108

4.2. Data and Methods 111

4.2.1. CMIP5 model data 111

4.2.2. Methods 113

4.3. Results 115

4.3.1. CCSM4 116

4.3.2. HadGEM2-CC 118

4.3.3. IPSL-CM5A-LR 120

4.4. Discussion 121

4.5. Summary 123

CHAPTER 5 ..... **135**

SUMMARY **135**

References **141**

LIST OF TABLES

Table 2.1 Information about the selected DMI stations and POSS..... 47

Table 2.2 Correlation coefficients between the ASRv1 precipitation and the DMI/POSS precipitation. All values are statistically significant ($p \leq 0.05$)..... 48

Table 2.3 Mean values of monthly precipitation of DMI (POSS) and the corresponding ASRv2 values from the three different coverage sizes..... 49

Table 2.4 Linear regression constants and accuracy measures between the ASRv2 precipitation and the DMI/POSS precipitation..... 50

Table 3.1 September and December SIE low and high periods from 1979 to 2014. Refer to section 3.2.1. Data and Fig. 2 for the methodology of determining the low and high ice years..... 91

Table 3.2 Summary of seasonal cyclone counts variations..... 92

LIST OF FIGURES

Figure 2.1 DMI stations used for this study and Summit where the POSS is located..... 51

Figure 2.2 Scatterplot of the ASRv1 1x1-patch precipitation and the DMI/POSS precipitation and numbers at top right corners show the correlate coefficients. Solid lines indicate linear regressions. Statistical significance of the correlation can be found in Table 2.2..... 52

Figure 2.3 (a) time series of the ASRv1 1x1-patch precipitation at the DMI stations and (b) corresponding DMI precipitation. Each graph is plotted in optimized range for precipitation (y-axis) at the corresponding location. The blue line shows local polynomial regression fitting and the gray shading shows the 95% confidence intervals..... 53

Figure 2.4 Time series of the POSS and ASRv1 1x1-patch precipitation at the corresponding location. The blue line shows local polynomial regression fitting and the gray shading shows the 95% confidence intervals..... 55

Figure 2.5 Time series of the POSS and ASRv1 1x1-patch precipitation at the corresponding location. The blue line shows local polynomial regression fitting and the gray shading shows the 95% confidence intervals..... 56

Figure 2.6 Boxplots of seasonal variations in the POSS and ASRv1 1x1-patch precipitation..... 58

Figure 2.7 Map of Greenland regions and surrounding waters, comprising Northwest (NW), Southwest (SW), Southeast (SE), Northeast (NE), the Baffin Bay (BB), the Davis Strait (DS), the North Atlantic (NA), the Greenland Sea (GS), the Lincoln Sea (LS), and the Arctic Basin (AB)..... 59

Figure 2.8 Mean monthly ASRv1 precipitation and the NAO index over four regions in Greenland. Dotted lines indicate linear regressions and numbers at top right corners show the correlate coefficients..... 60

Figure 2.9 Same as Figure 2.8, but for four regions of the surrounding waters..... 61

Figure 3.1 The entire Arctic (ARC) north of 60 N includes the high-latitude North America (HNA), the Chukchi and East Siberian Seas (CHU), Central Russia (CRU), the Greenland, Norwegian and Barents Seas (GNB), Greenland (GRE), and all areas north of 80N (TOP)..... 93

Figure 3.2. Standardized SIE (a) September and (b) December time series from 1979 to 2014. The extremely high ice years are listed in Table 3.1. Box symbols correspond to those extreme years..... 94

Figure 3.3. (a) Annual cycle of extreme cyclones determined from daily NCEP/NCAR SLP field of 1981-2010. (b) Annual mean count of extreme cyclones from 1979 to 2014..... 95

Figure 3.4. (First row) Composite September sea ice area change ratio from the high ice years to low ice periods. (Second row) mean sensible heat flux, (third row) mean latent heat flux, (fourth row) mean 925-hPa air temperature, and (fifth row) mean precipitable water. Each column period can be referred to Table 1. ERA-Interim is utilized except for the first row…… 96

Figure 3.5. The mean temperature difference between 500 and 925 hPa of (a) NCEP/NCAR, (b) MERRA, and (c) ERA-Interim during the low and high sea ice extreme composites and the entire study period…….. 97

Figure 3.6. Regional trends of grid cell numbers exceeding the threshold =1.5 day-1 which is based on NCEP/NCAR reanalysis. GRE region demonstrate a statistically significant trend. The dotted lines are linearized trends……... 98

Figure 3.7. Normalized mean counts of grid cells exceeding the threshold =1.5 day-1 in autumn derived from the (a) NCEP/NCAR, (b) MERRA, and (c) ERA-Interim reanalyses during the high- and low-ice composite periods over the six regions (bars represent standard deviation of the mean) …….. 99

Figure 3.8. Time series of seasonal cyclone counts derived from NCEP/NCAR reanalysis over the Arctic. The linearized trends are illustrated by dotted lines…….. 100

Figure 3.9. Average of maximum cyclone deepening rates derived from NCEP/NCAR reanalysis, (a) from 1979 to 2014, during (b) + 1.0 SD high and (c) - 1.0 SD low ice years…….. 101

Figure 3.10. Frequency of averaged maximum cyclone deepening rates derived from NCEP/NCAR reanalysis, from 1979 to 2014, during high and low ice years…….. 102

Figure 3.11. The temporal and spatial resolution of NCEP/NCAR reanalysis is 6-hourly on a 2.5 x 2.5 degree global grid, respectively. (First row) Composite September sea ice area change ratio from the high ice years to low ice periods. (Second row) mean cyclone frequency from NCEP/NCAR, (third row) cyclone center mean SLPs from NCEP/NCAR, (fourth row) cyclone center mean Laplacian from NCEP/NCAR. Each column period is the same as Figure 3.4……. 103

Figure 3.12. The temporal and spatial resolution is 6-hourly on a 100km x 100km degree global grid, respectively. (First row) mean cyclone frequency differences derived from ERA-Interim between the high ice years to low ice periods. (Second row) same as row 1, but derived from MERRA. (Third row) cyclone center mean SLPs differences derived from ERA-Interim between the high ice years to low ice periods. (Second row) same as row 3, but derived from MERRA. (Fifth row) cyclone center mean Laplacian differences derived from ERA-Interim between the high ice years to low ice periods. (Sixth row) same as row 5, but derived from MERRA. Each column period is the same as Figure 3.4…….. 104

Figure 3.13. Time series of (a) DJF extreme cyclone counts from NCEP/NCAR over GNB and the Arctic, and (b) mean DJF Arctic Oscillation (AO) index..... 104

Figure 3.14. Extreme cyclone frequency difference in winter, "Low ice years" minus "High ice years"..... 105

Figure 4.1 Arctic map showing locations of marginal seas. North of the red outline shows the ocean area of near-surface air temperature data that are used to train the SOM [from Cassano and Cassano (2017)]..... 126

Figure 4.2 Master SOM of near-surface temperature anomaly from six model runs..... 127

Figure 4.3 Mean sea ice concentration (above) and sea ice thickness (bottom) over autumn months (September – November) from 1979 to 2014 for CCSM4, HadGEM2-CC, and IPSL-CM5A-LR..... 128

Figure 4.4 Composite atmospheric fields of CCSM4 created by compositing anomaly fields for the days clustered on the top-left SOM pattern shown in Figure 4.2: rows from top to bottom show near-surface temperature, sea ice concentration, sea ice thickness, total surface energy flux, near-surface temperature, 1000 to 500 hPa thickness, geopotential height at 500 hPa, and sea level pressure, respectively. Columns, from left to right show composites at weeks 0, 2, 6, 8, and 10, respectively..... 129

Figure 4.5 As in Figure *4*.4 but for HadGEM2-CC with columns, from left to right showing composites at weeks 0, 2, 6, 10, and 12, respectively..... 131

Figure 4.6 As in Figure 4.4 but for IPSL-CM5A-LR..... 133

CHAPTER 1

INTRODUCTION

Once, the idea of global warming induced primarily by carbon dioxide was underrated even in the research community (Broecker 1975). As stated in the Intergovernmental Panel on Climate Change (IPCC) fifth assessment report (AR5), there have been obvious changes in many types of extreme weather and climate events since the 1950s (IPCC 2013). Consequently, in recent years, the general public's perception of its influence on long-term socioeconomic activity has changed. Under abnormal conditions such as unusually high or low temperatures, sudden heavy rainfall, or long-lasting drought, human health and well-being are undoubtedly threatened. The current infrastructure cannot be maintained as originally planned and economic losses due to extreme weather events will keep rising. Thus, for long-range planning, it is important to assess the likelihood, intensity, and frequency of extreme weather events related to global climate change.

While the polar bear may be the poster boy of animals threatened with extinction, primarily due to the global warming trend (Hunter et al. 2010), it is indisputable that the habitat of all life on this planet are experiencing significant environmental changes. However, it is the polar bears' habitat, the Arctic, that appears to be experiencing the most rapid of these changes (ACIA 2005). The Arctic lower troposphere has been warming more than twice as fast as the global average,

a phenomenon known as Arctic amplification (Serreze et al. 2009; Screen and Simmonds 2010; Inoue and Hori 2011; IPCC 2013).

Other striking Arctic climate changes are the increased mass loss from the Greenland ice sheet (GrIS) and the decline in sea ice extent (SIE) corresponding to Arctic amplification. While Antarctica and Greenland hold enough ice to raise global sea levels by some 70 m, about seven meters contribution from GrIS is estimated (ACIA 2005). Many major cities are located in low-lying coastal areas, where erosion, temporary flooding, and permanent inundation are anticipated due to sea-level rise. These potential hazards are becoming crucial political and social issues for the management of high-risk coastal areas. The rate of ice loss from the GrIS has accelerated following the summer melt increase over the last two decades (IPCC2013). It increased from 51 ± 65 Gt per year (1992 - 2000) to 263 ± 30 Gt per year (2005-2010) (Shepherd et al. 2012). Another estimate of the mass loss rate between 2002 and 2015 is 265 ± 25 Gt per year and this is equivalent to 0.72 mm per year average global sea level rise (Forsberg et al. 2017).

Similarly, Arctic SIE retreat can influence global weather and climate: reduction in albedo and expanding open water would have significant effects on energy budget and atmospheric and oceanic circulation in the high latitude. As a consequence, anomalous weather patterns could happen more frequently both locally in the Arctic and potentially in lower latitudes. Serreze et al. (2007) documented that the SIE decline during all calendar months over the period 1979 to 2006 was linear, and the largest trends occurred at the end of the melt season in

September (Stroeve et al. 2012: Serreze and Stroeve 2015; Simmonds 2015). Following sea ice loss, the air above the expanding areas of open water and thinner sea ice is warmed and further influences air temperature and precipitation through atmospheric advection and mixing.

Johannessen et al. (2004) presented hypothesis concerning Arctic warming and a shrinking ice cover. In addition to the effects on energy balances and atmospheric and oceanic circulation, they discussed the possibility of the Arctic Ocean becoming new sink of atmospheric CO_2 (Anderson and Kaltin 2001) and the altering global thermohaline circulation from various changes in the Nordic and Greenland Seas (Rahmsdorf 1999; Alekseev et al. 2001). Beyond the changes in geophysical environment, Arctic and sub-Arctic marine biodiversity would be substantially transformed (Beaugrand 2002). Those environmental changes are expected to threaten the native flora and fauna. Eventually, we need to anticipate the potential to reverse the improvements of health and longevity from economic development (Watts et al. 2015).

Here, we wish to address the fundamental question: how do weather patterns in the northern hemisphere respond to the rapid changes in the Arctic, especially sea ice loss? Sea ice plays a fundamental role in the global energy budget, and ice loss is already having impacts on Arctic temperatures (Serreze et al. 2009; Screen and Simmonds 2010; Serreze et al. 2011; Serreze and Barry 2011; Kim et al. 2014; Screen et al. 2014), precipitation patterns (Stroeve et al., 2011; Simmonds and

Kaey 2009; Screen et al. 2014) and atmospheric circulation (Francis et al., 2009, 2012; Overland and Wang, 2010).

To study changes in Arctic climate, we need a good understanding of precipitation, since there is a direct influence of global warming on precipitation (Trenberth 2011) and it is one of the main components of the fresh water budget in the Arctic (Serreze et al. 2006). However, there is great uncertainty in measuring precipitation in a cold environment with a sparse ground observation network. As the GrIS mass deficit and SIE loss affect the Arctic climate system, the water cycle, surface gas exchange, sea level, and eventually the global climate system through its impact on the surface energy budget, it would be beneficial to have improved precipitation reanalysis data over Greenland and the vicinity, including information regarding the reanalysis uncertainty. Arctic System Reanalysis (ASR) is a recently developed Arctic regional reanalysis having an improved depiction of mesoscale processes (Bromwich et al. 2010). While Bromwich et al. (2016) compared the ASR monthly precipitation totals with gauge observations on land, the comparison was performed for a limited time period of just one year. Chapter 2 of this dissertation aims to assess the accuracy of the ASR precipitation fields over Greenland for the entire ASR time-period (2000-2012) through comparisons with ground-based station data and X-band Doppler radar measurements at Summit, Greenland.

In order to demonstrate the causal link between the warming Arctic and atmospheric changes, both in the Arctic and mid-latitudes, it is important to determine which measures of the atmospheric state will be explored. Cyclone

activity represent a major measure of the state of the atmosphere since its passage is associated with strong wind, precipitation, and temperature changes. Information on the intensity and tracks of cyclones is closely related to local weather and a key aspect of climate (Ulbrich et al. 2009). Most day to day weather changes are linked to the passage of the transient, synoptic-scale disturbances in the tropospheric wind field (Wallace and Hobbs 2006). Thus, synoptic-scale analysis can help us to observe both Arctic and mid-latitude responses to changes in the Arctic climate system. In Chapter 3, several cyclone metrics in the high latitudes are analyzed to examine if a connection exists between recent Arctic sea ice loss and cyclone activity. Mid-latitude atmospheric responses to anomalously warm surface air temperature patterns in the Arctic are presented in Chapter 4.

Each individual chapter is written as an independent study: Chapter 3 was published in 2017 in Journal of Climate (Koyama et al. 2017) and Chapters 2 and 4 will be submitted for publication in the spring of 2018. Chapter 5 summarizes the results from this dissertation.

Greenland precipitation analysis from the arctic system reanalysis (ASR): 2000-2012

Tomoko Koyama[1,2]

Julienne Stroeve[3,1]

[1]**National Snow and Ice Data Center, University of Colorado, Boulder, CO, USA**

[2]**Department of Atmospheric and Oceanic Sciences, University of Colorado Boulder, 311 UCB, Boulder, CO, USA**

[3]**Centre for Polar Observation and Modelling, Earth Sciences, University College London, London, UK**

This manuscript will be submitted to Polar Science for publication in the spring of 2018

CHAPTER 2

GREENLAND PRECIPITATION ANALYSIS FROM THE ARCTIC SYSTEM REANALYSIS (ASR): 2000-2012

2.1. Introduction

The Greenland ice sheet (GrIS) has been losing mass in recent decades (1992 - 2011) at an estimated rate of 142 ± 49 Gt per year, with an increase in mass loss rate from 51 ± 65 Gt per year (1992 - 2000) to 263 ± 30 Gt per year (2005-2010) (Shepherd et al. 2012). Another estimate based on measurements by NASA's Gravity Recovery and Climate Experiment (GRACE) showed similar mass loss rate, 265 ± 25 Gt per year (2002-2015), corresponding to 0.72 mm per year average global sea level rise (Forsberg et al. 2017). This mass loss has been dominated by increased ice sheet melt, which in recent years has contributed more to GrIS mass loss than that from ice dynamics (Enderlin et al. 2014). While surface albedo primarily governs ice sheet surface mass balance (SMB) (Bougamont et al. 2005; Tedesco et al. 2011; Fitzgerald et al. 2012), summer snowfall events can counterbalance the positive melt-albedo feedback (Stroeve 2001), by covering dark ice and/or metamorphosed snow with a highly reflective fresh snow layer (Noël et al. 2015).

At the same time, large reductions in Arctic sea ice extent (SIE) have occurred (e.g. Stroeve et al. 2012a; Serreze and Stroeve 2015), leading to strong solar heating of the upper ocean. Increased ocean mixed layer heat content during summer results in large exchanges of heat and moisture during autumn and winter

as the ice reforms. Enhanced heat and moisture fluxes from the ocean to the atmosphere is one of the drivers behind increased moisture content of the Arctic atmosphere (Serreze et al. 2012) as well as Arctic Amplification (AA), the outsized warming of the Arctic compared to the Northern Hemisphere or the global average (Serreze et al. 2009; Screen and Simmonds 2010). Increased moisture content of the Arctic atmosphere may in turn be responsible for increased autumn and winter precipitation over Siberia (Cohen et al. 2012; Ghatak et al. 2012; Orsolini et al. 2013) as well as increases in Arctic snowfall extremes (Liu et al. 2012; Bintanja and Selten 2014). The impact of sea ice loss on Greenland accumulation, however, remains less clear.

Expanding open water areas however do appear to be in part responsible for locally sourced moisture that could impact precipitation over Greenland. Kopec et al. (2016) found an increase of the proportion of moisture sourced from the Arctic with respect to sea ice reductions in the Canadian Arctic and Greenland Sea regions over the past two decades. However, precipitation observations do not show a significant increasing trend with respect to sea ice loss in these two regions. On the other hand, several studies have examined how Arctic warming and associated changes in turbulent fluxes may impact cyclone activity in the Arctic (McCabe et al. 2001; Yin 2005; Bengtsson et al. 2006; Bengtsson et al. 2009; Ulbrich et al. 2009; Inoue et al. 2012; Akperov et al. 2015; Koyama et al. 2017). Some regional features have emerged, such as a northward shift in cyclones tracking through the North Atlantic (Zhang et al. 2004; Yin 2005; Ulbrich et al. 2009; Koyama et al. 2017) with

the potential to impact GrIS precipitation. Koyama et al. (2017) showed an increased potential for cyclogenesis around Greenland during low sea ice years. The combination of more moisture availability and increased cyclogensis, may further increase the intensity of cyclones, and increase the amount of cyclone-associated precipitation, leading to increased snowfall.

While the quantitative link between precipitation and SIE remains poorly constrained, Appenzeller et al. (1998) found a linear relationship between snow accumulation and the North Atlantic Oscillation (NAO) (Hurrell et al. 1995) index in western central Greenland. The NAO describes a tendency toward simultaneous strengthening or weakening of the subpolar (Icelandic) Low and the subtropical (Azores) High, impacting general climate conditions for the North Atlantic Ocean basin and the strength of meridional transport (Koerner and Russell 1979). Bromwich et al. (1999) retrieved the precipitation from wind, geopotential height, and moisture fields over Greenland utilizing an indirect dynamic approach. Chen et al. (1997) showed this approach, the ω equation method based on an equivalent isobaric geopotential height in σ coordinates. The results showed that increased precipitation in southern Greenland occurs with variations in the position and intensity of the Icelandic Low, which is related to the NAO. Mosley-Thompson et al. (2005) documented that the NAO influence on Greenland precipitation weakens along the west-central side of the ice sheet and strengthens in the southeastern region when temperature rises.

As the sea ice is forecasted to continue to decline through the end of the twenty-first century (e.g. Stroeve et al. 2012b; Massonnett et al. 2012; Notz and Stroeve 2015; Jahn et al. 2016; Stroeve and Notz 2016), precipitation over the Arctic Ocean is projected to increase (Kattsov et al. 2007; Bintanja and Selten 2014), with the potential to increase the GrIS mass balance if the precipitation falls as snow. When the precipitation falls as rain, only the part of rainfall that refreezes can contribute to mass gain and it decreases surface albedo which enhances surface melt (Vizcaíno et al. 2014). On the other hand, Lim et al. (2016) found that the negative phase of the NAO is associated with warm and dry conditions for the GrIS, leading to SMB decreases. Thus, it is important to better understand how precipitation has and may change in the future, as a warmer troposphere is more likely to produce rainfall rather than snowfall. Unfortunately, such an assessment is challenged by the lack of observations. Observations of Greenland precipitation are limited, and the ones that exist (e.g. gauge measurements) suffer from wind effects contamination and are generally confined to the coastal regions.

The lack of reliable and accurate observations of precipitation has led to many studies using atmospheric reanalysis data to evaluate changing Arctic precipitation (Serreze et al. 2015; Kopec et al. 2016). Atmospheric reanalyses are retrospective forms of numerical weather forecasts that assimilate observational data into a short-term forecast model using the observations as a first guess of the state of the atmosphere. Recently, an Arctic-focused reanalysis product was developed to specifically assess and monitor variability and change over the greater

Arctic region, the Arctic System Reanalysis (ASR) (Bromwich et al. 2010). The growing need for enhanced understanding of Arctic climate change inspired the Study of Environmental Arctic Change (SEARCH), which is a U.S. program with a mission to provide a foundation of Arctic change science through collaboration with the research community, funding agencies, and other stakeholders. Consequently, the ASR was developed as a synthesis tool for assessing and monitoring variability and change in the Arctic system. Bromwich et al. (2016) compared the ASR forecast monthly precipitation totals with gauge observations on land from the Global Historical Climate Network version 2 (GHCN2) (Peterson and Vose 1997) and the Adjusted Historical Canadian Climate Data (AHCCD) (Mekis and Hogg 1999) within the ASR domain, including Greenland, for the period December 2006 to November 2007. While they showed that the ASR precipitation is generally less (more) during cool (warm) months than observed, the comparison was performed for a limited time, over 12 months.

This study aims to assess the accuracy of the ASR precipitation fields over Greenland for the entire ASR time-period (2000-2012) through comparisons with ground-based station data and X-band Doppler radar measurements at Summit. The results of our study complement the findings of Bromwich et al. (2016) by utilizing different observations over a different study period and different region. Additionally, we explore the relationship between the NAO index and ASR precipitation over Greenland.

2.2 Datasets and Methodology

Three datasets are used to evaluate precipitation over Greenland: the ASR version 1 (ASRV1) precipitation data; gauge-based precipitation measured by the Danish Meteorological Institute (DMI) (Cappelen et al. 2014); and precipitation retrieval from the Precipitation Occurrence Sensor System (POSS), which is a bistatic, continuous-wave, X-band Doppler radar utilized in the Integrated Characterization of Energy, Clouds, Atmospheric state and Precipitation at Summit (ICECAPS) project (Sheppard and Joe 2008; Castellani et al. 2015; Castellani et al. 2015). The first dataset, ASRv1, spans 2000-2012 and the spatial coverage extends beyond the boundaries of the Arctic Ocean. The spatial resolution of ASRv1 is 30 km, and the temporal resolution is 3-hourly. Among six ASRv1 products, variables designated as "accumulated total grid scale precipitation" and "accumulated total cumulus precipitation" in the Final 30 km 2D surface forecast product are utilized to derive total precipitation since they are non-convective and convective precipitation, respectively. The accumulated amount of this total precipitation over a month is defined as the ASRv1 monthly precipitation in this study. Note that cumulus convection is not accurately represented in numerical models and excessive precipitation tends to be produced (Fonseca et al. 2015). Bromwich et al. (2015) reported that convective precipitation over land in summer is excessive, but the issue is resolved in version 2 (ASRv2). ASRv2 also has improved spatial resolution of 15 km, and while fields of precipitation and radiation are expected to be improved, ASRv2 was not available in time for this study.

The second dataset is the DMI historical data collection 1873-2012 for Greenland. Eighty-eight DMI weather stations are located in coastal or near-coastal (less than 100 m a.s.l.) regions. Measurement periods of the DMI gauges vary significantly among these stations resulting in many stations lacking data during our study period. DMI stations, where counts of observations reached more than a third of the study period of the data available from the ASRv1 (156 months of data from 2000-2012) are selected for comparison, i.e., stations having at least 52 monthly observations during the 13 years. This resulted in only 10 stations being identified for comparison with the ASRv1 precipitation. In addition, the observed data quality among stations may vary due to differences in the automated observation system and frequencies of maintenance and calibration (Cappelen et al. 2014). Table 2.1 and Figure 2.1 show the locations of those selected stations including the Summit POSS (described below). In order to derive 24 hours accumulated precipitation, considering wind-induced undercatch, wetting loss, and trace precipitation amounts, a precipitation bias is corrected following Yang et al. (1999):

$$P_c = \frac{CR}{100}(P_g + \Delta P_w + \Delta P_e) + \Delta P_t$$

where P_C, P_g, ΔP_w, ΔP_e, and ΔP_t in millimeters are corrected precipitation, gauge-measured precipitation, wetting loss, evaporation loss, and trace precipitation, respectively. ΔP_w is varied by precipitation type and the number of times the gauge is emptied. ΔP_e depends on gauge type and time of the year. ΔP_t is

inversely proportional to the gauge-measured annual precipitation and this correction is important in northern Greenland (Yang et al. 1999). Daily catch ratio (CR in %) is a function of daily wind speed and three precipitation types: snow, rain, and mixed precipitation. Although precipitation types were unknown at the selected stations, a simple assumption based on the near-surface air temperature was made to determine the type of precipitation. If all the observations in a single day indicate below (above) zero Celsius, i.e., freezing point, the daily precipitation type is snow (rain), and otherwise, it is mixed precipitation. The monthly DMI precipitation used for the comparison is represented as the accumulations of those daily corrected precipitation data, which is based on the reported 24-hour accumulated precipitation (Cappelen 2014).

The third dataset is from the POSS located at Summit, one of the highest elevation locations within the Arctic, and is used to assess ASRv1 precipitation within the interior of the ice sheet. POSS operated from September 2010 to present under the project ICECAPS, resulting in 27 months of snowfall data that overlap with the ASRv1 dataset. Snowfall retrieval from POSS is based on the so-called Z-S relationship between the equivalent reflectivity factor and water equivalent (w.e.) snowfall rate using the T-matrix scattering model (Mischenko 2000). The Z-S relationship is expressed as $Z = BS^{\beta}$, where Z is the equivalent reflectivity factor or reflectivity, S is snowfall rate, and B and β are coefficients. These coefficients depend on crystal habits and the snow size distribution, which are not observed, leading to a certain level of uncertainty in the POSS snowfall rate is inevitable.

Associated with the time-space comparison, the effective uncertainty of POSS reflectivity is likely to be within 3dB which is equivalent to a factor two difference uncertainty in snowfall (Castellani et al. 2015). Consequently, the POSS monthly precipitation used for the comparison consists of this daily precipitation accumulated over a month. Further information about POSS and/or radar-based snowfall retrievals can be found in Matrosov (2007), Matrosov et al. (2009), Sheppard and Joe (2008), and Castellani et al. (2015).

The nearest ASRv1 grid point to each DMI station or the POSS location was initially selected for comparison. Recalling that precipitation depends on subgrid-scale physical processes, we do not know whether precipitation amount at the nearest ASRv1 grid point represents that at the corresponding station with acceptable uncertainty. In order to find an adequate area to represent each measurement location, three patches of various sizes (1x1, 3x3, and 5x5 grid points) are defined. While a 1x1 patch is equal to the nearest grid point to the measurement site, 3x3 and 5x5 patches are defined as areas having the nearest grid points in the center. Consequently, monthly ASR 1x1-patch precipitation is the same as the ASRv1 monthly precipitation at the nearest point to the measurement site, and the corresponding spatial mean values are defined as 3x3- and 5x5-patch monthly precipitation. The Pearson's correlation coefficient between the ASRv1 monthly precipitation and the DMI (POSS) monthly precipitation is computed to measure the linear correlation. The seasonal and interannual variability of the DMI, ASRv1, and POSS monthly precipitation are visually examined at each site.

The NAO index data used in this study is obtained from the National Oceanic and Atmospheric Administration (NOAA) Climate Prediction Center (CPC; www.cpc.ncep.noaa.gov/products/precip/CWlink/pna/nao.shtml). The monthly NAO index is defined as principal component of the Atlantic centered rotated empirical orthogonal function analysis of the monthly mean 500-mb height north of 20°N. Further information can be found on the CPC website.

2.3 Results

2.3.1 Comparison of monthly precipitation

Table 2.2 lists the correlation coefficients between the DMI (POSS) precipitation and the ASRv1 precipitation obtained from the three different coverage sizes described in the previous section. These correlations are all statistically significant at $p \leq 0.05$. Overall, they are positively correlated, and the range is from 0.37 to 0.86, indicating that temporal representativeness of the ASRv1 precipitation varies strongly by location. While the ASRv1 1x1-patch and the DMI precipitation have larger correlations in the south and northeast of Greenland, correlation coefficients with respect to the 5x5-patch are larger than those with respect to the 1x1- or 3x3-patches in eastern and western Greenland. However, correlation coefficients for the different spatial resolutions generally only differ by +/- 0.04, suggesting precipitation at the nearest ASRv1 grid point is representative of the corresponding DMI station. Table 2.3 summarizes the mean values of monthly precipitation from DMI (POSS) and the corresponding ASRv1 values derived from the three different coverage sizes. In general, the ASRv1 1x1-patch

values show the best agreement with the DMI (POSS) values, further confirming the nearest ASRv1 grid point is sufficient to represent the corresponding DMI station. The following figures only show results for the 1x1 patch.

Figure 2.2 shows the ASRv1 1x1-patch precipitation against the DMI (POSS) precipitation at each station location. Table 2.4 lists the corresponding linear regression coefficients and the mean and root mean square errors (rmse). In general, precipitation at the DMI stations located on the east side of Greenland (04310, 04320, 04339, 04360, 04270, and 04272) show the best agreement with the corresponding ASRv1 precipitation, with correlation coefficients in the range of 0.75-0.86. ASRv1 precipitation at three northeastern stations, 04310, 04320, 04339, and a southern station 04270 exhibit apparent positive biases that are not dependent on precipitation amount received. On the other hand, ASRv1 precipitation at stations 04360 and 04272 show positive biases during light precipitation periods, and negative biases during heavy precipitation. While moderate correlations (0.57-0.76) appear at stations 04390, 04231, and 04220, station 04250 (Nuuk) shows the lowest correlation (0.37) among all the DMI stations. Nuuk receives about 100 mm per month of precipitation (Aðalgeirsdóttir et al. 2009), and the majority of the corresponding ASRv1 data show a negative bias.

It is known that there are challenges in measuring solid precipitation, such as blockage of the gauge orifice by snow capping the gauge; accumulation on the side of the orifice walls; wind undercatch of snow due to the formation of updrafts

over the gauge orifice; the unknown role of turbulence on gauge catch; and the large variability in gauge catch efficiency for a given gauge and wind speed (Rasmussen et al. 2012). Thus, the wind field around the gauge can significantly affect the quality and accuracy of precipitation data. While gale-force winds frequently occur in Southern Greenland from westerly or easterly tip jets, northeasterly barrier winds, or northwesterly katabatic winds (Moore et al. 2016), topography-induced airflow can also influence local precipitation. The effects of area-specific variability in winds is less likely to be reflected in the coarse resolution ASRv1 precipitation estimates where terrain is complex. For example, Nuuk at the mouth of Nuup Kangerlua is part of the large Nuuk fjord system and the smoother topography used in the model can cause high bias in surface wind forecast there. Moore et al. (2016) documented that a horizontal grid size on the order of 15 km is needed to characterize the impact that Greenland's topography has on the regional wind field and climate. Station 04390 (Ikerasassuaq) shows large scatter between the station data and ASRv1, and this too may also be a result of topographic effects. Moore and Renfrew (2005) studied surface winds over Southern Greenland from December to February using Quick Scatterometer (Quick-SCAT) data and found highly localized maxima wind speeds just to the south and east of Cape Farewell, which is near Ikerasassuaq. It is plausible that the ASRv1 forecast precipitation error is likely to be larger when stronger wind is observed.

While we find generally good agreement between the gauge and ASRv1 precipitation data at coastal locations, there is a large discrepancy between the

ASRv1 precipitation and retrieved POSS precipitation at Summit (Figures 2.2 and 2.4). The ASR monthly precipitation is always larger than the corresponding POSS retrievals. The correlation coefficient is about 0.5 and the rmse is 9.47 mm as shown in Tables 2 and 4, respectively. As for the estimated POSS precipitation, the annual values for 2011 and 2012 are 51.8 and 79.1 mm water equivalent (w.e.), respectively. Assuming the reflectivity uncertainty is a factor of two, the maximum limit of the estimations are 103.6 and 158.2 mm w.e. for 2011 and 2012, respectively. These uncertainties are inevitable due to the inherent indirect nature of radar observations. According to observations by Castellani et al. (2015), the mean annual POSS snowfall was 92.5 mm w.e. with potential values of 81.1 to 126.7 mm w.e. due to uncertainty in the assumed undercatch ratio. On the other hand, the ASRv1 annual precipitation at Summit is 134.3 and 192.2 mm w.e. for 2011 and 2012, respectively. Therefore, the estimated POSS precipitation amounts are still smaller than the ASRv1 retrieval at Summit. This result is not conclusive since the comparison is over only 27 months and the p-value is 0.30. In fact, other estimations of the annual precipitation are in the range of 170-200 mm w.e. in the area near Summit (Bales et al. 2001; Ettema et al. 2009). Given that little to no net water vapor exchange occurs at the surface at Summit (Berkelhammer et al. 2016), interannual variability of precipitation is likely to be related to frequency of synoptic-scale cyclones, which can deliver precipitation to this high-altitude site. Koyama et al. (2017) found that distinct changes in the frequency of winter Arctic cyclones (December through February) are not observed in the post-satellite era. It

is plausible to assume that cyclones have commensurate influence on precipitation at Summit during the study period. Thus, annual POSS precipitation values evaluated here are less likely to be a statistical outlier.

Figure 2.3 shows the time series of the ASRv1 1x1-patch and DMI precipitation at the target DMI stations, respectively. The blue line shows local polynomial regression fitting and the gray shading shows the 95% confidence intervals. The majority of the ASRv1 precipitation values are outside of the 95% confidence intervals, but interannual variability at stations 04270 and 04272 are similar to each other as they are located in the vicinity in the southern coast of Greenland (Figure 2.3a). Gradual precipitation increase (decrease) is observed from 2000 to 2004 (2006 to 2008) at the two stations. Trends at stations 04310 and 04320 located in the northeastern coast of Greenland are also similar to each other. Local maximum values appear in 2006 at the both stations, which are reflections of the extremely large observed values (Figure 2.3a). Similar to the ASRv1 precipitation trends, the majority of the DMI precipitation values are outside of the 95% confidence intervals of the local polynomial regression fitting (Figure 2.3b). The station 04250 trend looks unique since it shows an extreme precipitation amount (over 1500 mm per month). However, it is reasonable to assume this extreme value is an erroneous observation. It is still difficult to discuss the trends from the available DMI data since some stations have discontinuous observations, but the stations 04220, 04231, 04272, and 04390 show increasing trend at the end of the

study period. The lowest Arctic sea ice extent during the satellite era was recorded in this year.

Figure 2.4 shows the time series of precipitation at Summit, the POSS and ASRv1 1x1-patch precipitation. As we see in Figure 2.2, the ASRv1 precipitation is larger than the retrieved POSS precipitation and the trend lines for the two datasets do not agree. However, the time period of available monthly precipitation data (a little over two years) is not sufficient time to adequately identify interannual variability at Summit.

Finally, a boxplot approach is utilized to examine seasonality in the retrieved precipitation. Figures 2.5 shows seasonal variability in the ASRv1 1x1-patch and DMI precipitation. For the ASRv1 precipitation (Figure 2.5a), stations in similar geographical locations show similar variability. For the northeastern stations (04310 and 04320), the interquartile ranges (IQRs) are relatively small. The median values are under 50mm for all seasons and precipitation in colder seasons tends to be greater than in warmer seasons. For the eastern stations (04339 and 04360), the IQRs are about 50mm except lower values during summer at station 04339. For southern stations (04270 and 04272), minimum median precipitation occurs during winter. The median at these stations is a maximum in autumn and the IQRs are relatively large except for spring. While stations 04390 (in southeastern Greenland) and stations 04270 and 04272 (in southwestern Greenland) are relatively close to each other (about 260 and 330 km, respectively), there is no resemblance in

seasonal precipitation variability. Station 04390 has more precipitation during winter, the amount decreases in warmer seasons and the IQRs are larger than 50 mm. For the western stations (04220 and 04231), the IQRs are smaller than that of 04390 and the median precipitation is less than 50mm throughout the year. The seasonal cycle at station 04390 is most similar to those the eastern stations (04339 and 04360) and the larger IQR corresponds to its scatterplot (Figure 2.2). The median values and IQRs at station 04250 are larger than those in the northwestern stations (04220 and 04231), but there is no obvious seasonality.

For the DMI precipitation (Figure 2.5b), the IQRs of the precipitation at stations 04220, 04231, 04270, 04310, 04320, 04360, and 04390 are similar to the corresponding ASRv1 IQRs. However, similar seasonality of the median values to the ASRv1 can only be found at stations 04231, 04310, and 04320, where less precipitation is observed.

Figure 2.6 shows boxplots of seasonal variations in the POSS and ASRv1 1x1-patch precipitation. Again, there are discrepancies between the two precipitation measurements, even if the sample size is limited. While the POSS exhibits the largest IQR in summer, the ASRv1 precipitation values are the smallest range during summer.

2.3.2 The Northern Atlantic Oscillation (NAO) and precipitation

The spatial distribution of precipitation is governed by atmospheric circulation, proximity to large bodies of water, and topography. Thus, it is better to

divide Greenland and surrounding waters into regions with similar characteristics to study the relationship between local precipitation and the NAO index. Greenland is divided into four regions, based on the major ice sheet topographical divides following Stroeve et al. (2017): Northwest (NW), Southwest (SW), Southeast (SE), and Northeast (NE). Also, the surrounding waters, i.e., the Baffin Bay (BB), Davis Strait (DS), North Atlantic (NA), Greenland Sea (GS), Lincoln Sea (LS), Arctic Basin (AB), are defined as shown in Figure 2.7. Note that the entire AB is not depicted in the figure due to the map projection (the Lambert conformal conic). The defined AB is approximately bordered by the continental shelves of Eurasia and North America.

Figure 2.8 shows the relationship between the area averaged monthly ASRv1 precipitation over the divided regions and the corresponding monthly NAO index. The spatially averaged precipitation is derived from monthly ASRv1 precipitation at all available grid points in the region. The data period is from 2000 and 2012, and all 12 months of data are utilized as well as the monthly precipitation analysis. Correlation coefficients for the NW, SW, NE, and SE regions are -0.36, 0.09, 0.32, and 0.25, respectively. These values are statistically significant ($p \leq 0.05$) except for the SW (p-value of 0.24). Figure 2.9 shows the relationship between the regionally averaged ASRv1 precipitation over surrounding waters, the BB, NA, GS, and AB regions, and the NAO index, in which the correlation coefficients are -0.27, 0.49, 0.46, and -0.14, respectively. The correlation coefficients are statistically significant ($p \leq 0.05$) for the BB, NA, and GS regions. The corresponding scatter plots for the

LS and DS regions are not shown here, but their correlation coefficients are 0.01 and 0.11, respectively. Since the NAO is strongest and its most climatologically effective expression occurs during the cold season months (Rogers 1984; Hurrell 1995; Jones et al. 1997), the same analysis during the colder months (September-April) is performed. The colder months' correlation coefficients for the NW, SW, SE, SW, BB, DS, NA, GS, LS, and AB are -0.42, -0.01, 0.09, 0.39, -0.32, -0.01, 0.50, 0.48, 0.10, and -0.14, respectively. Among these values, the results for the NW, NE, BB, NA, and GS are statistically significant ($p \leq 0.05$) and their magnitudes are larger than the corresponding coefficients derived from the entire period except for the GS.

These results suggest that precipitation over Greenland and the surrounding waters is influenced by the phase of the NAO, yet it is clear geographical dependencies are important as well. Where negative correlation coefficients appear, NW, BB, and AB, precipitation tends to decrease along with the increasing NAO index (Figures 2.8 and 2.9). When NAO is positive, the greater pressure gradient between the subpolar low and the subtropical high can induce stronger westerlies, with speeds 8 m/s greater during high NAO winters than low NAO winters and anomalous northerly flow occurs across western Greenland (Hurrell 1995). Consequently, the southwesterly flow that brings moisture to Greenland is weakened and results in a reduction of precipitation. On the other hand, regions on the east side of Greenland: NE, SE, GS, and NA, show positive correlation coefficients (Figures 2.8 and 2.9); precipitation over those regions tends to increase along with the increasing NAO index. When the NAO is in the positive phase, the

Arctic Front occurring along the southeastern Greenland coast is possibly enhanced by the Icelandic Low, which can lead to increased pre-frontal rainfall over eastern coastal Greenland. Almost no correlations appear over the rest of the regions, SW, DS, and LS between monthly precipitation and the NAO index.

2.4. Summary and concluding remarks

In the Arctic, precipitation arrives as snow during nearly nine months out of the year and sublimation directly returns moisture to the atmosphere (Liston and Sturm 2004). Given that strong and frequent winds prevent us from measuring accurate precipitation, it is extremely challenging to observe precipitation at any place in the Arctic. Therefore, it is beneficial to understand the characteristics of the newly developed ASRv1 precipitation data for Arctic climate research. Arctic sea ice decline has increased the heat flux from the ocean to atmosphere in autumn and early winter (Vihma 2014). Consequently, sea ice loss is strongly tied to increased tropospheric moisture, precipitation and cloud cover (e.g. Francis et al. 2009; Kay and Gettelman 2009; Screen et al. 2013; Abe et al. 2016; Vazquez et al. 2017). In regard to the GrIS, changes in accumulation, mostly driven by precipitation, may help to counter ice mass loss from increased ice melt. Mernild et al (2015) investigated coastal annual precipitation trends and showed positive (negative) trends in western (southern and eastern) Greenland over the 1991-2012 period. Similarly, Wong et al. (2015) showed positive annual precipitation trends at Thule air base in northwestern Greenland over the 1981-2012 period. While these results were based on gauge observations, mean precipitation in the interior of the GrIS

was estimated from snow pits and ice cores in both studies and negligible changes in precipitation in the GrIS interior were found.

In this study, monthly ASRv1 precipitation was compared with bias-corrected DMI precipitation around coastal Greenland and precipitation retrieved from POSS at Summit. While three different spatially averaged ASRv1 values are compared to the DMI precipitation to evaluate the spatial representativeness of the individual ASR grid point, the differences in the correlation coefficients between modeled data and observations for the different spatial averaging was found to be negligible (Table 2.2). Thus, ASRv1 precipitation data at the nearest grid point to the stations were used for comparison. The ASRv1 and DMI precipitation on the east and south side of Greenland showed good agreement, but uncertainty at Ikerasassuaq, the station nearest to Cape Farewell, South Greenland, in both datasets, appears to be larger (Figure 2.2). The ASRv1 precipitation at Nuuk, the capital city of Greenland on the west coast of Greenland on the shore of the Labrador Sea, showed a negative bias when the observations exceeded 100 mm per month. One of suspected causes is that local wind events account for the differences between the reanalysis and gauge data there. Even allowing for the reflectivity uncertainty of the POSS, which is a Doppler radar, the ASRv1 precipitation is overestimated at Summit, a high-elevation and inland research station (Figures 2.2 and 2.5). While no independent precipitation gauges exist there, it is advisable to have further observations for comparison to confirm the ASRv1 overestimation. A possible approach is utilizing

measurements by the Millimeter-wave Cloud Radar (MMCR), one of the ICECAPS instruments.

The time series of precipitation illustrate pronounced high-frequency variability: each monthly precipitation value from both observed and modeled data is often beyond the 95% confidence intervals of the local polynomial regression fitting (Figures 2.3). The ASRv1 fitted local polynomial regression of the southern stations show similar trends to each other as well as trends from the northeastern stations. It can be assumed that the similarity is coming from the numerical model's reproduction of synoptic-scale circulation effects on precipitation. However, the DMI regression results do not show similar trends among the stations (Figure 2.3b) and this suggests that local effects on precipitation, including several types of wind events and/or orographic effects, can surpass synoptic-scale circulation patterns in the observations and that these local effects are not captured in the ASRv1 data.

Comparable seasonal variability in the ASRv1 precipitation, shown using the boxplot approach, is found among stations that are geographically close, especially the IQRs and median values (Figure 2.5a). The IQRs become larger moving from more northeasterly stations to southerly ones. The median values along the eastern stations and at the southernmost gauge show similarity: precipitation values are smallest in summer and become larger in colder seasons. The median values at the western coastal stations do not appear to be similar to each other. The IQRs of the DMI precipitation instruments show similar variations to those of the ASRv1, but

the variability of the median values is not necessarily comparable (Figure 2.5b). This also suggests that there are local wind effects on observed precipitation in Greenland that are not captured by the 30 km ASRv1 data. It is important to note that there is still uncertainty in observed and modeled precipitation in the Arctic. Serreze and Barry (2014) provided major issues regarding measurement of precipitation: significant gauge undercatch of solid precipitation, the sparse station network, and large biases in precipitation estimates based on satellite observations or from atmospheric reanalyses. We can also assume that spatial and temporal patterns of precipitation are linked to moisture circulation caused by multi-scale dynamics. Thus, it is difficult to reach a solid understanding of ASRv1 precipitation utilizing a few sets of analyses. Future comprehensive work will entail further understanding of precipitation in the Arctic.

The relationship between the NAO index and ASRv1 precipitation over Greenland and surrounding waters is explored for different geographical areas of Greenland (split into 4 regions based on the major ice sheet topographical divides in this study) and the surrounding waters (Figures 2.7, 2.8 and 2.9). The NAO index is moderately related to precipitation amount over northern Greenland, the North Atlantic, and Greenland Sea, where the magnitude of the correlation coefficients are between 0.32 and 0.49. Since the NAO is associated with changes in the surface westerlies across the North Atlantic and into Europe (Hurrell 1995), moisture from the Labrador Sea can also vary along with NAO phases. However, the large and cold Greenland plateau can cause distinct local wind events originating from

different mechanisms, such as westerly and easterly tip jets, barrier winds, katabatic wind, and cyclones that can significantly affect precipitation amount and its spatial distribution. Thus, it is feasible to have a low correlation depending on the geographical effects. Sodemann et al. (2008) applied a Lagrangian method to the European Centre for Medium-Range Weather Forecasts' ERA-40 reanalysis and showed that the North Atlantic and Nordic Seas are moisture sources for Greenland precipitation. They found that the location of the identified moisture sources strongly varied with the NAO phase. Calder et al. (2008) studied a relationship between Greenland ice core-derived accumulation and NAO and identified the linear accumulation-NAO relationship is stronger in western Greenland. Wong et al. (2015) confirmed that recent (1981–2012) changes in northwest Greenland annual precipitation are likely a response to a weakening NAO.

Overall, the ASRv1 precipitation agrees with the corrected DMI gauge-based precipitation measured at coastal or near-coastal stations in Greenland. In contrast, the ASRv1 precipitation at Summit, i.e., in a higher continental environment, is overestimated compared with the POSS observations. While similar variability is not found in the ASRv1 and DMI precipitation, the limited study period is not adequate for a detailed discussion. The NAO index and ASRv1 precipitation show moderate correlation over northern Greenland, the North Atlantic, and Greenland Sea. It is suspected that local wind events have larger influence on precipitation where smaller correlation coefficients appear. Suggested future work to understand the discrepancies between the ASRv1 and DMI precipitation in Greenland coastal

regions could use case studies of local wind events and the corresponding precipitation variations utilizing in-situ measurements during both strong positive and negative NAO phases.

Acknowledgements

This study was supported by National Science Foundation grants PLR-1304807. The ASRv1 forecast precipitation data have been produced by the Polar Meteorology Group/Byrd Polar and Climate Research Center/The Ohio State University and available at Research Data Archive at the National Center for Atmospheric Research, Computational and Information Systems Laboratory website. The POSS data and corrected DMI precipitation data were kindly provided by Matthew D. Shupe from Cooperative Institute for Research in Environmental Science, University of Colorado, and NOAA/Earth System Research Laboratory and Arno Hammann from Rutgers University, respectively. Elizabeth Cassano, John Cassano, and David Bromwich are acknowledged for providing helpful advice and comments on the draft manuscript.

Table 2.1. Information about the selected DMI stations and POSS

Station ID	Location	Monthly data counts	Latitude	Longitude	Elevation (a.s.l.)
04310	Station Nord	58	81.6°N	16.7°W	36 m
04320	Danmarkshavn	71	76.8°N	18.7°W	11 m
04339	Ittoqqortoormiit	108	70.5°N	22.0°W	65 m
04360	Tasiilaq	142	65.0°N	37.6°W	53 m
04390	Ikerasassuaq	127	60.0°N	43.2°W	26 m
04270	Mitt. Narsarsuaq	105	61.2°N	45.4°W	27 m
04272	Qaqortoq	150	60.7°N	46.1°W	32 m
04250	Nuuk	110	64.2°N	51.8°W	54 m
04231	Kangerlussuaq	111	67.0°N	50.8°W	50 m
04220	Aasiaat	111	68.7°N	52.8°W	43 m
POSS	Summit	27	72.6°N	38.5°W	3260 m

Table 2.2. Correlation coefficients between the ASRv1 precipitation and the DMI/POSS precipitation. All values are statistically significant ($p \leq 0.05$).

Station ID	1x1 patch	3x3 patch	5x5 patch
04310	0.833	0.804	0.753
04320	0.784	0.769	0.746
04339	0.810	0.821	0.823
04360	0.804	0.817	0.818
04390	0.594	0.587	0.573
04270	0.843	0.833	0.797
04272	0.845	0.856	0.839
04250	0.365	0.384	0.397
04231	0.662	0.668	0.615
04220	0.702	0.725	0.757
POSS	0.567	0.535	0.497

Table 2.3. Mean values of monthly precipitation of DMI (POSS) in mm and the corresponding ASRv1 values from the three different coverage sizes

Station	DMI (POSS)	ASR 1x1	ASR 3x3	ASR 5x5
04310	23.06	40.47	35.32	30.67
04320	14.91	23.83	24.02	25.12
04339	36.29	54.80	54.92	58.58
04360	67.00	84.57	90.60	99.79
04390	138.25	166.90	154.00	143.41
04270	50.09	85.92	100.89	118.39
04272	73.62	76.34	81.62	94.67
04250	84.25	53.97	60.77	66.49
04231	14.89	21.46	24.34	31.42
04220	26.94	32.10	32.46	33.42
POSS	5.45	13.62	13.71	14.11

Table 2.4. Linear regression constants and accuracy measures between the ASRv1 precipitation and the DMI/POSS precipitation.

Station ID	Intercept [mm]	Slope [mm]	Mean Absolute Error [mm]	Root Mean Square Error [mm]
04310	6.98	1.14	13.90	18.19
04320	11.37	1.41	18.10	24.67
04339	21.56	1.02	25.66	33.27
04360	34.73	0.77	28.13	35.66
04390	73.76	0.59	61.68	81.20
04270	33.79	1.21	45.00	58.77
04272	26.96	0.65	23.97	31.08
04250	49.88	0.07	55.24	161.73
04231	11.31	1.06	13.41	19.42
04220	13.19	0.87	14.55	19.81
POSS	10.02	0.67	8.17	9.47

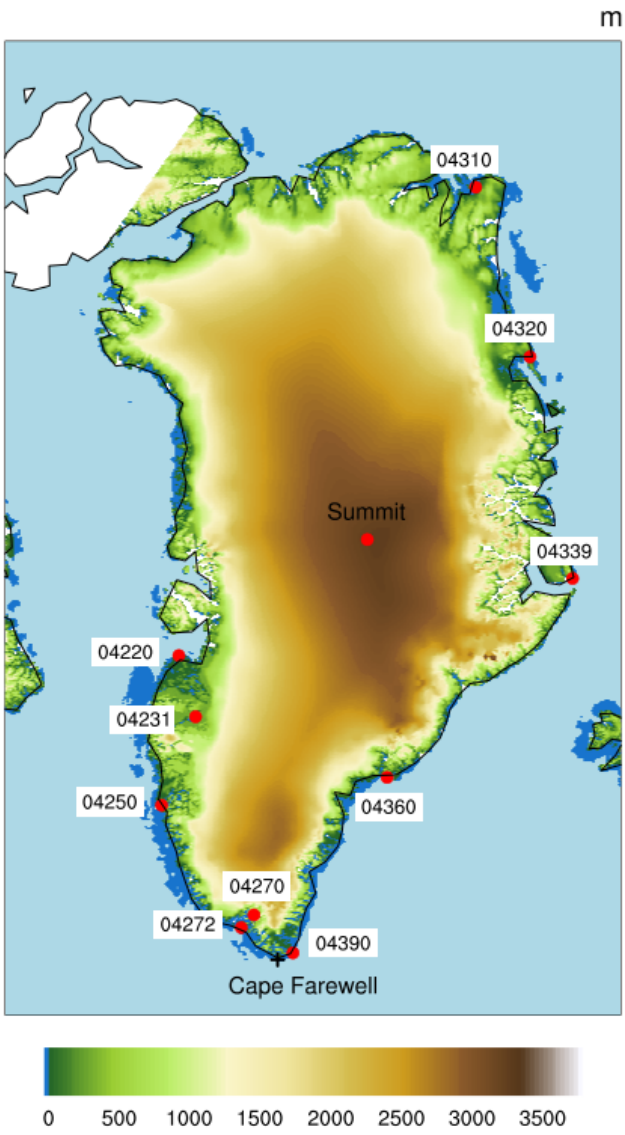

Figure 2.1. DMI stations used for this study and Summit where the POSS is located.

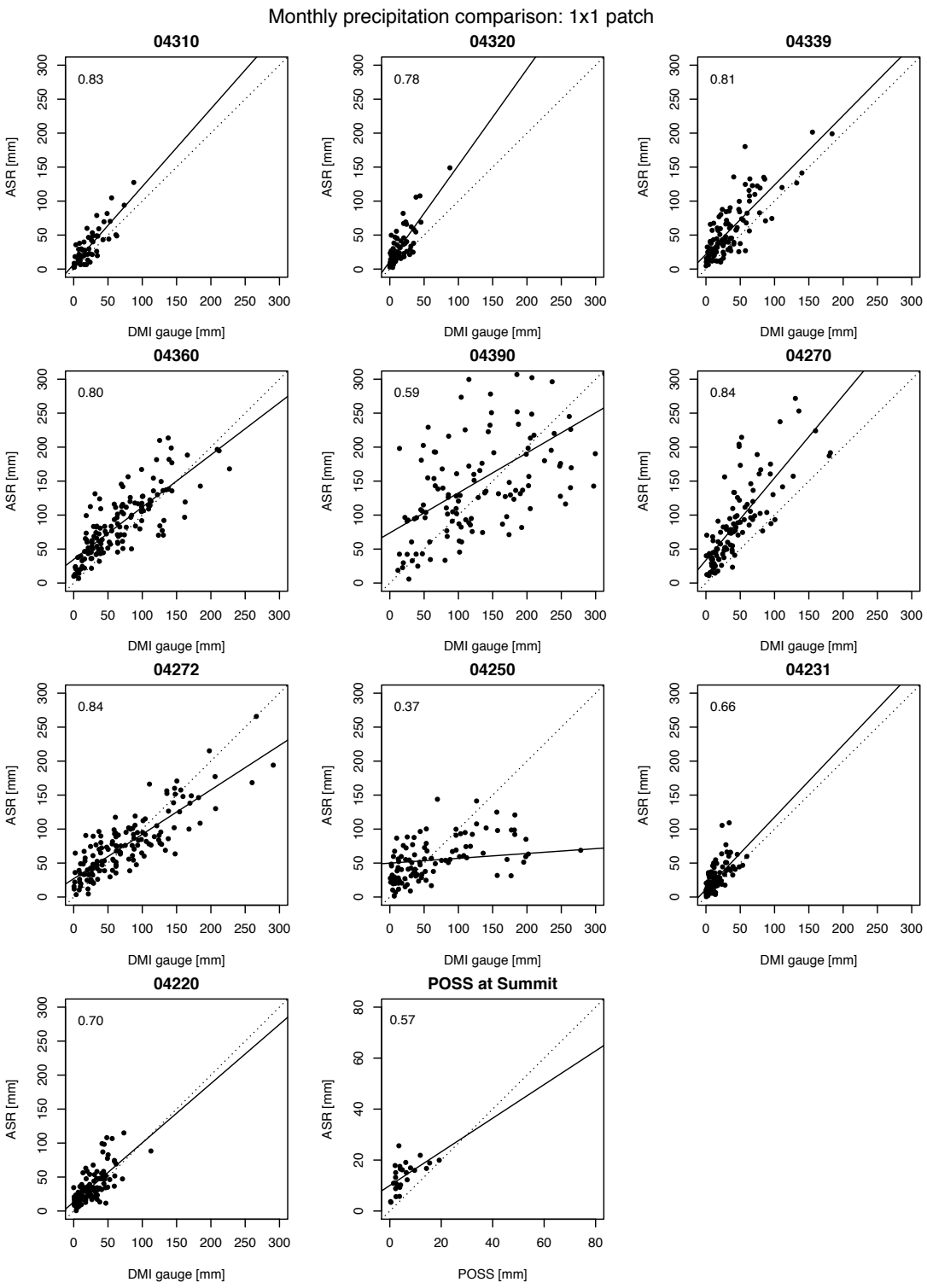

Figure 2.2. Scatterplot of the ASRv1 1x1-patch precipitation and the DMI/POSS precipitation and numbers at top right corners show the correlate coefficients. Solid lines indicate linear regressions. Statistical significance of the correlation can be found in Table 2.2.

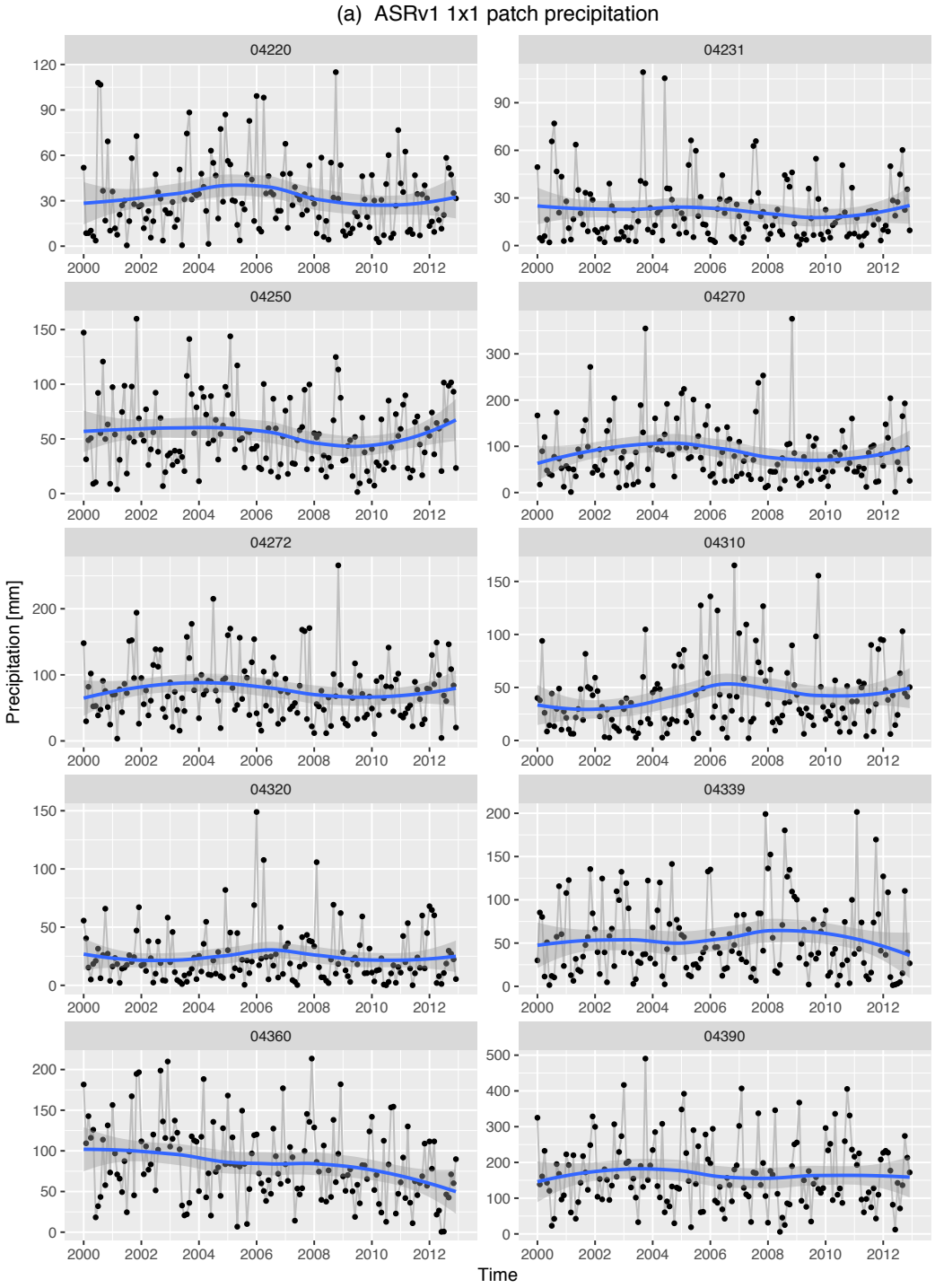

Figure 2.3. (a) time series of the ASRv1 1x1-patch precipitation at the DMI stations and (b) corresponding DMI precipitation. Each graph is plotted in optimized range for precipitation (y-axis) at the corresponding location. The blue line shows local polynomial regression fitting and the gray shading shows the 95% confidence intervals.

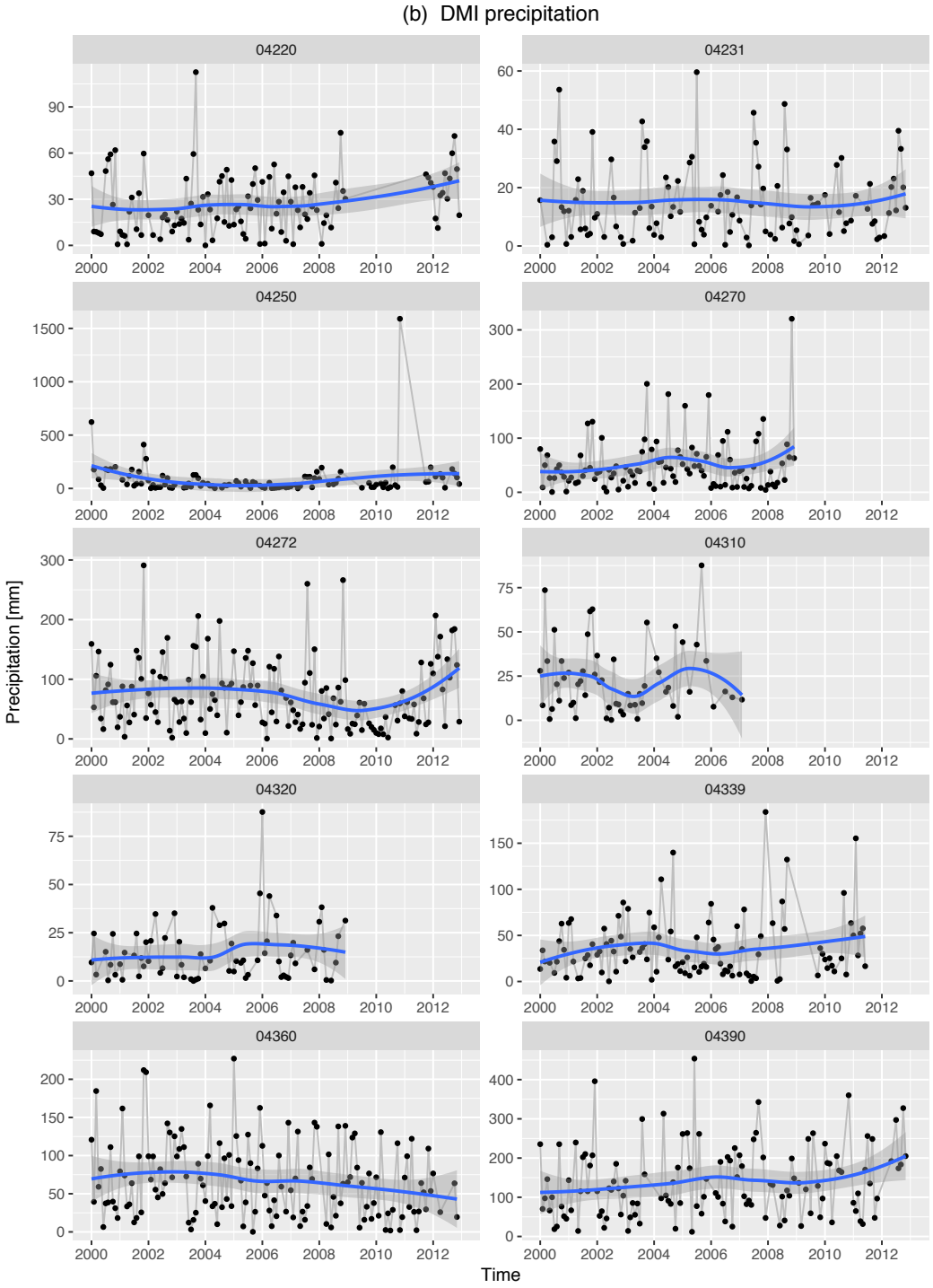

Figure 2.3. (Continued)

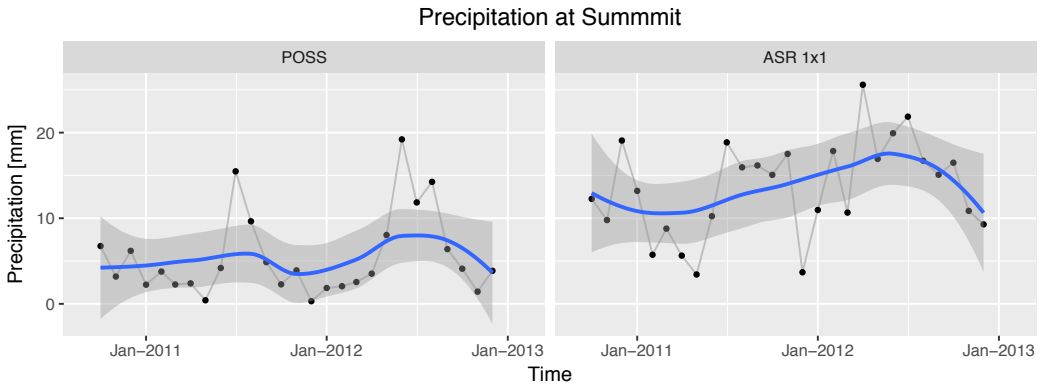

Figure 2.4. Time series of the POSS and ASRv1 1x1-patch precipitation at the corresponding location. The blue line shows local polynomial regression fitting and the gray shading shows the 95% confidence intervals.

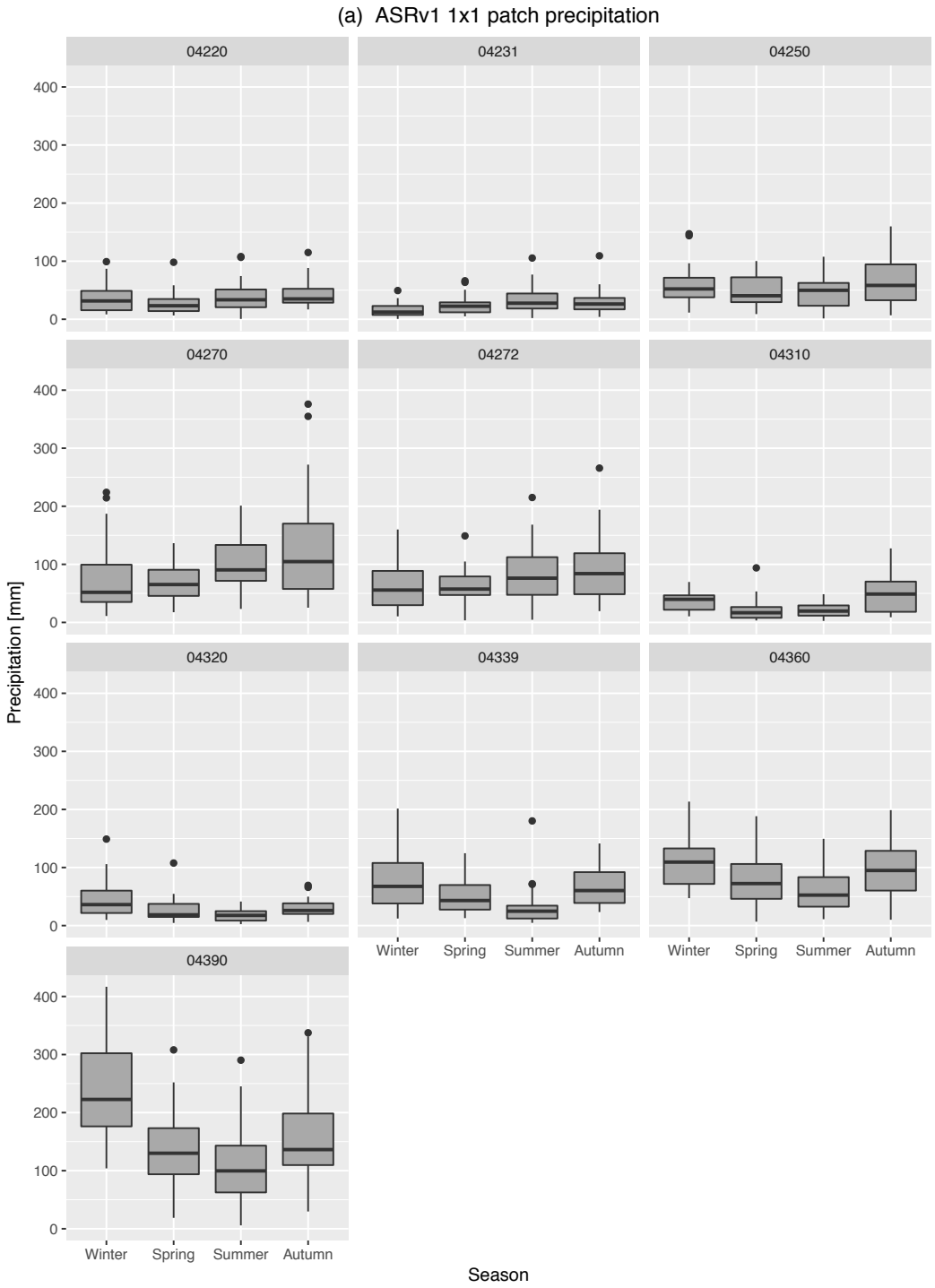

Figure 2.5. Boxplots of seasonal variations in the (a) ASRv1 1x1-patch precipitation and (b) DMI precipitation. The four seasons, spring, summer, autumn, and winter are defined from March to May, June to August, September to November, and December to February, respectively.

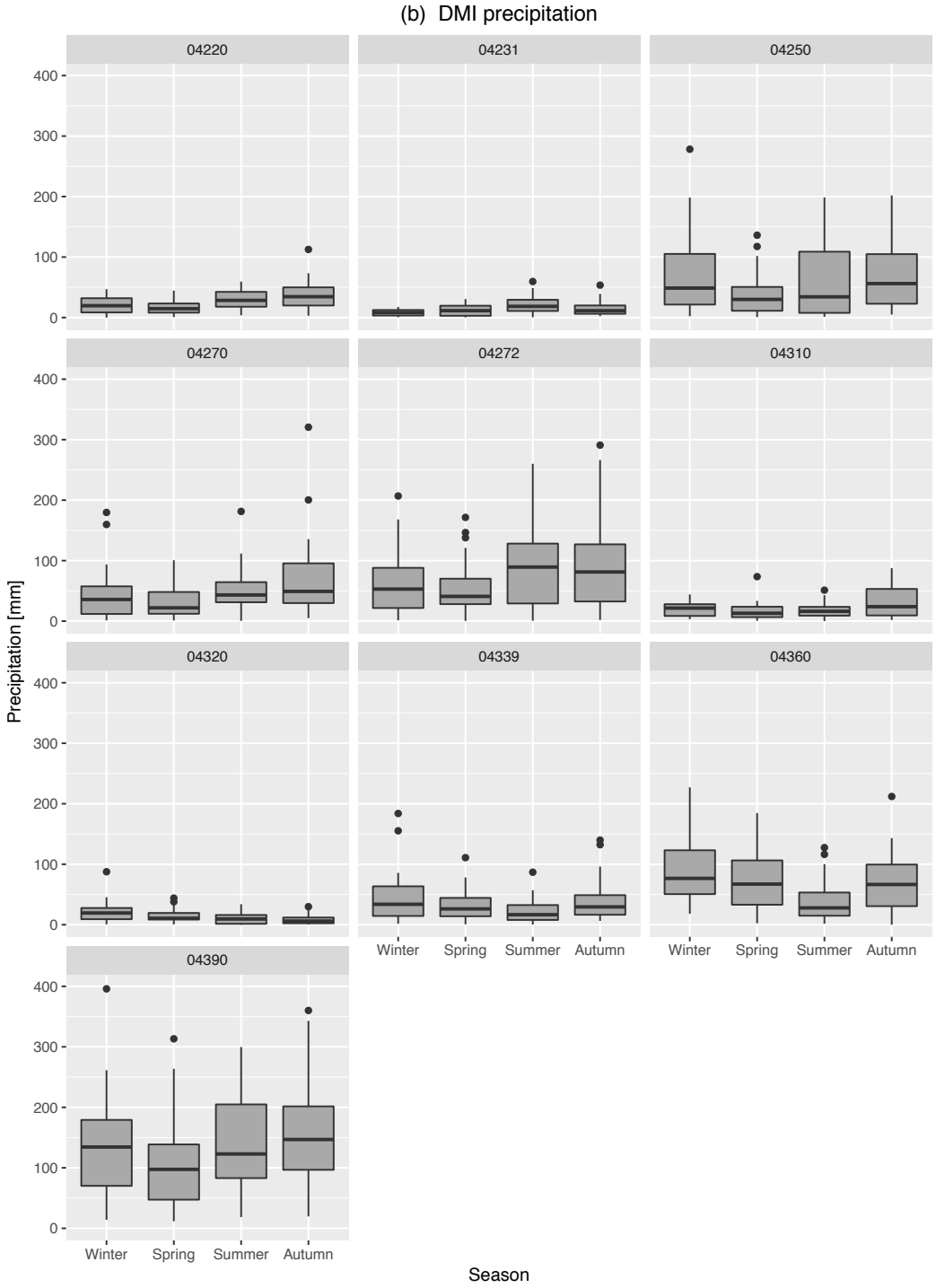

Figure 2.5. (Continued)

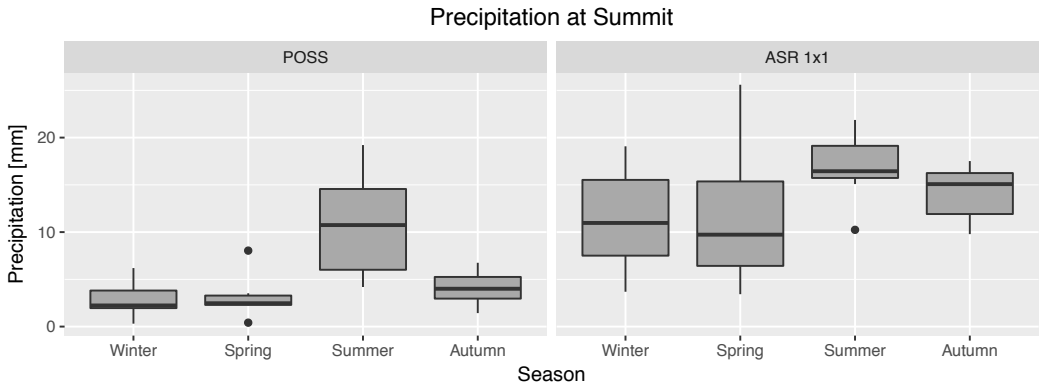

Figure2.6. Boxplots of seasonal variations in the POSS and ASRv1 1x1-patch precipitation.

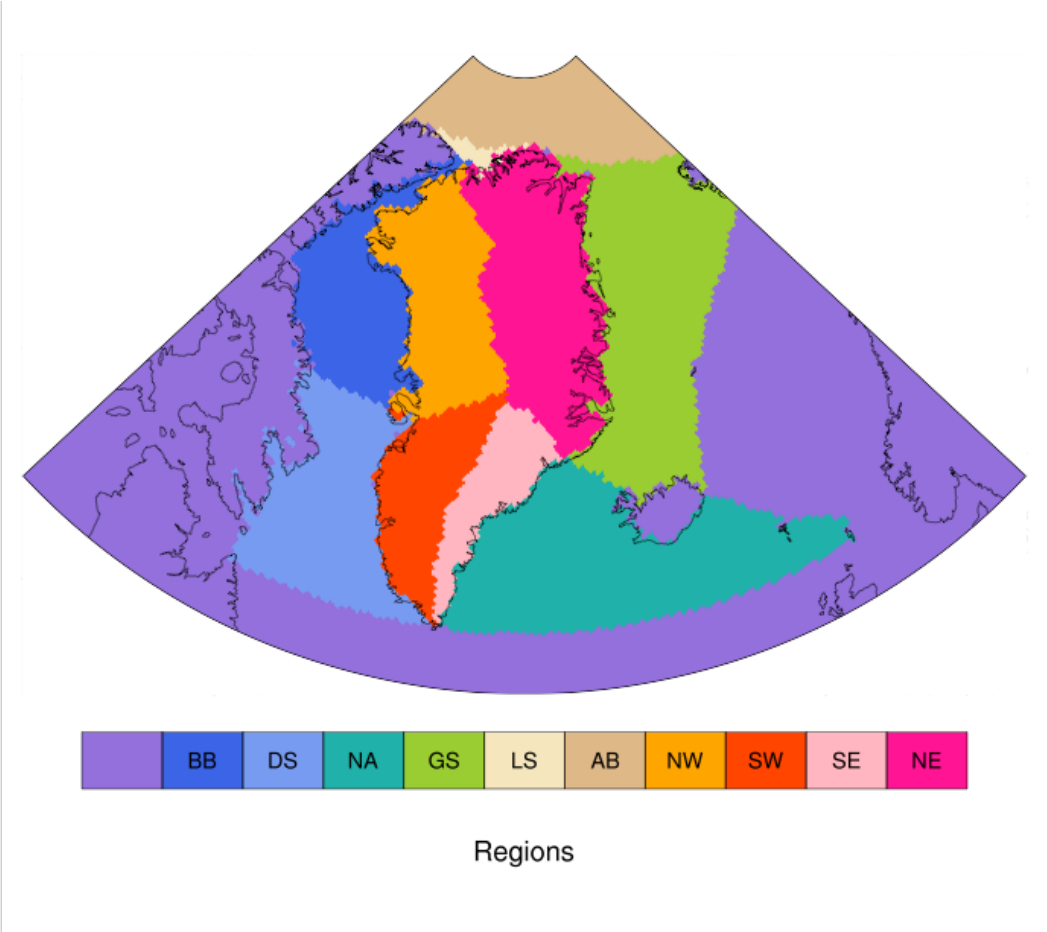

Figure 2.7. Map of Greenland regions and surrounding waters, comprising Northwest (NW), Southwest (SW), Southeast (SE), Northeast (NE), the Baffin Bay (BB), the Davis Strait (DS), the North Atlantic (NA), the Greenland Sea (GS), the Lincoln Sea (LS), and the Arctic Basin (AB).

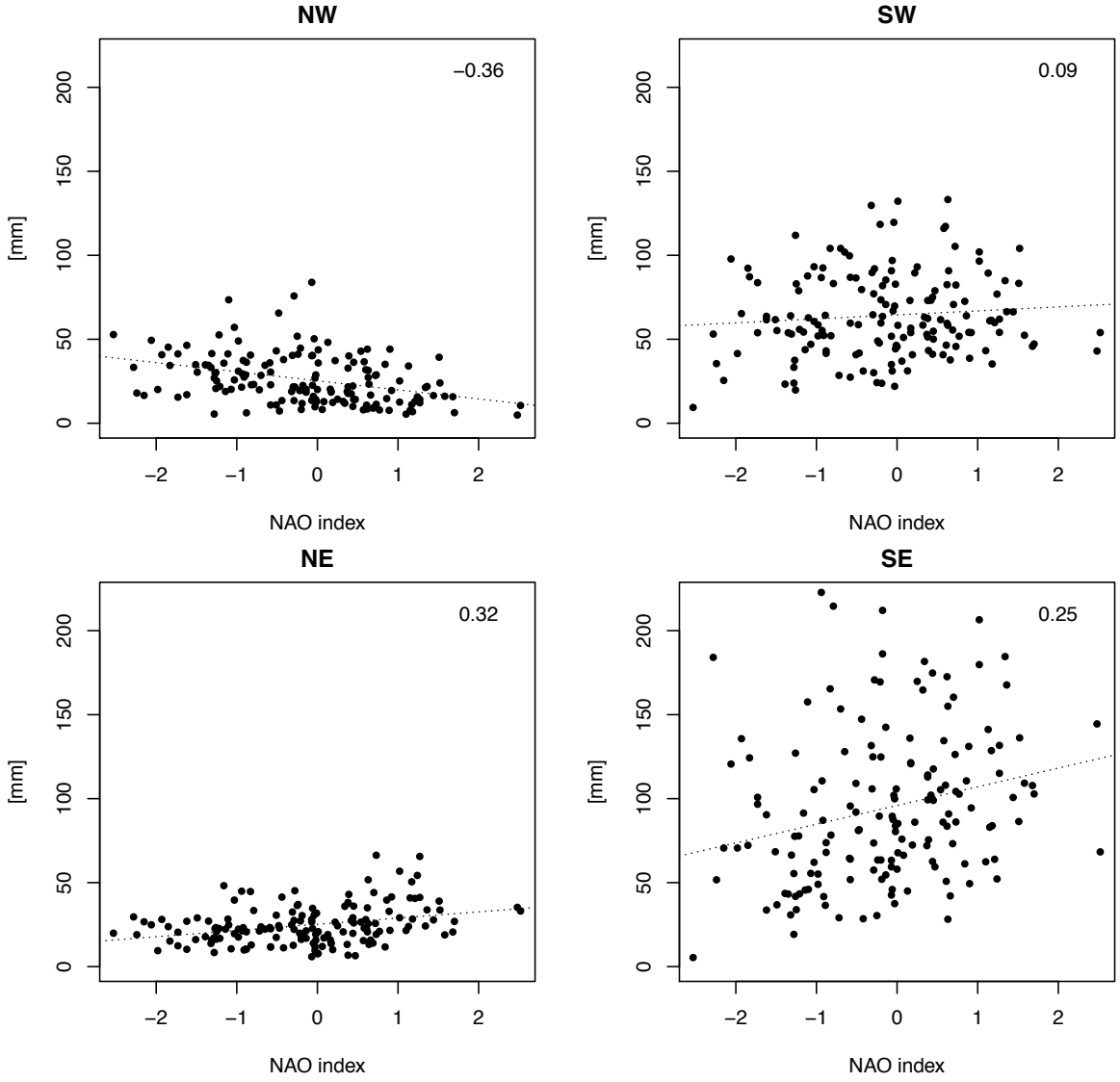

Figure 2.8. Mean monthly ASRv1 precipitation and the NAO index over four regions in Greenland. Dotted lines indicate linear regressions and numbers at top right corners show the correlate coefficients.

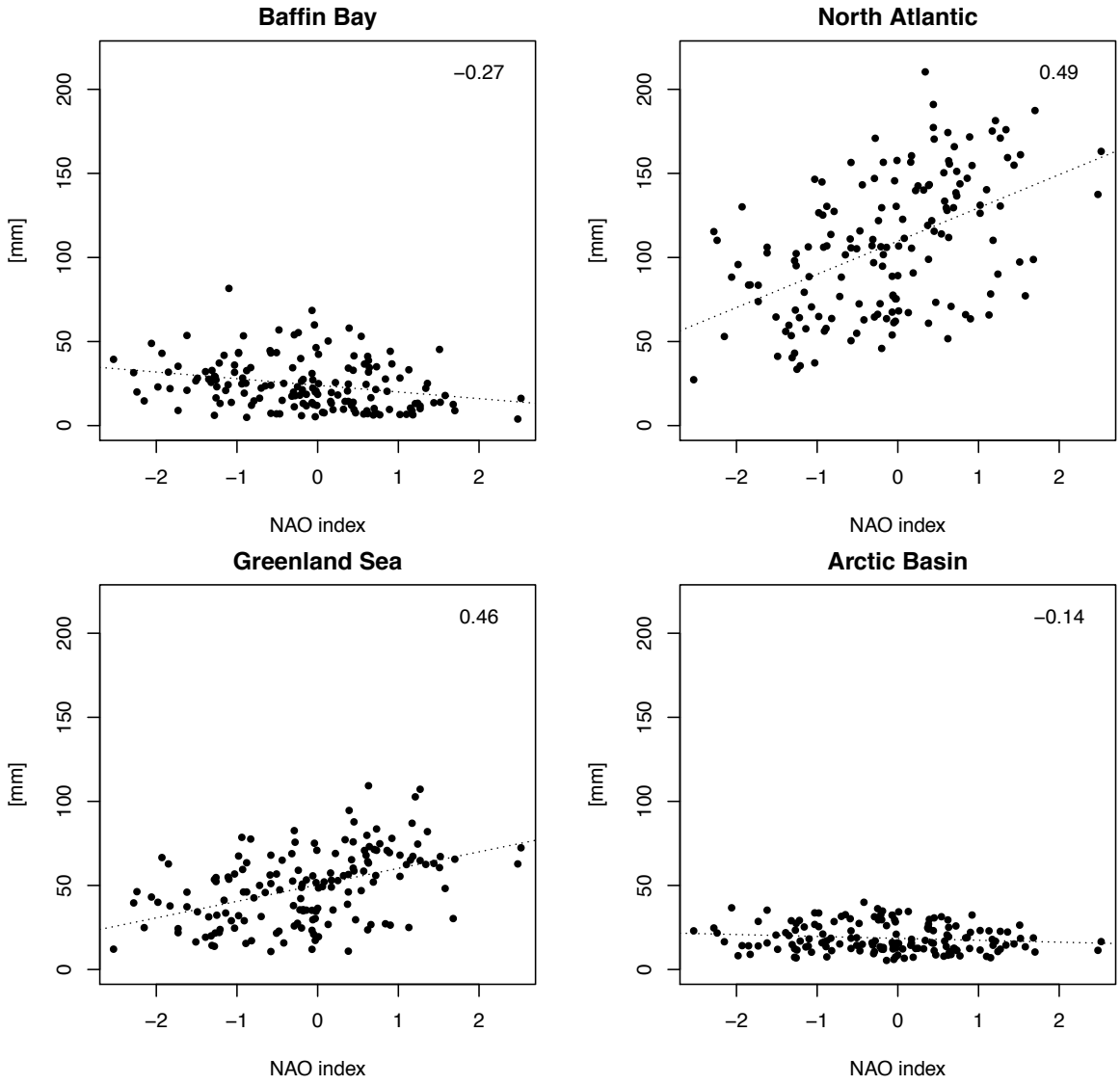

Figure 2.9. Same as Figure 2.8, but for four regions of the surrounding waters.

Sea ice loss and Arctic cyclone activity from 1979 to 2014

Tomoko Koyama[1,2]

Julienne Stroeve[3,1]

John Cassano[4,2]

Alex Crawford[1]

[1]**National Snow and Ice Data Center, University of Colorado, Boulder, CO, USA**

[2]**Department of Atmospheric and Oceanic Sciences, University of Colorado Boulder, 311 UCB, Boulder, CO, USA**

[3]**Centre for Polar Observation and Modelling, Earth Sciences, University College London, London, UK**

[4]**Cooperative Institute for Research in Environmental Sciences, University of Colorado Boulder, 216 UCB, Boulder, CO, USA**

Published in Journal of Climate on 25 May 2017 Vol. 30, Issue 12, JCLI-D-16-0542.1, doi:10.1175/JCLI-D-16-0542.1.

CHAPTER 3

SEA ICE LOSS AND ARCTIC CYCLONE ACTIVITY FROM 1979 TO 2014

3.1. Introduction

Extratropical storms transport atmospheric energy from lower latitudes into the polar regions. These cyclones initially form as waves in regions of enhanced temperature contrasts, referred to as baroclinic zones. In summer, when the central Arctic Ocean experiences a cyclone maximum (Serreze and Barrett 2008), cyclogenesis (the formation and intensification of cyclones) is particularly common over the Eurasian continent (Crawford and Serreze 2016). Whereas Arctic cyclone formation over Eurasia peaks in the summer, the autumn and winter show a predominance of storm tracks originating in the northern North Atlantic and propagating towards the Greenland, Norwegian, and Barents seas (e.g. Zhang et al. 2004). Shallow baroclinic zones typically found along the ice edge may provide the initial conditions for some of these storms (Tsukernik et al. 2007), which play an important role in our climate system by impacting precipitation, the radiation budget, cloudiness, and poleward heat and moisture transport (Bengtsson et al. 2006; Sorteberg and Walsh 2008). For example, at the end of December 2015, a strong cyclone entered the Arctic, transporting warm and humid air over the sea ice areas, resulting in localized thinning and retreat of sea ice (Boisvert et al. 2016).

During the last four decades, Arctic sea ice extent (SIE) has declined by more than 40% during summer (e.g. Stroeve et al. 2012; Serreze and Stroeve 2015; Simmonds 2015), leading to large open water areas in autumn that result in stronger heat and moisture transfers from the ocean to the atmosphere: turbulent fluxes of sensible and latent heat from the ocean are increased, as is longwave radiation emitted by the sea surface (e.g. Serreze et al. 2009; Screen and Simmonds 2010a). This leads to large increases in near surface air temperatures, which have been particularly strong in recent years during the month of October, a month after the seasonal minimum of sea ice occurs. This amplified autumn and winter warming contributes to a phenomenon called Arctic Amplification (e.g. Serreze et al. 2009; Screen and Simmonds 2010b; Inoue and Hori 2011), which in turn alters the meridional temperature gradient between the equator and the pole, especially at the surface. This ice loss has also increased the moisture content of the Arctic atmosphere (Serreze et al. 2012), which may in part explain the observed increase in cyclone-associated precipitation during the recent warm period (Li et al. 2014). Several other studies document an increase in autumn/winter snowfall over the adjacent boreal land in recent years of anomalously low summer sea ice, particularly over Siberia (e.g. Ghatak et al. 2010, 2012; Cohen et al. 2012; Liu et al. 2012; Orsolini et al. 2012).

Nevertheless, how these atmospheric changes in response to sea ice loss manifest on cyclone frequency and intensity within the Arctic remains unclear. Changes in cyclone tracks, frequency, and intensity reflect competing processes,

such as changing temperature gradients between mid-latitudes and the pole, and changes in specific humidity as the atmosphere warms. This has resulted in studies reaching different conclusions, with some studies suggesting a reduction in mid-latitude cyclone frequency and intensity during winter (e.g. Gitelman et al. 1997; Geng and Sugi 2003), while others suggesting an increase in frequency and strength of winter cyclones (Bengtsson et al. 2006; Simmonds et al. 2008; Sorteberg and Walsh 2008; Simmonds and Keay 2009; Stroeve et al. 2011), depending on the time-period evaluated and the metrics used to identify cyclones.

One consequence of sea ice loss and associated autumn warming that appears less uncertain is the potential for a poleward shift of storm tracks related to a northward shift in the region of greatest baroclinic instability (e.g. Hall et al. 1994; Carnell et al. 1996). Several studies report that a northward shift of storm tracks has already occurred, related to reduced winter sea ice in the Barents and Kara Seas, which may in turn be partly responsible for the warm Arctic - cold Eurasian continent pattern (e.g. Bengtsson et al. 2006; Inoue et al. 2012; Tang et al. 2013), although the role of sea ice loss in the cold continent pattern is disputed (Sun et al. 2016; Sorokina et al. 2016). Future projections for the end of this century in an anthropogenically warmed climate also suggest a northward shift will occur, yet the number of cyclones in the North Atlantic will actually decrease as a result of the mid-troposphere warming faster than the ocean surface, thereby increasing vertical stability (Zahn and von Storch 2010).

In summary, while the position of the sea ice edge might be expected to impact cyclone development and their tracks, it remains uncertain if the recent northward progression of the summer ice edge has already influenced autumn and winter cyclone frequency and intensity. This study is motivated by these large uncertainties. We aim to not only document whether or not cyclone frequency and intensity have changed in response to sea ice retreat, but also to evaluate the physical mechanisms governing changes in cyclone activity and how that may change in a further warmed climate. It is hypothesized that reductions in summer SIE and expanding open water areas in September have already transformed moisture availability, regional baroclinicity and atmospheric vertical stability in autumn. Building on previous work by Stroeve et al. (2011), this study uses data through 2014 and analyzes not only cyclone frequency and intensity, but also changes in extreme cyclones and the Eady growth rate, which can be strongly influenced by changes in the meridional temperature gradient. By comparing various cyclone metrics for low and high ice years, we hope to shed more light on the potential impacts of northward retreat of the ice edge on Arctic cyclone activity.

This paper is structured as follows: Section 2 briefly describes the data and methods used in this study, and how summer sea ice loss impacts the atmosphere is presented in section 3. Sections 4, 5, 6, and 7 report changes in baroclinic instability, vertical temperature difference, cyclone activity, and extreme cyclone activity, respectively, with respect to sea ice loss. Section 8 summarizes the results and presents discussion.

3.2 Methodology

There is no universal agreement on how exactly to define what constitutes an extratropical cyclone and where it is located. Despite their inherent complexity, many researchers have explored objective cyclone identification and tracking methods over the last two decades (Neu et al. 2013). Among currently available schemes, the Serreze et al. (1997) cyclone detection method has been used in numerous studies to monitor extratropical cyclones, mainly in the Northern Hemisphere (e.g. McCabe et al. 2001; Serreze and Etringer 2003; Wang et al. 2006; Finnis et al. 2007; Tsukernik et al. 2007; Serreze and Barrett 2008; Stroeve et al. 2011). We also rely on the Serreze et al. (1997) method to identify and track cyclones, where cyclones are tracked based on a series of search patterns to define occurrences when sea level pressure (SLP) is at least 1hPa lower than adjacent grid points (described in more detail below).

We additionally evaluate vertical temperature difference, baroclinic instability, cyclone intensity, and frequency of extreme cyclones. The Eady growth rate (Hoskins and Valdes 1990) provides a measure of baroclinicity and is determined by changes in static stability and vertical wind shear. Cyclone intensity is given by the cyclone central pressure and the local Laplacian. Details on each cyclone metric evaluated are provided in Section 2.b through 2.d below. As in Stroeve et al. (2011) we summarize results for the entire Arctic and also for different regions as depicted in Figure 3.1.

3.2.1 Data

Among currently available reanalyses products, we mainly rely on the National Centers for Environmental Prediction and National Center for Atmospheric Research (NCEP/NCAR) reanalysis (Kalnay et al. 1996), in part to be consistent with earlier work by Serreze et al. (1997), and also to extend the Northern Hemisphere Cyclone Locations and Characteristics dataset originally developed by Serreze et al. (2009) and distributed by the National Snow and Ice Data Center (NSIDC) (https://nsidc.org/data/docs/daac/nsidc0423_cyclone/) through 2008. A drawback is that it has lower horizontal and vertical resolution than more modern reanalysis data sets. Accordingly, two more modern products, the ECMWF Interim Reanalysis (ERA-Interim) (Dee et al. 2011) and Modern-Era Retrospective Analysis for Research and Applications (MERRA) (Rienecker et al. 2011) are utilized to verify the robustness of the results.

The target period of this study, from 1979 to 2014, is inherently determined by the time period of available sea ice data observed by satellites. Sea ice observations by multi-channel passive microwave sensors did not become available until October 1978. While some prior satellite observations are available, these are not consistent in time or spatial coverage. We use observations of sea ice concentration from the NASA Team Scanning Multichannel Microwave Radiometer and Special Sensor Microwave/Imager data set (Cavalieri et al. 1999) obtained from NSIDC. SIE is defined as the total ice area with at least 15% sea ice concentration.

To isolate potential links between reduced summer sea ice and changes in cyclone activity during the following months, we focus our analysis on relationships between mean September SIE (the SIE at the end of the summer melt season) and indices of cyclone activity from September to November for several different time-periods. These are defined by sorting the September SIE north of 60°N in ascending order, pentad, decade, and 18-year (half of the entire record) duration periods, for which the lowest and highest SIE are selected for each time period. Extreme high and low sea ice years are additionally determined by selecting years with values greater than ± 1.0 standard deviation (SD) from the standardized time-series, i.e., the SIE time-series is depicted as areal unit variation standardized to have a unit SD and zero mean value. The linear trend is computed by minimizing the chi-square error statistic. Figure 3.2 shows the standardized September and December SIE time series and extreme years with box symbols. The December SIE trend is used for the extreme cyclone analysis discussed later. Table 3.1 lists the September and December low and high ice years corresponding to each of the four time-periods evaluated.

3.2.2. Eady growth rate

The theory of baroclinic instability pioneered by Charney (1947) and Eady (1949) provides a physical explanation of cyclogenesis (Descamps et al. 2007). The maximum Eady growth rate is commonly used to measure development of atmospheric wave disturbances and is used as a measure of the potential for cyclones to develop and strengthen (Hoskins and Valdes 1990; Paciorek et al. 2002;

Lim and Simmonds 2007; Serreze and Barrett 2008). Here we determine the Eady growth rate (σ) at each grid point for each day at 500hPa following Paciorek et al. (2002) and Vallis (2006):

$$\sigma \equiv 0.31 \frac{f}{N} \left| \frac{\partial v}{\partial z} \right| ,$$

where f is the Coriolis parameter, N is the Brunt-Väisälä frequency (Rogers 1978; Lee and Mak 1994), z is vertical distance, and v is the horizontal wind vector. The vertical wind shear ($\frac{\partial \mathbf{v}}{\partial z}$) is related to the horizontal temperature gradient via the thermal wind equation (Wallace and Hobbs 2006). The Brunt-Väisälä frequency, which is a measure of atmospheric static stability, is given by

$$N = \left(\frac{g}{\theta} \frac{d\theta}{dz} \right)^{1/2} ,$$

where g is the acceleration due to gravity and θ is the potential temperature. One can see the Eady growth rate depends on both the static stability and horizontal temperature gradients in the atmosphere. Following Simmonds and Lim (2009), the potential temperatures at 300, 500, and 700hPa are used to estimate N and $\frac{\partial \mathbf{v}}{\partial z}$. The zonal and meridional winds, air temperature, and geopotential height fields directly from NCEP/NCAR reanalysis and the potential temperature calculated from the reanalysis temperature and pressure are utilized for the derivation. Simmonds and Lim (2009) further showed that the Eady growth rate derived directly from the time-mean fields is not entirely suitable and instead

recommend computing σ at all relevant synoptic time-scales before averaging. Accordingly, daily products are utilized to estimate the Eady growth rate.

3.2.3. Cyclone detection

The Serreze et al. (1997) cyclone tracking algorithm uses a series of search patterns to detect cyclones: the cyclone center is assumed to be defined when the SLP is at least 1hPa lower than the adjacent grid points. The algorithm employs a nearest neighbor analysis of the positions of cyclones from temporally successive SLP fields. Assuming two thresholds, a maximum search distance and an allowable pressure difference, the tracking algorithm examines if a target cyclone has moved in sequential time steps. In order to track center jumps, those limiting values are set at 800km and 20hPa, respectively.

To select robust cyclone systems in the Arctic (60-90°N), only cyclones satisfying the following three criteria are considered: (1) cyclones must last more than 24 hours, (2) cyclones must not be stationary, and (3) a cyclone must deepen at least 2hPa during its life cycle (Serreze and Barrett 2008). Regions with surface elevations higher than 2000m are discarded since the tracking algorithm tends to detect spurious systems over mountainous terrain where there is larger uncertainty in the utilized SLP fields. For example, Rudeva et al. (2014) showed that the Serreze tracking algorithm tracked the highest number of cyclone tracks in a selected region in Central Asia among 13 schemes evaluated. By applying topographic filtering, the number of tracked cyclones becomes close to the ones

detected using other schemes. Similar terrain filtering is widely used as a part of cyclone tracking algorithms (Neu et al. 2013).

The intensity of an individual cyclone can be quantified in terms of the cyclone central pressure and local Laplacian at each cyclone center. However, cyclone central pressure only gives a rough indication of cyclone strength since airflow near the surface is largely affected by the pressure difference between cyclone center and SLP field on the periphery. Thus, it is necessary to consider an ambient pressure field when we discuss central pressure in the context of cyclone intensity. On the other hand, the Laplacian is proportional to the geostrophic relative vorticity and directly indicates the corresponding cyclone intensity.

We perform a further consistency check using ERA-interim and MERRA. While the horizontal resolution of the ERA-interim and MERRA are 0.75 x 0.75 degree and 2/3 degree longitude by 0.5 degree latitude, respectively, the SLP field is regridded into 100 x 100 km spatial resolution for the tracking algorithm application. Since the spatial resolution is still finer than the NCEP/NCAR reanalysis, a multi-center cyclone detection procedure is applied in the tracking: when there are two cyclone centers that are clearly part of the same system, the system will only be counted as one cyclone. Topographic filtering is not applied since ERA-Interim and MERRA use more advanced assimilation techniques.

3.2.4. Extreme cyclones

In this study, extreme cyclones are determined from daily SLP fields following previous studies (Chang et al. 2012; Vavrus 2013). The climatological

annual average SLP at each grid point is first determined from 1981 to 2010. When the SLP for a specific grid cell at a specific time is at least 40hPa lower than the climatological value at the same grid point, it is assumed that an extreme cyclone occurred in that location. There is an advantage of using "relative" central pressure to study cyclones (Simmonds et al. 2003). Strong local meridional pressure gradients over the subarctic region and the locations vary by season (Serreze and Barry 2014) so that when a mid-latitude cyclone migrates poleward, the central pressure may decrease even if it is not intensifying. Also, how cyclones are defined — as minima in the total SLP or as minima in SLP perturbations after a large scale, low-frequency background flow has been removed — has an impact on projection of change in the frequency of strong cyclones over the Pacific under global warming (Chang 2014). While this approach does not show cyclone tracks, it can identify instances of extremely strong cyclones without needing to consider anomalous cyclonic or anticyclonic systems.

Figure 3.3 (a) shows the climatological mean monthly occurrence of extreme cyclones based on NCEP-NCAR reanalysis. The southern boundary of the Arctic domain is extended from 60 to 50°N since the latitude of the climatological center for the Aleutian Low exists near 50°N. Seasonal variation of the annual cycle is apparent: while extreme cyclones hardly occur in summer, the number of extreme cyclones increases during autumn and winter, reaching a maximum in January. This seasonal cycle agrees with previous studies (Zhang et al. 2004; Vavrus 2013). Spatially, the highest frequency in annual extreme cyclones occurs over Iceland and

in the vicinity of the Icelandic Low (Figure 3.3 (b)). The surrounding area where the average count is above 1.5 extreme cyclones per year corresponds to the North Atlantic cyclone track. Another area of high frequency of extreme cyclones lies in the Bering Sea, corresponding to the winter Aleutian Low. The spatial pattern is similar to that obtained using MERRA reanalysis (Vavrus 2013), while the derived frequencies by MERRA are greater than those of NCEP-NCAR.

3.3. Atmospheric impacts of summer sea ice loss

Since cyclone intensification and dissipation is sensitive, amongst other influences, to heat exchange processes at the surface (e.g., Kuo et al. 1991), the presence or absence of sea ice might be expected to play an important role in this heat exchange, leading to changes in cyclone activity.

Figure 3.4 shows September sea ice area differences together with differences in autumn (SON) ERA-Interim sensible and latent heat fluxes, 925-hPa air temperatures, and precipitable water between low and high ice years, determined by subtracting the high ice period from the low ice period. By conducting paired t tests, these differences are found to be statistically significant except for mean sensible heat flux differences corresponding to the ± 1.0 SD period. Extensive sea ice loss is observed within the Beaufort, Chukchi, East Siberian, and Laptev Seas for the four composite time-periods, with the largest reductions observed for the pentad and the ± 1.0 SD composites. Reductions are considerably less in the East Greenland Sea, Baffin Bay, and Barents Sea.

The local autumn atmospheric response of ice loss manifests as negative anomalies in the turbulent heat fluxes. Note that the heat fluxes are defined positive downward. Local minima of the sensible and latent heat flux anomalies coincide with regions of large summer ice loss (e.g. Beaufort, Chukchi, Laptev, and Kara Seas as well as in the northern Barents Sea). On the other hand, positive differences are dominant in the Bering, Barents, East Greenland and Labrador Seas. Little difference is observed over the middle of the Arctic Ocean where sea ice coverage has been stable. It is suspected that decreases in turbulent heat fluxes during low ice years reflect a smaller vertical temperature gradient between the sea surface and overlying air in close proximity to each other, which is also influenced by advection of warm air. Over the open ocean farther south, the sensible and latent heat fluxes increase along with increased sea surface temperatures (SSTs) resulting in positive differences. Negative differences in Denmark Strait can be related to anomalous cooling of the Irminger Sea (e.g. de Jong and de Steur 2016).

Increased heat loss from the ocean to the atmosphere in autumn helps to explain positive anomalies in air temperature throughout the Arctic at 925hPa (Figure 3.4, fourth row). Particularly large anomalies extend from the East Siberian Sea shore to the west of Severnaya Zemlya via north of the Laptev Sea. The largest positive anomalies occur during the pentad and ± 1.0 SD composite periods, consistent with the time-periods with the largest ice loss. Woods and Caballero (2016) studied poleward intrusions of moist air across 70°N from October to January and showed that the vertical structure of the warming associated with

moist intrusion is bottom amplified: a trend toward a weakening of the climatological temperature inversion. However, it is still unknown how much the moisture flux into the Arctic affects the SON 925-hPa temperature field since the frequency of intrusion events in October and November does not show statistically significant increment.

The last row of Figure 3.4 shows corresponding anomalies in precipitable water. The areas of predominantly positive anomalies partially correspond to the areas of sea ice loss and 925-hPa temperature anomalies (i.e., near the East Siberian Sea and Severnaya Zemlya). This is expected since precipitable water is largely dependent on the moisture content in the lower troposphere, and a warmer atmosphere is able to hold more moisture. Furthermore, positive anomalies of precipitable water appear over the North Atlantic, Barents and Labrador Seas during the pentad and the ± 1.0 SD composites. More frequent moist intrusions into the central Arctic basin can be expected during low ice years (Woods and Caballero 2016). Consequently, the increases in precipitable water reflect increased moisture and temperature as well as a contribution from bottom-amplified warming. A transition from a "cold clear" to a "warm opaque" state can in turn yield increased downwelling longwave radiation (Stramler et al. 2011).

While these physical hypotheses are based on interpreting the composite results, composite patterns may be misleading (Boschat et al. 2016). Their analysis initially suggested that SST dipole conditions may form a necessary condition for summer heat waves. However, sensitivity tests indicated that the vast majority of

days when the dipole SST pattern appeared were not associated with heat waves (i.e., the SST dipole pattern was not a sufficient condition). Thus, more rigorous evaluation is required to confirm exactly how sea ice reduction affects the heat exchange processes. However, we aim to only broadly explore the association between Arctic sea ice loss and changes in different environmental variables, which can potentially impact cyclone development.

3.4. Changes in vertical temperature difference

Jaiser et al. (2012) documented that stronger heat release to the atmosphere such as observed above, reduces the atmospheric vertical static stability when sea ice concentration is low, leading to an earlier onset of baroclinic instability. Zahn and von Storch (2010) utilized a simplified measure of vertical stability, the temperature difference between sea surface and at 500hPa model levels, and showed that the increased vertical temperature gradient contributes to weakened polar lows: polar lows are intense maritime meso-scale cyclones forming at high latitudes during cold air outbreaks (Rasmussen and Turner 2003). Since this measure is useful to detect unstable conditions related to polar low development, it is utilized for operational forecasting in Norway (e.g. Noer and Ovhed 2003; Woollings et al. 2012). Given that polar lows cannot always be detected by our cyclone tracking algorithm due to coarse grid spacing of the reanalysis data fields, this measure is not only helpful to estimate favorable conditions for polar lows to form, but also for the potential for synoptic-scale cyclogenesis in the Arctic.

Figure 3.5 shows the mean values of the temperature difference between 500 and 925hPa within the Arctic and six regions as shown in Figure 3.1. Mean values are computed for the ± 1.0 SD low and high sea ice years. The vertical temperature difference in each region during low ice years is generally larger, suggesting more favorable conditions for cyclogenesis during low sea ice years. Thus the position of the ice edge appears to influence vertical stability, such that small-scale disturbances in low-level air flows formed during low ice years are more likely to develop into cyclones over most of the Arctic. While the results are generally consistent between the different reanalyses, the NCEP-NCAR reanalysis shows considerably smaller temperature gradients over GRE that are likely an artifact of the coarser spatial resolution and small size of the GRE region (all regions are shown in Fig.1).

3.5. Changes in baroclinic instability

Eady growth rate measures the baroclinic instability around the mid-troposphere level. This altitude is effective for depicting the synoptic-scale potential for storminess. Regional time series of all grid cells with an Eady growth rate exceeding a threshold of $\sigma > 1.5 day^{-1}$ in autumn from NCEP-NCAR reanalysis is shown in Figure 3.6. The average Eady growth rate over the domain during the study period is 0.52 day^{-1}. Since the threshold value is approximately three times the average, it is only exceeded when strong cyclones occur, such as the Great Arctic Cyclone (Simmonds and Rudeva 2012; Parkinson and Comiso 2013; Zhang et al. 2013; Yamazaki et al. 2015). The annually averaged number of cyclones within the

TOP, GRE, HNA, CHU, CRU, and GNB regions during the study period are 45.3, 130.8, 224.6, 58.0, 69.6, and 199.3, respectively, indicating cyclones are more likely to occur in the GNB and HNA regions during autumn, where baroclinic instability can contribute to intensification and persistence of cyclones. However, while positive trends in Eady growth rate are seen in several regions of the Arctic (e.g. GRE, HNA, CRU, and GNB regions), only the GRE region shows statistically significant increases in baroclinic instability ($p \leq 0.05$).

To examine the influence of the reanalysis data set, Figure 3.7 shows mean counts of grid cells where $\sigma > 1.5 day^{-1}$ in autumn from three reanalyses during the ± 1.0 SD high and low ice years. Mean counts are normalized by the total number of grid points over the domain since each reanalysis has different spatial resolution. NCEP-NCAR results in larger frequency of occurrence during low ice years in all regions, whereas MERRA and ERA-Interim give mixed results. The same analysis was performed on October and November SIE ± 1.0 SD composites (not shown). Only within the GRE region do we find consistency among the reanalysis products that there is a tendency for increased autumn baroclinicity during low sea ice years. In other words, baroclinic instability increases over Greenland following anomalously low sea ice conditions in autumn.

3.6. Changes in cyclone activity

3.6.1. Interannual variability and trend analysis

Given the above indications of a moist climate, potential for increased baroclinicity around Greenland, and larger vertical temperature difference during

low sea ice years, we now examine whether these changes have actually influenced cyclone activity in the Arctic. Cyclone counts show large seasonal and interannual variability (Figure 3.8 and Table 3.2). Cyclone frequency peaks in summer, in agreement with Serreze and Barrett (2008) and Simmonds et al. (2008). Spring and autumn generally show similar number of cyclones, but with slightly more frequent cyclones in autumn (85 versus 79). While monthly SIE shows negative trends in all months (not shown), positive trends in cyclone counts are only seen in autumn (+ 0.6 cyclones per decade), yet they are not statistically significant. The only season with a statistically significant trend is summer, decreasing at a rate of 3.3 cyclones per decade.

3.6.2. Cyclone deepening rates

Figure 3.9 shows averaged maximum cyclone deepening rates in autumn for three time-periods (a) 1979 - 2014, (b) + 1.0 SD high ice years, and (c) - 1.0 SD low ice years from NCEP-NCAR reanalysis. Cyclone deepening rate is defined as the change in 6-hourly cyclone central pressure. The location of maximum cyclone deepening is a good indicator of where the strongest development occurs (Serreze and Barrett 2008). The average maximum cyclone deepening rate is defined as the summation of the maximum deepening rates divided by the number of the maximum deepening events. Locally, deepening rates are largest from Denmark Strait to the Greenland Sea and there is some indication that maximum deepening rates are increasing poleward in the Barents Sea during low ice years. However, caution is needed as these results are influenced by sample size differences: while

the entire study period has samples over 36 years, those of high and low ice periods are collected from 8 and 6 year durations, respectively. The numbers of detected cyclones at a grid point during low ice periods are smaller than those of the entire study period. Since depicted cyclone deepening rates are the sample mean of maximum cyclone deepening rates, their confidence intervals are not consistent. Assuming a 95% confidence level, confidence intervals for the entire time series, high ice, and low ice periods are 0.4178-0.4281, 0.4307-0.4458, and 0.4220-0.4387, respectively. Thus, the lengths of confidence interval for the high and low ice years are larger than that for the entire study period.

Corresponding frequency distributions of maximum deepening rates show that the most frequent maximum deepening rate is between 0.3 and 0.4hPa per hour regardless of compositing (Figure 3.10). Mean values of the maximum cyclone deepening rates for 1979-2014, high and low ice years are 0.38, 0.38, and 0.37hPa hour $^{-1}$, respectively, suggesting no specific tendency in cyclone deepening rates between the high and low ice years.

3.6.3. Spatial pattern of cyclone activity

Cyclone activity with respect to SIE variation is analyzed in an analogous way to the surface energy budget analysis. Figure 3.11 shows low minus high ice year differences in SON sea ice area, mean cyclone counts, cyclone center mean SLPs, and the local Laplacian derived from NCEP/NCAR reanalysis.

Small and unevenly shaped positive and negative anomalies in cyclone frequency are found for all different composites throughout the Arctic (Figure 3.11,

second row). Weak positive anomalies occur in Baffin Bay, south of Denmark Strait, north of Norway, the vicinity of Severnaya Zemlya, and the Bering Strait. Considering patterns of the pentad and the ± 1.0 SD composites, positive anomalies north of Norway might correspond to a marked increase in autumn cyclone activity within the GNB region previously reported by Stroeve et al. (2011), however the spatial pattern is more limited and less coherent. In particular, positive anomalies are interspersed with negative anomalies, and it is difficult to find a specific pattern of anomalies along with the area where extreme cyclones frequently occur. In addition, differences are statistically significant ($p \leq 0.01$) for the decade and ± 1.0 SD years, but not for the pentad and the 18-year composite.

Regions with large summer ice losses generally show little change in cyclone activity except for some small increases in frequency in the Laptev, Kara, and Barents seas, but again, these regions are interspersed with declines in cyclone activity as well, making it difficult to ascribe these changes directly to sea ice loss. Interestingly, no real change in cyclone activity is found over North America. The correlation coefficients between mean changes in sea ice area and mean changes in cyclone frequency for the pentad, decade, 18-year, and ± 1.0 SD periods are 0.04, 0.13, 0.07, and 0.07, respectively, which are not statistically significant. Thus, the results do not suggest cyclone frequency has changed in response to sea ice loss.

Turning our attention towards cyclone intensity, we find that all Laplacian differences and the pentad and decade composites of SLPs are statistically significant ($p \leq 0.01$), while the 18-year and ± 1.0 SD composites of SLPs are not

(Figure 3.11, rows 3 and 4). Changes in intensity might be expected to occur when the sea ice area represents a major change, (i.e., because of averaging, the longer the duration becomes, the less the corresponding anomalies show). Thus, we can expect that spatial patterns are better defined for the pentad and $\pm$ 1.0 SD composites than for the decade and 18-year composites. Positive SLP differences are found in the Chukchi Sea, near the North Pole and over large parts of Eurasia, combined with negative differences over Baffin Bay, the North Atlantic and north of the Barents and Kara Seas during the pentad and $\pm$ 1.0 SD composites. Positive (negative) SLP differences demonstrate that SLP during low ice years is higher (lower) than during high ice years, which indicates that cyclone intensity is weakened (intensified) with respect to sea ice loss. On the other hand, positive Laplacian differences indicate strengthened intensity since the local Laplacian is proportional to the geostrophic relative vorticity. Together the cyclone SLP and Laplacian suggest that while cyclone frequency may not be changing in the GNB and northern Barents and Kara Seas, cyclones are becoming more intense. However, correlation coefficients between area-weighted mean September SIE and area-weighted mean local Laplacian in autumn are not statistically significant in any of the six regions. Since the GNB region tends to be ice-free in summers, intensification of cyclones may be more related to observed increases in precipitable water.

Finally, to test the robustness of the results, corresponding differences in composite mean cyclone frequency, cyclone center mean SLPs, and the local

Laplacian in SON derived from ERA-Interim and MERRA are shown in Figure 3.12. Results remain noisy, and differences between low and high ice years are found to not be statistically significant by conducting paired t tests. Nevertheless, features seen in the NCEP-NCAR reanalysis are also seen in MERRA and ERA-Interim, such as positive differences in mean cyclone frequency in northern Baffin Bay, the vicinity of the Icelandic Low region, off the Kola Peninsula, Norway, and near the North Pole, together with weak negative differences in the Beaufort Sea. Less agreement is seen around Siberia. MERRA further indicates negative differences from Ellesmere Island to northwestern Greenland, which may be a spurious signal. Further study is required to assess if this a limitation of the tracking algorithm, which is optimized for NCEP-NCAR reanalysis or if it is a characteristic of the MERRA SLP field.

Spatial difference patterns in central SLPs and local Laplacian also generally agree among the reanalysis, the exception being that the magnitude of changes between the two composites is less in MERRA and ERA-Interim (Figures 3.11 row 4; Figure 3.12, rows 5 and 6). It is hypothesized that the local Laplacian derived from NCEP-NCAR has larger discretization error due to the coarse spatial resolution, resulting in larger differences between the high and low ice years. Overall, comparison among the three reanalysis products suggest cyclone intensity is likely to be weakening in the Bering and Chukchi seas, but the increase in cyclone intensity in the northern Barents, Kara Seas as well as in the North Atlantic is not robust.

3.7. Changes in extreme cyclone activity

Finally, we turn our attention to changes in extreme cyclone activity. Extreme cyclones mostly occur in winter (DJF) (Figure 3.3 (a)). Accordingly, high and low ice years are composited based on the December SIE (Table 3.2). Time series of DJF extreme cyclone counts over the GNB region and the entire Arctic (60-90°N) show decreasing trends on the order of -2.84 and -6.71 counts per year, respectively, yet are not statistically significant (Figure 3.13). Variability in extreme cyclones appears closely linked with the winter Arctic Oscillation (AO) (Thompson and Wallace 1998) (Figure 3.13 b). Correlation coefficients between the DJF AO index and extreme cyclone counts in the GNB region and Arctic-wide regions are 0.52 ($p=0.001$) and 0.47 ($p=0.004$), respectively. This suggests that when the AO index is positive, there is an increase in baroclinicity, increasing cyclogenesis and the number of extreme cyclones in the Arctic. Thus, the AO constitutes part of the decadal-scale variability in extreme cyclones, particularly in the GNB region but also on a pan-Arctic scale. However, several studies have suggested that the relationship between the North Atlantic Oscillation (NAO) (Hurrell et al. 2003) index and other climatic variables such as SLP, SST, or surface air temperature is not stationary in time (e.g. Rogers 1997; Zveryaev 1999; Polyakova et al. 2006; Haylock et al. 2007). Thus, if there is strong interdecadal variability in the relationship between the DJF AO index and extreme cyclone counts, it is possible that those coefficients can be varied by the length of study period.

Nevertheless, extreme cyclone frequency differences between low and high ice years are statistically significant ($p \leq 0.01$) from paired t tests, with positive differences in the vicinity of the Aleutian Islands for all periods and within the Barents Sea and North Atlantic during the pentad and ± 1.0 SD composites combined with negative differences within the North Pacific Ocean, Greenland, Norwegian, Barents and Kara seas (Figure 3.14). Further, there appears to be a westward shift in extreme cyclones in the North Pacific Ocean, while a northward progression in the North Atlantic is less certain. Small areas near Svalbard and south of Iceland during the pentad and ± 1.0 SD period show increases in extreme cyclones, as well as near Iceland during the last decade, but other regions show reductions.

3.8. Summary and discussion

To study whether or not a linkage between sea ice loss and cyclone activity has already emerged in the Arctic, we evaluated several metrics relevant to cyclones over the period 1979 to 2014. Cyclones are influenced by many factors, including land-sea temperature contrasts, local topography, near surface temperature and specific humidity, and large-scale transient eddies leading to climate patterns such as the AO. The reduced spatial extent of Arctic sea ice (Figure 3.2) impacts the heat and moisture content of the overlying atmosphere, and can therefore potentially influence atmospheric circulation patterns and impact storm frequency and intensity. The combined changes of cyclones and SIE may have a significant impact not only on the Arctic ecosystem but also human activity. For example, strong

winds from extreme cyclones produce storm surges and extensive wave action, especially as fetch (distance to the ice edge) has grown in the coastal areas of the Beaufort, Chukchi, East Siberian, Laptev, and Kara Seas (Figure 3.4, row 1). Consequently, storms can cause disastrous damage to local communities as well as erosion and flooding. Thus, assessing how cyclone frequency and intensity will change under an Arctic with less sea ice is important for long-range planning.

To gain insight, we first examined heat exchange processes at the surface in response to sea ice loss. Enhanced turbulent heat fluxes and longwave radiation in autumn and winter from sea ice loss have reduced the atmospheric static stability (Figure 3.4), as evidenced by increases in vertical temperature differences between 500 and 925 hPa (Figure 3.5). A similar result has been found in other studies (e.g. Francis et al. 2009; Overland and Wang 2010; Stroeve et al. 2011; Jaiser et al. 2012). This has made the Arctic atmosphere more prone to baroclinic instability, which could in turn lead to more or stronger cyclones within the Arctic. Eady growth rate, which provides a measure of changes in the baroclinicity and the potential for cyclogenesis, further suggests that baroclinic instability over Greenland has increased as Arctic sea ice cover has decreased in autumn (Figure 3.7). Combined these results suggest an increased potential for cyclogenesis in the Arctic during low sea ice years.

In addition, to the increased potential for cyclogenesis in the Arctic, expanding open water areas at the end of the melt season have lead to substantial changes in moisture availability during subsequent months (Figure 3.4), which may

further increase the intensity of autumn and wintertime cyclones, and increase the amount of cyclone-associated precipitation, leading to increased snowfall. Yet it is important to note that changes in cyclone-associated precipitation do not necessarily imply a corresponding increase in cyclone intensity. Furthermore, Willison et al. (2013) suggest the response of cyclone intensity to atmospheric moisture increases may be a function of resolution of the reanalysis dataset.

While the observed atmospheric changes suggest the potential for increased cyclone activity and intensity, applying the Serreze et al. (1997) cyclone detection and tracking algorithm to the NCEP-NCAR atmospheric reanalysis does not suggest there has been an increase in autumn cyclone activity following years with low September SIE. On the other hand, results suggest that cyclones are becoming stronger (as evaluated by the cyclone central SLP and local Laplacian) within limited areas: the northern Greenland, Norwegian, Barents, and Kara Seas (Figure 3.11). Crawford and Serreze (2016) documented that the summer Arctic Frontal Zone, a narrow band of strong horizontal temperature gradients along the Arctic coastline, acts as an intensification area for systems forming over Eurasia. While the well-defined summer Eurasian frontal zone breaks down in autumn, frontal activity in the vicinity of Greenland is redeveloped (Serreze et al. 2001). Thus, it is hypothesized that the frontal activity from the Denmark Strait to Barents Sea is strengthened along with sea ice loss and acts as a modest intensifier of storms passing through the area in autumn. However, we find intensification of cyclones is

dependent on the choice of atmospheric reanalysis used, in agreement with previous studies (e.g. Raible et al. 2008; Ulbrich et al. 2009; Neu et al. 2013).

Finally, since a small change in the mean of a climate variable can result in a large change in the frequency of extremes (Mearns et al. 1984), extreme cyclones, identified as having anomalous deviation from a regionally mean SLP, were examined. Results suggest DJF extreme cyclone tracks are shifted westward in the North Pacific Ocean while the frequency of extreme cyclones in the north Atlantic storm track has generally declined in response to sea ice loss (Figure 3.14). This is counter to previous studies that have documented an increase in intensity and frequency of extreme Atlantic cyclones (Paciorek et al. 2002; Lehmann et al. 2011), and others that showed opposite trends in the eastern Pacific and North America (Gulev et al. 2001). Simmonds and Rudeva (2014) analyzed a subset of the most intense Arctic cyclones throughout the year using 10 different cyclone tracking algorithms and showed agreement among the algorithms as to location of the cyclone center. Thus, we have confidence that our results are robust. Romero and Emanuel (2017) suggest that while the annual number of North Atlantic polar lows will decline by 10-15% in the future (2081–2100), a northward shift along the north Atlantic storm track is expected.

In summary, expanding open water areas in the Arctic have led to increased transfer of heat and moisture from the ocean to the atmosphere, warming and moistening the Arctic atmosphere and increasing the potential for cyclogenesis. However, a coherent change in autumn cyclone frequency has not yet manifested

despite evidence of a relationship between extreme cyclones and sea ice loss. This suggests that while there is some evidence that sea ice changes are impacting the potential for cyclogenesis, their effect on cyclone metrics is indistinct.

Acknowledgements

This study was supported by National Science Foundation grants PLR-1304807 and DGE-1144083 and NASA grant NNX14AH89G. NCEP-NCAR reanalysis data have been provided by the NOAA/OAR/ESRL PSD, Boulder, Colorado, through their website.

Table 3.1. September and December SIE low and high periods from 1979 to 2014. Refer to section 3.2.1. Data and Fig. 2 for the methodology of determining the low and high ice years.

Period	Sept low years	Dec low years	Sept high years	Dec high years
Pentad	2007, 2008, 2010, 2011, 2012	2006, 2007, 2010, 2011, 2012	1980, 1983, 1986, 1992, 1996	1980, 1981, 1983, 1988, 1989
Decade	2005, 2006, 2007, 2008, 2009, 2010, 2011, 2012, 2013, 2014	2000, 2006, 2007, 2008, 2009, 2010, 2011, 2012, 2013, 2014	1979, 1980, 1981, 1982, 1983, 1986, 1987, 1988, 1992, 1996	1979, 1980, 1981, 1982, 1983, 1986, 1988, 1989, 1993, 1994
18-year	1990, 1993, 1995, 1999, 2000, 2002, 2003, 2004, 2005, 2006, 2007, 2008, 2009, 2010, 2011, 2012, 2013, 2014	1984, 1987, 1999, 2000, 2001, 2002, 2003, 2004, 2005, 2006, 2007, 2008, 2009, 2010, 2011, 2012, 2013, 2014	1979, 1980, 1981, 1982, 1983, 1984, 1985, 1986, 1987, 1988, 1989, 1991, 1992, 1994, 1996, 1997, 1998, 2001	1979, 1980, 1981, 1982, 1983, 1985, 1986, 1988, 1989, 1990, 1991, 1992, 1993, 1994, 1995, 1996, 1997, 1998
$\geq 1.0 \lvert SD \rvert$	2007, 2008, 2010, 2011, 2012, 2014	2006, 2007, 2010, 2011, 2013	1980, 1982, 1983, 1986, 1987, 1988, 1992, 1996	1980, 1981, 1983, 1988, 1999

Table 3.2. Summary of seasonal cyclone counts variations.

Season	Mean	Standard Deviation	Trend (count / year)	P-value
Winter (DJF)	48.4	8.5	-0.15	0.29
Spring (MAM)	79.4	7.4	-0.14	0.23
Summer (JJA)	101.2	9.1	-0.33	0.020
Autumn (SON)	84.5	7.2	0.06	0.60

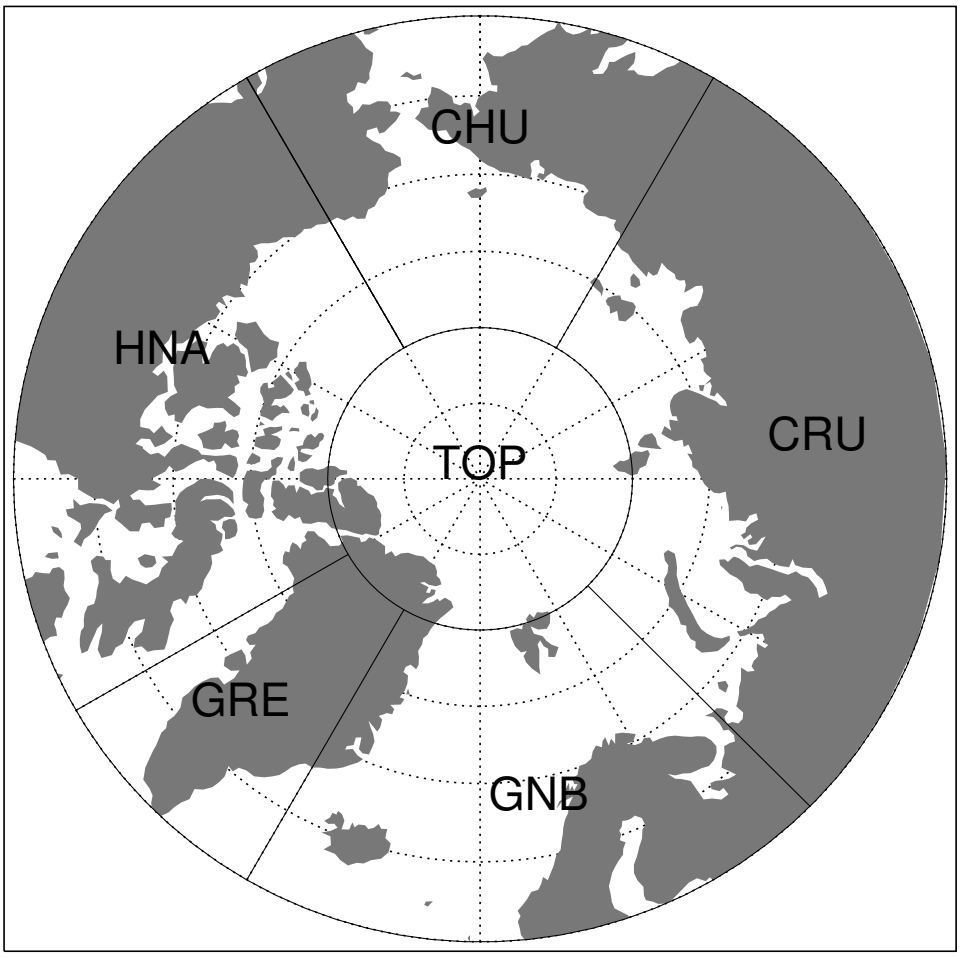

Figure 3.1. The entire Arctic (ARC) north of 60 N includes the high-latitude North America (HNA), the Chukchi and East Siberian Seas (CHU), Central Russia (CRU), the Greenland, Norwegian and Barents Seas (GNB), Greenland (GRE), and all areas north of 80N (TOP).

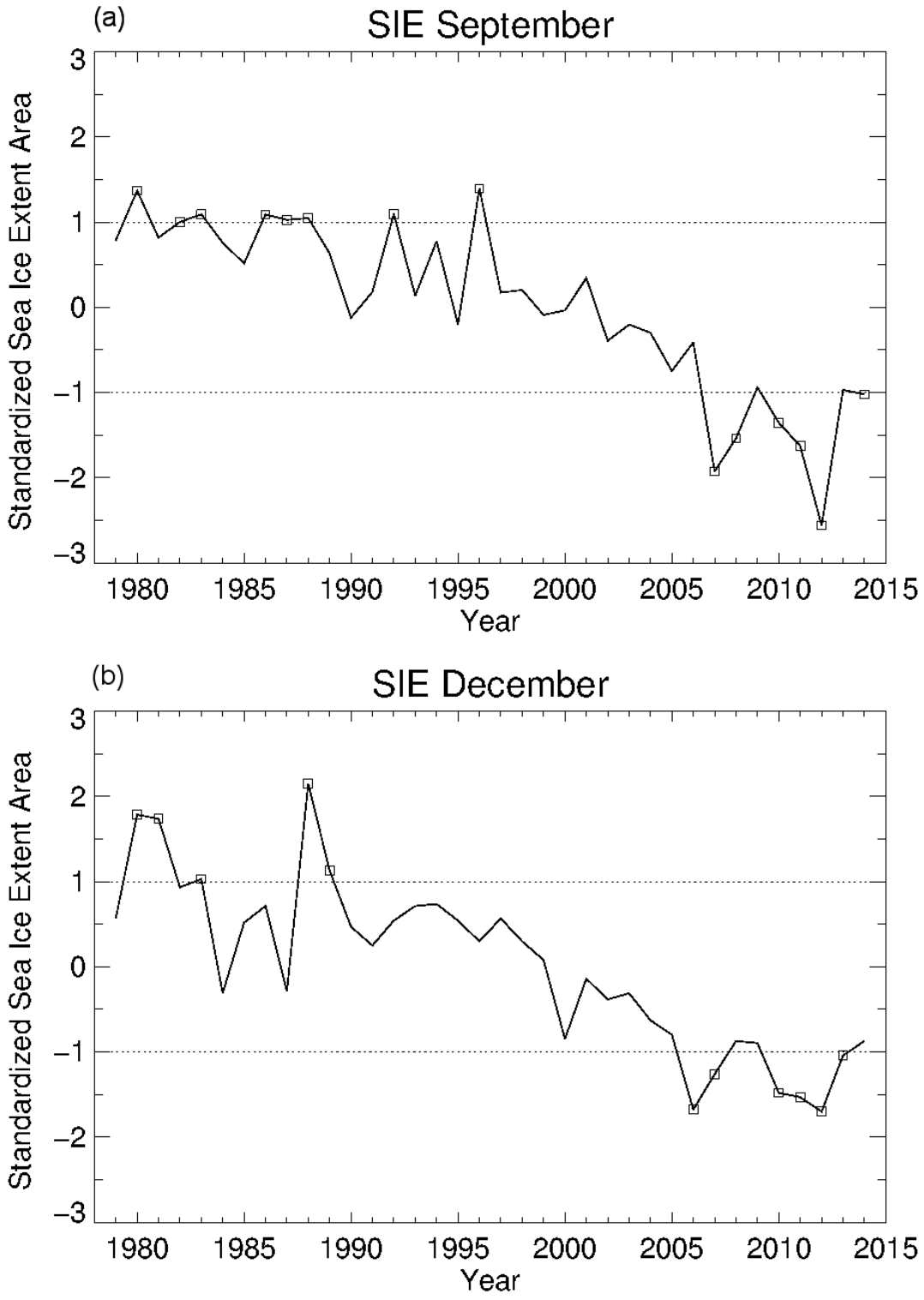

Figure 3.2. Standardized SIE (a) September and (b) December time series from 1979 to 2014. The extremely high ice years are listed in Table 3.1. Box symbols correspond to those extreme years.

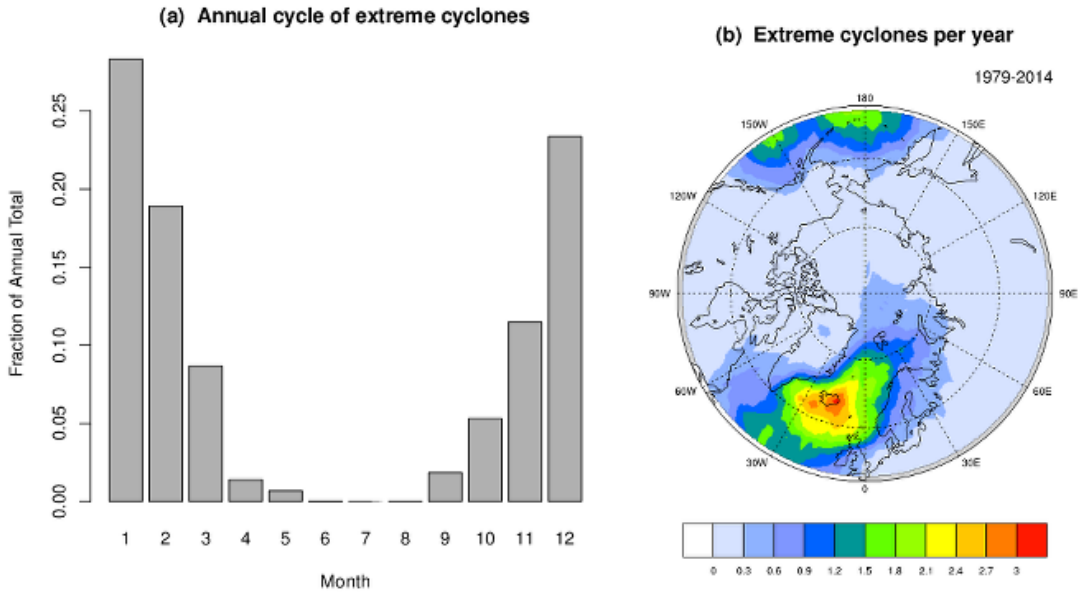

Figure 3.3. (a) Annual cycle of extreme cyclones determined from daily NCEP/NCAR SLP field of 1981-2010. (b) Annual mean count of extreme cyclones from 1979 to 2014.

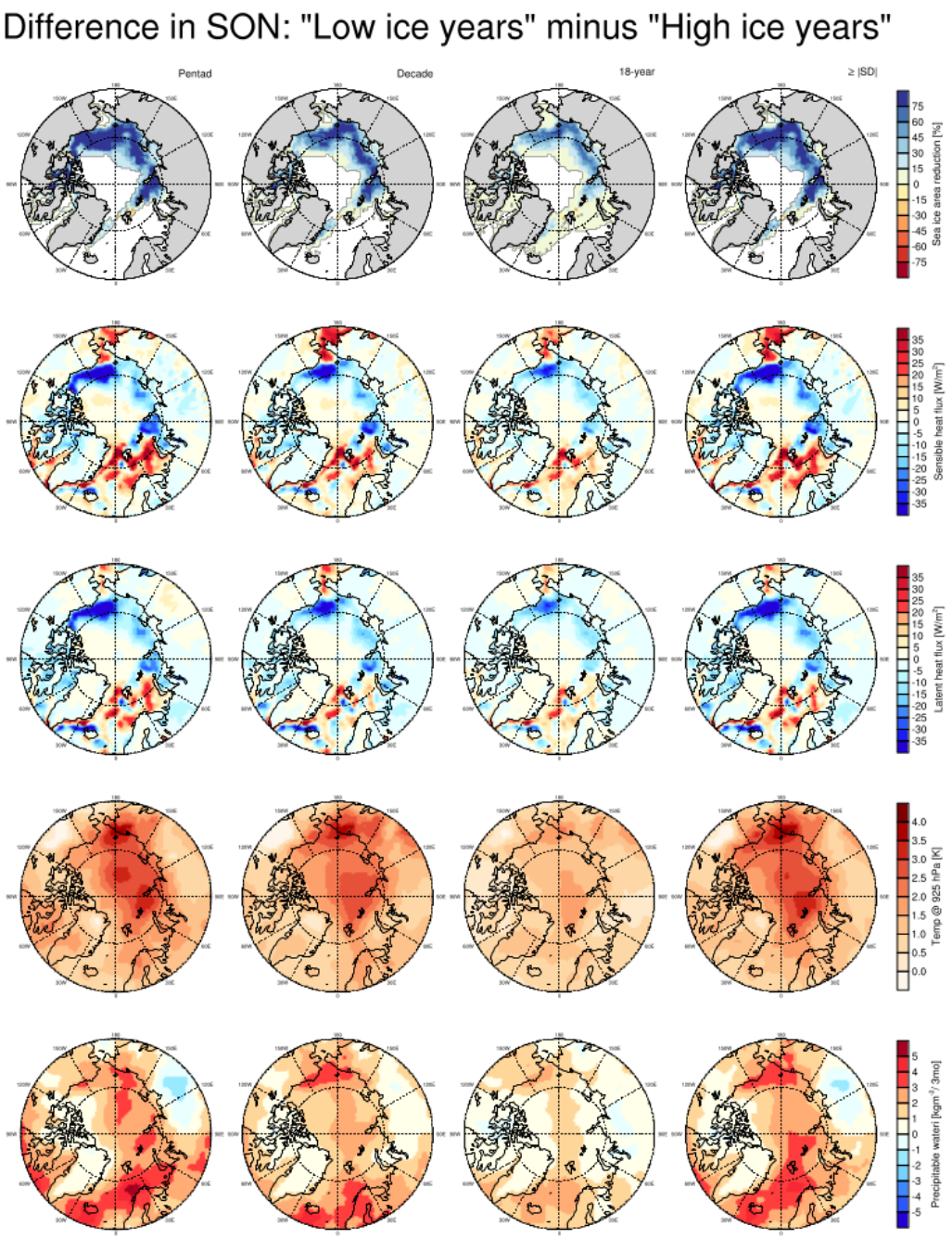

Figure 3.4. (First row) Composite September sea ice area change ratio from the high ice years to low ice periods. (Second row) mean sensible heat flux, (third row) mean latent heat flux, (fourth row) mean 925-hPa air temperature, and (fifth row) mean precipitable water. Each column period can be referred to Table 1. ERA-Interim is utilized except for the first row.

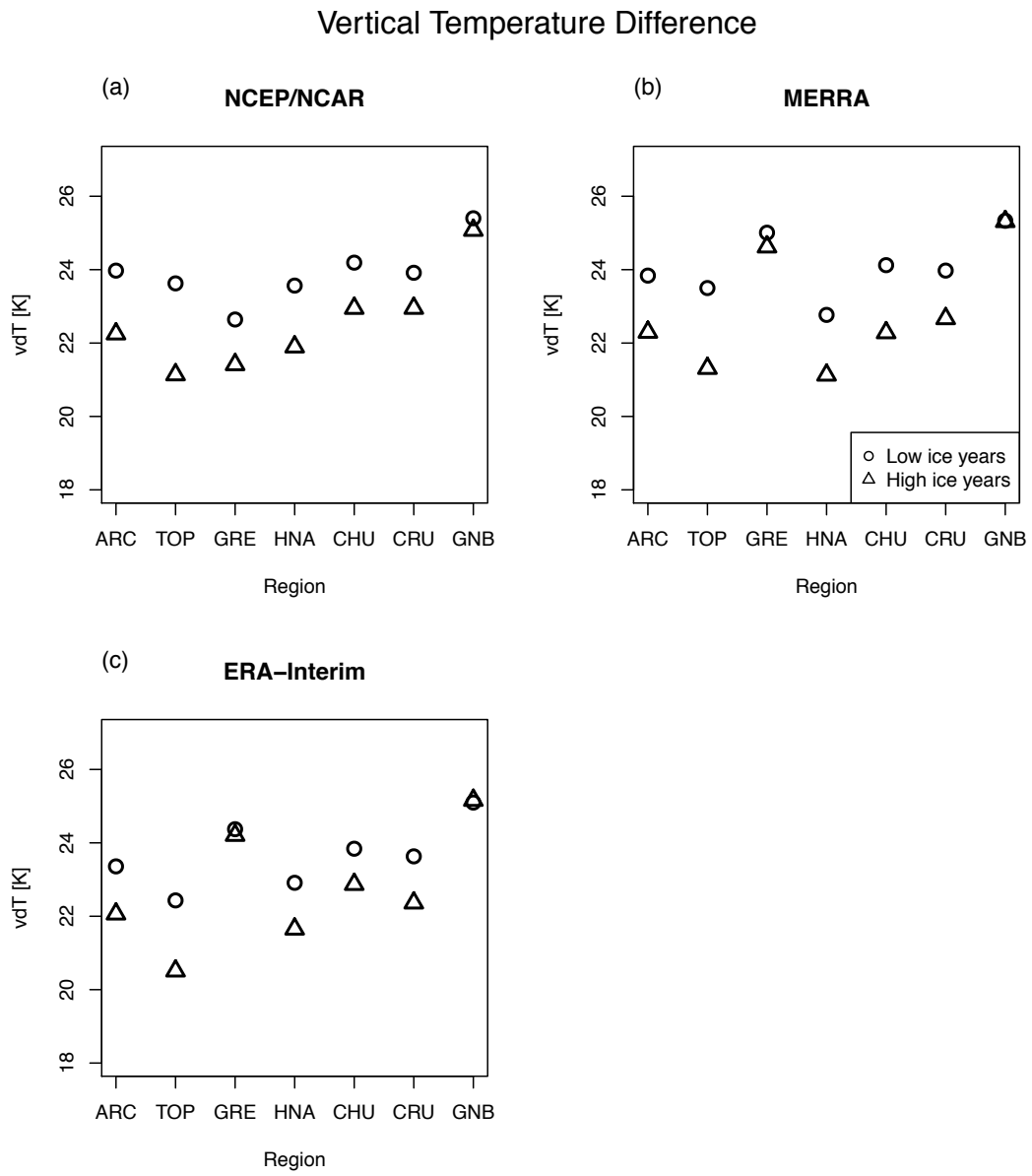

Figure 3.5. The mean temperature difference between 500 and 925 hPa of (a) NCEP/NCAR, (b) MERRA, and (c) ERA-Interim during the low and high sea ice extreme composites and the entire study period.

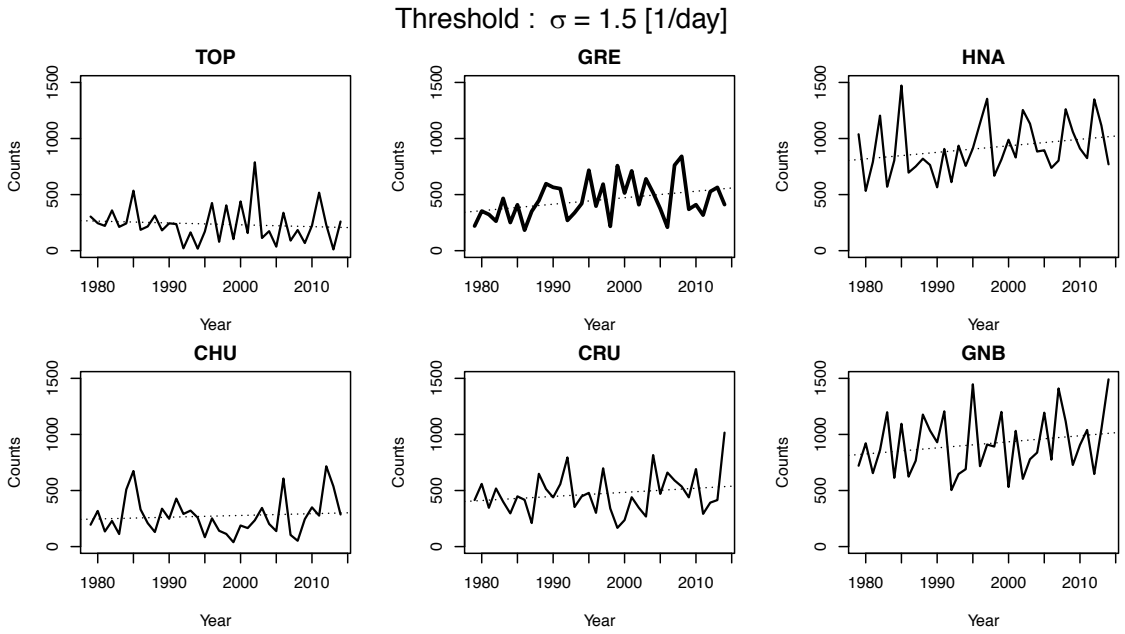

Figure 3.6. Regional trends of grid cell numbers exceeding the threshold =1.5 day^{-1} which is based on NCEP/NCAR reanalysis. GRE region demonstrate a statistically significant trend. The dotted lines are linearized trends.

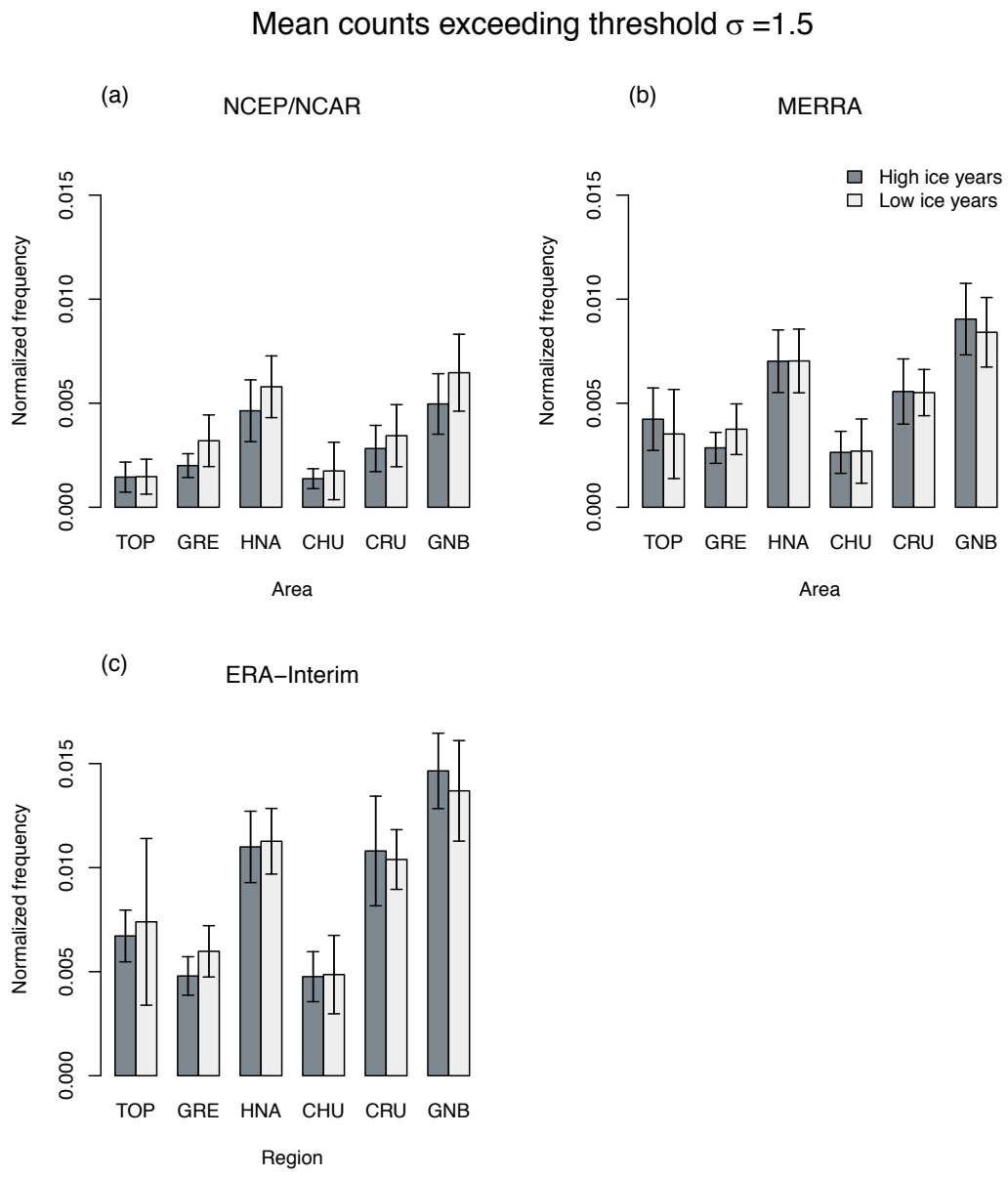

Figure 3.7. Normalized mean counts of grid cells exceeding the threshold =1.5 day^{-1} in autumn derived from the (a) NCEP/NCAR, (b) MERRA, and (c) ERA-Interim reanalyses during the high- and low-ice composite periods over the six regions (bars represent standard deviation of the mean).

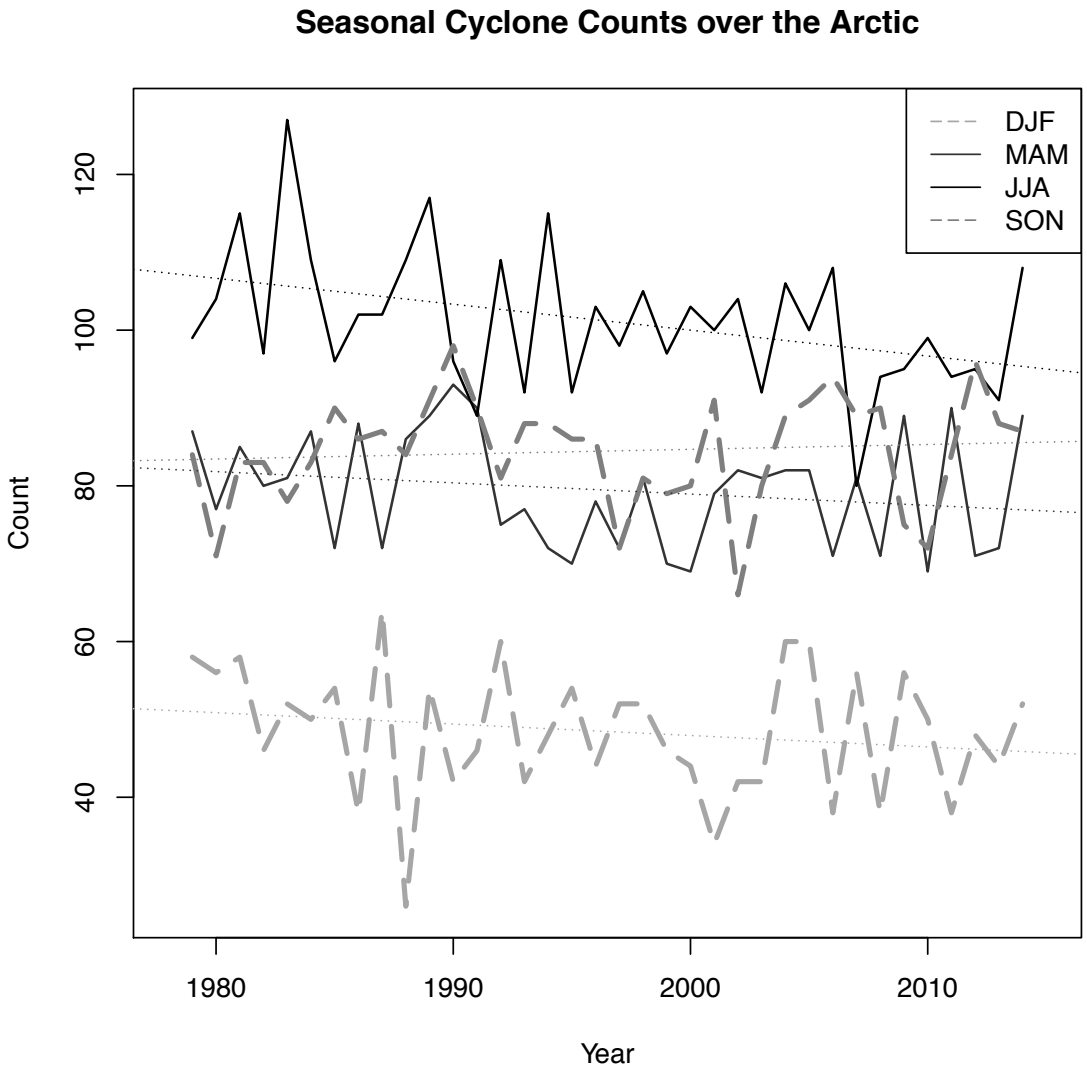

Figure 3.8. Time series of seasonal cyclone counts derived from NCEP/NCAR reanalysis over the Arctic. The linearized trends are illustrated by dotted lines.

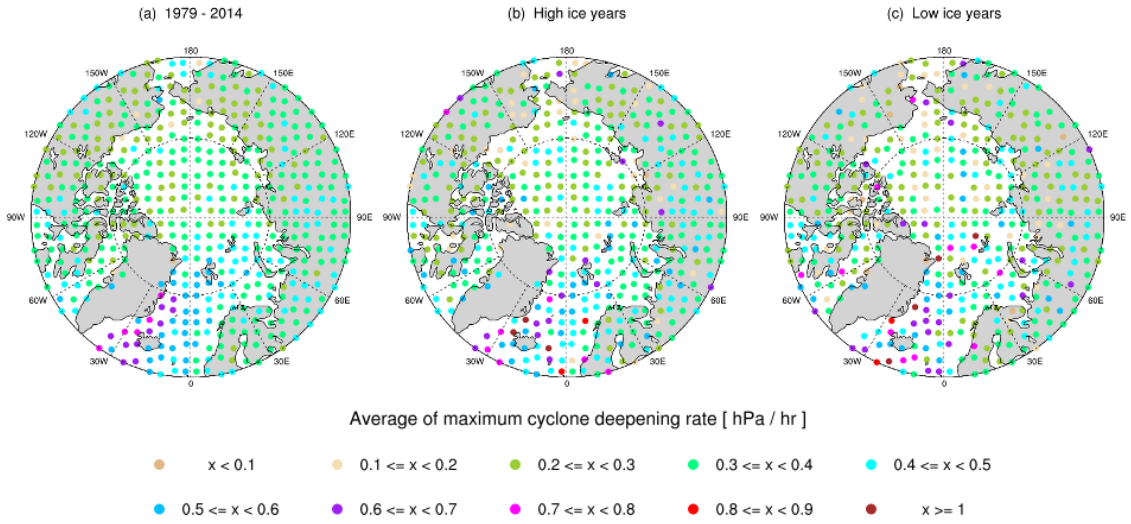

Figure 3.9. Average of maximum cyclone deepening rates derived from NCEP/NCAR reanalysis, (a) from 1979 to 2014, during (b) + 1.0 SD high and (c) - 1.0 SD low ice years.

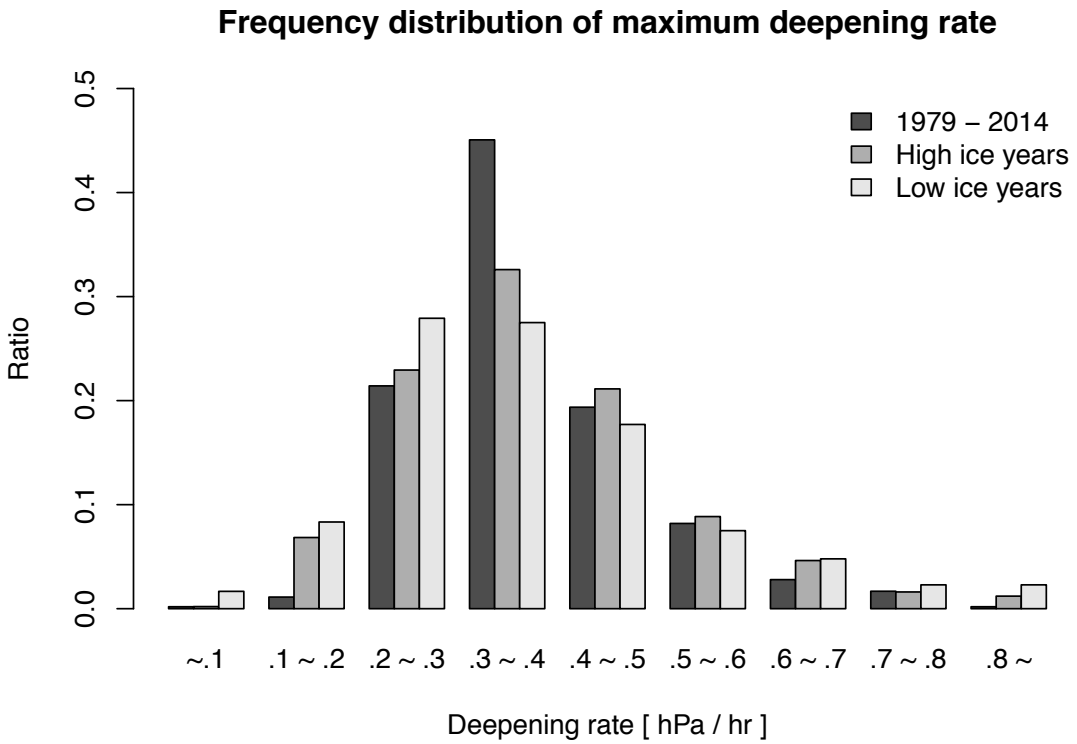

Figure 3.10. Frequency of averaged maximum cyclone deepening rates derived from NCEP/NCAR reanalysis, from 1979 to 2014, during high and low ice years.

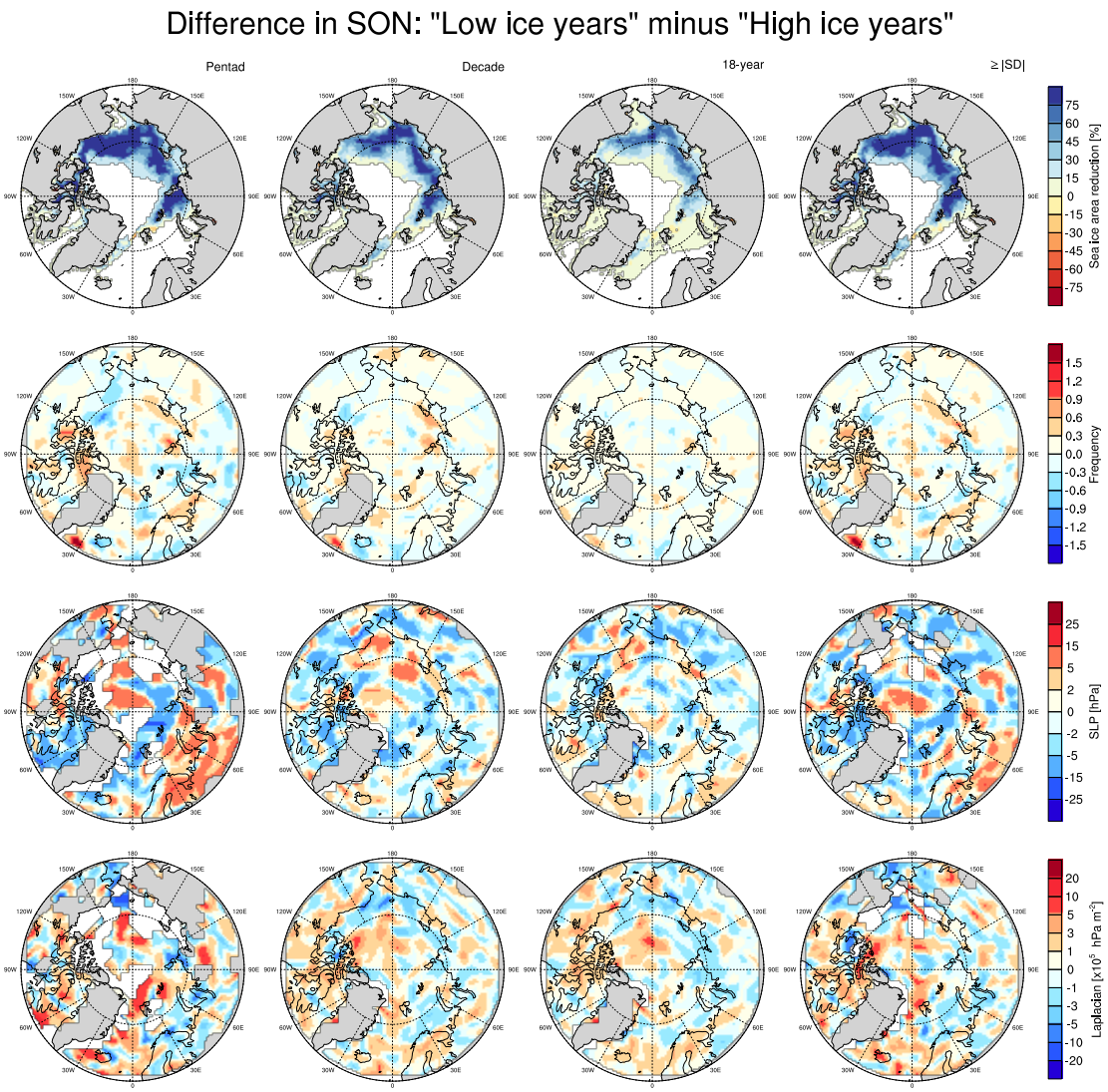

Figure 3.11. The temporal and spatial resolution of NCEP/NCAR reanalysis is 6-hourly on a 2.5 x 2.5 degree global grid, respectively. (First row) Composite September sea ice area change ratio from the high ice years to low ice periods. (Second row) mean cyclone frequency from NCEP/NCAR, (third row) cyclone center mean SLPs from NCEP/NCAR, (fourth row) cyclone center mean Laplacian from NCEP/NCAR. Each column period is the same as Figure 3.4.

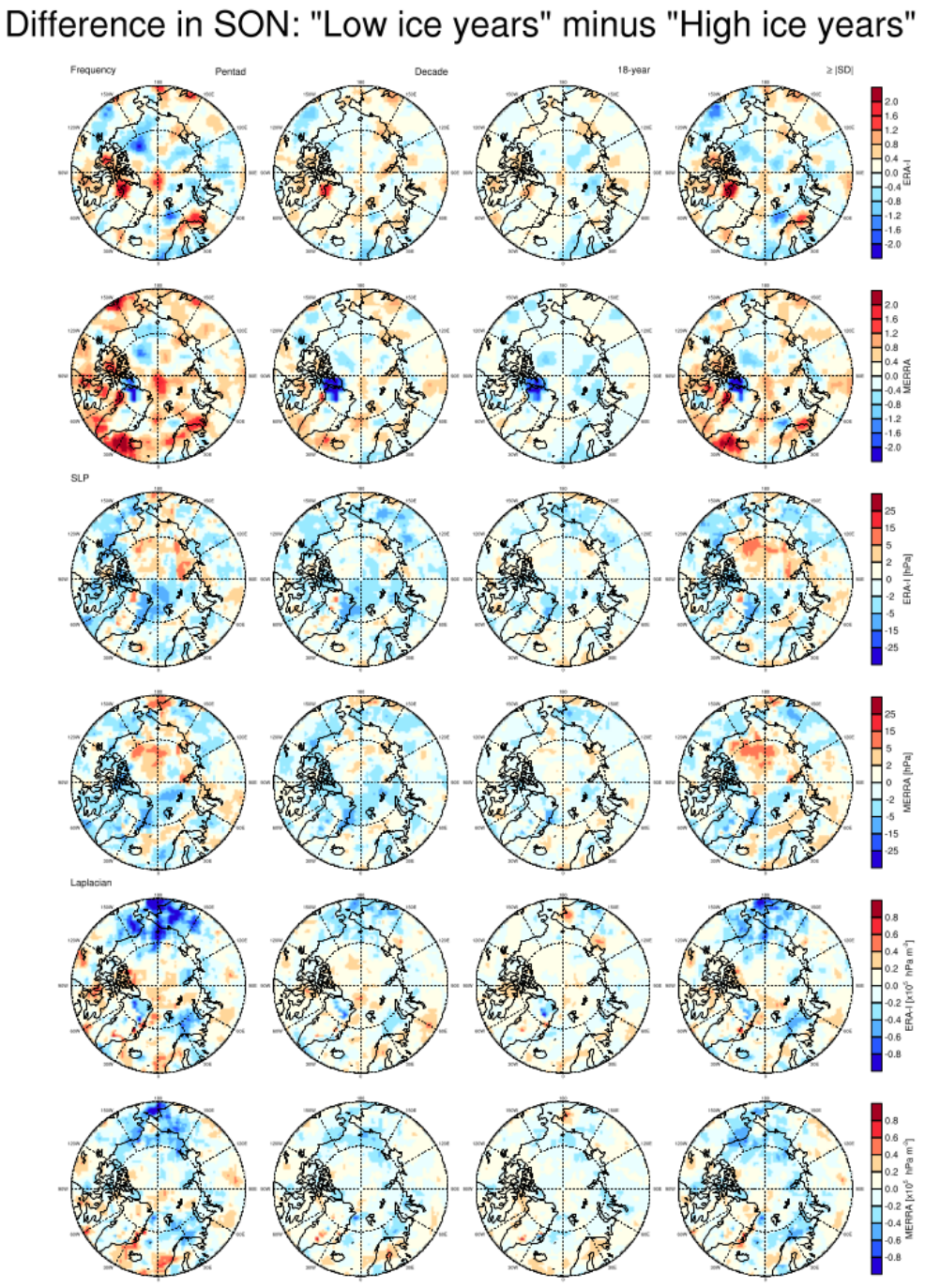

Figure 3.12. The temporal and spatial resolution is 6-hourly on a 100km x 100km degree global grid, respectively. (First row) mean cyclone frequency differences derived from ERA-Interim between the high ice years to low ice periods. (Second row) same as row 1, but derived from MERRA. (Third row) cyclone center mean SLPs differences derived from ERA-Interim between the high ice years to low ice periods. (Second row) same as row 3, but derived from MERRA. (Fifth row) cyclone center mean Laplacian differences derived from ERA-Interim between the high ice years to low ice periods. (Sixth row) same as row 5, but derived from MERRA. Each column period is the same as Figure 3.4.

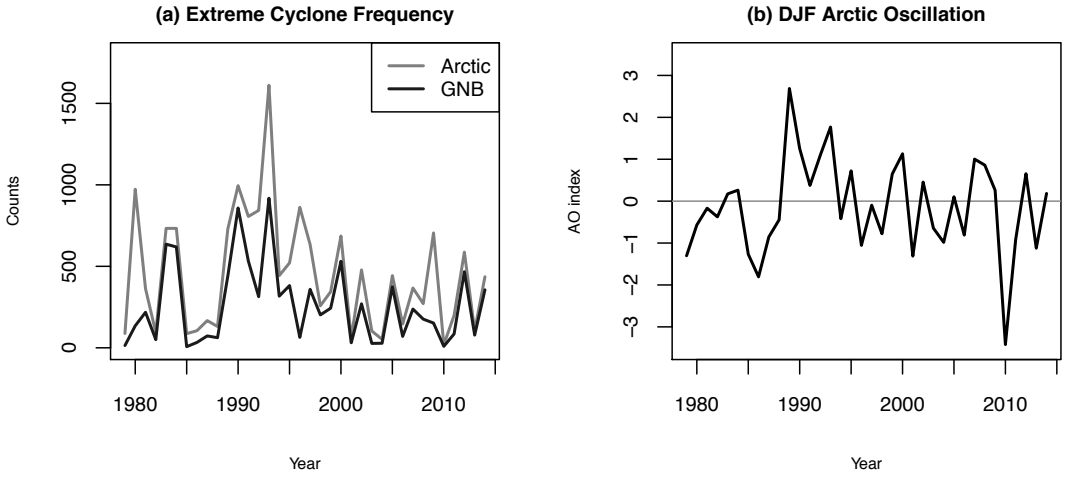

Figure 3.13. Time series of (a) DJF extreme cyclone counts from NCEP/NCAR over GNB and the Arctic, and (b) mean DJF Arctic Oscillation (AO) index.

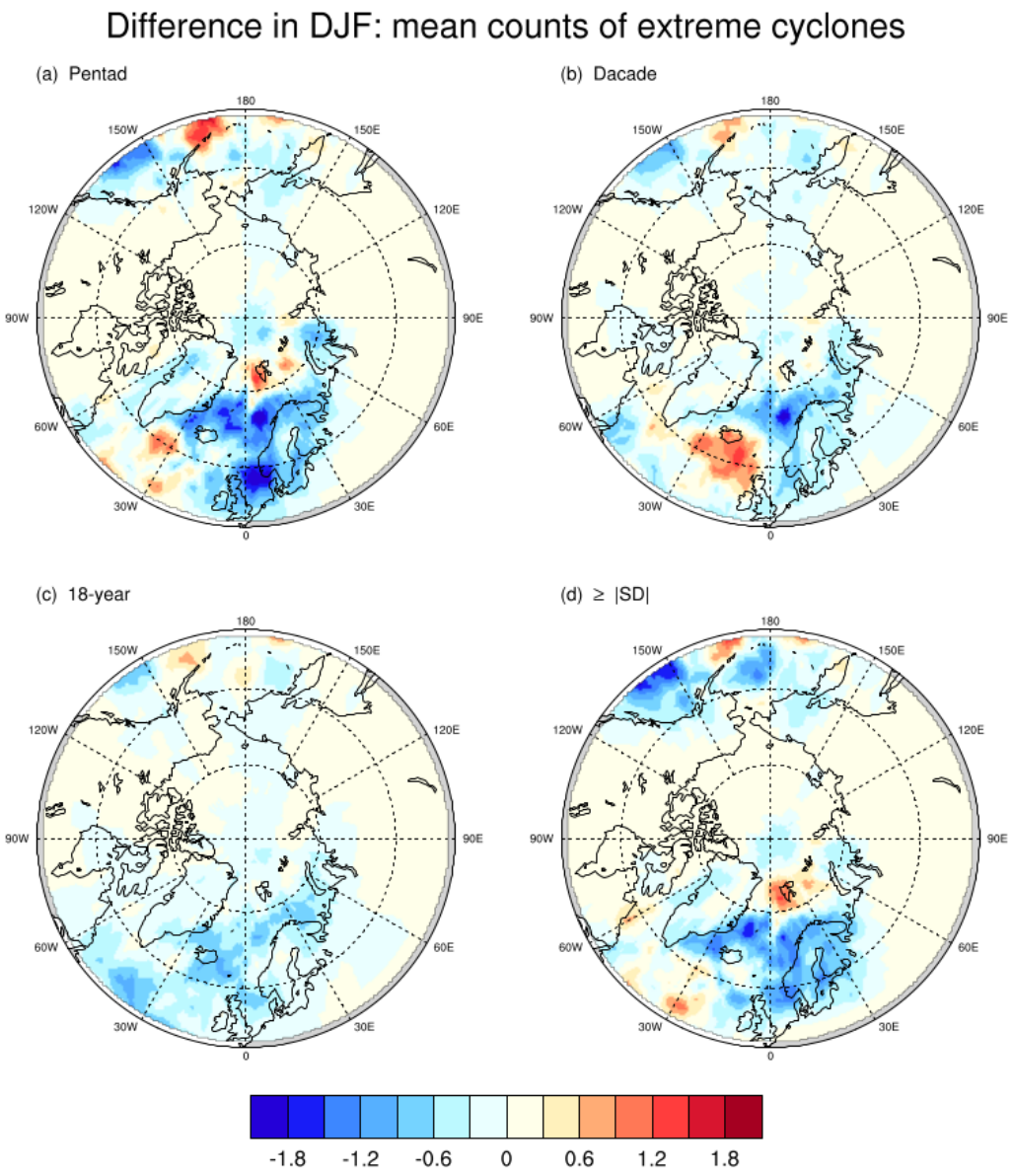

Figure 3.14. Extreme cyclone frequency difference in winter, "Low ice years" minus "High ice years".

Mid-latitude atmospheric responses to autumn Arctic near-surface temperature anomalies in CMIP5 models

Tomoko Koyama[1,2]

John J. Cassano[3,2]

Elizabeth N. Cassano[3]

Julienne Stroeve[4,1]

[1]**National Snow and Ice Data Center, University of Colorado, Boulder, CO, USA**

[2]**Department of Atmospheric and Oceanic Sciences, University of Colorado Boulder, 311 UCB, Boulder, CO, USA**

[3]**Cooperative Institute for Research in Environmental Sciences, University of Colorado Boulder, 216 UCB, Boulder, CO, USA**

[4]**Centre for Polar Observation and Modelling, Earth Sciences, University College London, London, UK**

This manuscript will be submitted to the Journal of Geophysical Research (JGR) for publication in the spring of 2018

CHAPTER 4

MID-LATITUDE ATMOSPHERIC RESPONSES TO AUTUMN ARCTIC NEAR-SURFACE TEMPERATURE ANOMALIES IN CMIP5 MODELS

4.1. Introduction

The Arctic occupies only four percent of the Earth's surface, but has a significant role in modulating global climate: the atmosphere and oceans continuously move excess heat from the tropics toward the polar regions. In recent decades, rapid changes have been observed in the Arctic. Satellite observations of sea ice extent (SIE) have shown a distinct decline over the Arctic Ocean since 1979. In particular, summer SIE has decreased considerably (e.g., Stroeve et al. 2012; Parkinson 2014; Serreze and Stroeve 2015; Simmonds 2015). In addition, sea ice thickness (SIT) has decreased (e.g., Kwok and Rothrock 2009; Laxon et al. 2013; Lindsay and Schweiger 2015) and snow-cover changes are substantial in the Arctic (e.g., Callaghan et al. 2011; Bokhorst et al. 2016). Open water areas have increased in parallel with the sea ice reduction and this enhances sensible and latent heat transfers from the ocean to the atmosphere, as well as longwave radiation emitted by the sea surface (e.g., Serreze et al. 2009; Screen and Simmonds 2010a). At the same time, the net heat input to the atmosphere from thin ice in the 0- to 0.4-m range is significantly larger than for thick ice (Maykut 1978). Accordingly, as a result of recent sea ice declines near-surface air temperature has increased notably.

In fact, temperature has increased almost twice as fast in the Arctic than elsewhere in the world, a phenomenon called Arctic amplification (AA) (e.g., Serreze et al. 2009; Screen and Simmonds 2010b; Inoue and Hori 2011).

These rapid changes in the Arctic climate system pose a new question: Can these changes in the Arctic climate system influence mid-latitude weather? It has been argued that AA has effects on the polar jet stream and planetary waves and those changes may increase the frequency of particular regional weather extremes (Overland et al. 2011; Francis and Vavrus 2012, 2015; Liu et al. 2012; Outten and Esau 2012; Screen and Simmonds 2014). However, there are contrasting viewpoints. For example, Barnes and Screen (2015) stated that "internal atmospheric variability may obscure the influence of Arctic warming and/or the Arctic influence may be small compared with other factors that control mid-latitude weather". Cohen et al. (2014) and Overland et al. (2016) both confirmed that it is a major challenge to unravel the linkage between a rapidly warming Arctic and mid-latitude atmospheric circulation and further study and community coordination are necessary to advance our understanding of the linkages.

Mills et al. (2016) assessed the possibility of Arctic ice variability forcing a mid-latitude response. By utilizing the self-organizing map (SOM) technique and CCSM4, they found that positive sensible heat flux anomalies in the Beaufort and Chukchi Seas produced low-level warm anomalies that built an upper level ridge and a planetary wave train. Subsequently, it induced robust surface cold anomalies

in eastern North America 6-8 weeks later. Cassano and Cassano (2017) followed Mills et al. (2016) approach and their results from four reanalyses showed that positive anomalies of skin temperature and surface energy fluxes in the Barents and Kara Seas coincided with lower SIC in this region. This led to ridging at 500 hPa and a positive SLP anomaly downstream of the ridge over the Barents and Kara Seas. Eventually, the surface high pressure system led to cold-air advection (CAA) into central and northern Asia. Similar mechanisms for lower level sensible heat fluxes producing low-level warming that builds and modulates eastward propagating planetary waves was reported by other studies (Serreze et al. 2009, 2011; Stroeve et al. 2012). Kug et al. (2015) documented that regional Arctic warming could induce cold mid-latitude winters: warming over the Barents–Kara Sea region is likely to lead to East Asian cooling, whereas northern North America cooling is closely related to warming over the East Siberian–Chukchi Sea region.

The focus of this study is on the impact of the rapidly changing autumn surface state in the Arctic on downstream weather in the mid-latitudes. Six models from the fifth phase of the Coupled Model Intercomparison Project (CMIP5) are analyzed with the SOM framework used by Mills et al. (2016) and Cassano and Cassano (2017). Composites for anomalously warm surface conditions in the Arctic are used to assess the atmospheric evolution over seasonal periods up to 12 weeks after the initial warm anomaly.

4.2. Data and Methods

4.2.1. CMIP5 model data

Coupled global climate models (CGCMs) have been used as the major objective tools to provide future climate projections. The CMIP5 archive provides a set of standardized simulations aimed at bridging major gaps in understanding of past and future climate change (Taylor 2012). It is desirable to utilize all the CMIP5 model runs to enable us to analyze more detailed and certainty in projected changes in atmospheric state (Knutti and Sedláček 2012), but it also requires expensive computational cost and resources to analyze data from all CMIP5 models. Therefore, models having well-simulated or overestimated sea ice thickness (SIT) are selected to assess the evolution of the atmospheric state with respect to changes in surface state over the Arctic Ocean. The six models selected for our analysis are the fourth version of the Community Climate System Model (CCSM4) (de Boer et al. 2011), the Hadley Global Environment Model version 2 Carbon Cycle and Earth System configurations (HadGEM2-CC and HadGEM2-ES) (the HadGEM2 Development Team 2011), a single version of the Institut Pierre Simon Laplace (IPSL) CM5 model (IPSL-CM5A-LR) (Dufresne et al. 2013), the Model for Interdisciplinary Research on Climate version 5 (MIROC5) (Watanabe et al. 2010), and the Norwegian Climate Center's Earth System Model (NorESM1-M) (Bentsen et al. 2013). While SIT simulated by CCSM4, HadGEM2-CC, HadGEM2-ES show relatively good agreement with Pan-Arctic Ice Ocean Modeling and Assimilation System (PIOMAS) SIT data (Zhang and Rothrock 2003), the IPSL-CM5A-LR, NorESM1-M, and MIROC5 overestimate SIT (Stroeve et al. 2014).

We characterize the Arctic surface state in the models listed above by using near-surface air temperature. This follows the approach taken by Mills et al. (2016) and Cassano and Cassano

(2017). Surface air temperature has been a primary metric to assess the climate system and it is largely influenced by conditions at the surface. In the Arctic, sea ice concentration and thickness influence local surface air temperature since sea ice reduces the exchange of heat between the ocean and atmosphere while the heat exchange is enhanced in areas of open water or thin ice. The albedo difference between ice and water is also a major factor in radiative forcing. As surface temperature responds to radiative and nonradiative forcing at the surface, changes in near-surface temperature are used as a proxy to represent changes in surface state.

We focus on autumn months (September-November), following Mills et al. (2016) and Cassano and Cassano (2017), when the difference in surface temperature between open water, thin ice, and thick ice becomes large. Consequently, we expect to see the strongest response to changes in sea ice cover at this time of year. The length of the open water season has increased in recent years (Comiso et al. 2008; Stroeve et al. 2008; Wang and Overland 2009). When the sea ice is melting in late summer reflecting the gain in oceanic sensible heat, there is not as much of a difference between the surface and atmospheric temperature: open water temperature is just a few degrees above the melting point. In autumn, air temperature rapidly decreases as the surface receives less downward shortwave radiation resulting in an increased temperature difference between open water and the atmosphere.

In this study, the atmospheric state for different near-surface air temperature regimes is evaluated by analyzing weekly running mean air temperature and geopotential height at the significant pressure levels, sea level pressure, 1000-500hPa thickness, and total surface energy fluxes (the sum of net shortwave and longwave radiative and latent and sensible heat fluxes, with positive values indicating fluxes upward from the surface to the atmosphere). Sea ice conditions are examined utilizing SIT and sea ice concentration (SIC).

4.2.2. Methods

The time period for analysis is 1979-2014 following Cassano and Cassano (2017). Satellite observations have provided a consistent continuous record of sea ice since 1979. Similarly, variables having daily temporal resolution are utilized to produce a synoptic climatology following Mills et al. (2016) and Cassano and Cassano (2017). Among the core simulations within the suite of CMIP5 long-term experiments, the historical (1979-2005) and the high emissions scenario (RCP8.5) (2006-2014) runs are chosen for a realistic climatology. As a first step, daily variables are interpolated to a common grid which is a 100 km Equal-Area Special Sensor Microwave Imager (SSM/I) grid (Brodzik et al. 2012). Next, running weekly means are created for each day by calculating the average of the previous and following 3 days of data (e.g., 4 September is the average of 1-7 September). Running weekly means have intrinsic information of the original daily data but short term variability is reduced. Anomalies are calculated for each of those averages by removing the weekly average over the entire study period for that particular day. This is done separately for each of the six models used in this study.

The self-organizing map (SOM) technique (Kohonen, 2001) is utilized to classify anomalous conditions of the near-surface temperature field and to examine changes in the atmosphere related to different surface temperature regimes. The SOM technique is an artificial neural network algorithm using unsupervised learning that can group high-frequency spatial data into a small number of common patterns in the form of a two-dimensional spatially organized array. This organized array and each representative pattern are referred to as a map and a node, respectively. The nodes are determined in an iterative process based on patterns that occurred during the training period, and thus the SOM approach may be considered a clustering technique, but involves no a priori assumptions about the distribution of the data. A detailed description of

the SOM technique as applied to climate data can be found in Hewitson and Crane (2002), Sheridan and Lee (2011), and Cassano et al. (2015).

The spatial domain used to train the SOM is the same as that used by Mills et al. (2016) and Cassano and Cassano (2017), covering grid points north of 70°N latitude excluding climatological open water in the North Atlantic and partially including the waterways in the Canadian Archipelago (Figure 4.1). Satellite observation confirms that SIE and SIT have decreased rapidly in this area as discussed in the Introduction.

Running weekly mean anomalies of the near-surface temperature from the six selected model runs and output from the Model for Interdisciplinary Research on Climate Earth System Model (MIROC-ESM) (Watanabe et al. 2011) are utilized to train the SOM. Since the MIROC-ESM SIT is underestimated compared to the PIOMAS, the output is added to widen a range of synoptic patterns for the SOM training. The formulation and simulation characteristics of CGCMs are different due to differences in the discretization of the governing equations and parameterizations of each model (Kalnay 2003). Thus, we can consider various synoptic conditions by utilizing multiple models' output to train the SOM. The training method cycles through the input data set and sorts each daily anomaly field into a 3 column by 2 row array of patterns (or nodes) following Mills et al. (2016) and Cassano and Cassano (2017). While different SOM sizes can be used, the six anomaly patterns chosen for this work provide generalized synoptic conditions that occur in autumn. Also, for a smaller SOM size, such as used here, more days can be evaluated for each individual nodes' synoptic conditions. Consequently, it is helpful to comprehend the large scale response to the forcing by choosing a smaller SOM map size. The master patterns created by the procedure described above are shown in Figure 4.2.

The running weekly mean anomalies from each individual model that were used to train the SOM are compared with the master SOM to determine the best-matching pattern among the six nodes. A list of dates associated with each SOM pattern is generated based on this pattern matching. Using this list of days, concurrent atmospheric and cryospheric states with respect to the initial near-surface temperature signal are created. Composite fields of one to 12 weeks after the initial conditions are similarly created to observe the evolution of the atmospheric state. These composites are created over the entire Northern Hemisphere to 30°N to capture signals propagating into mid-latitude regions. We focus on node (0,0) in the top left corner of Figure 4.2, which shows an anomalously warm pattern over the Arctic. Mills et al. (2016) and Cassano and Cassano (2017) found downstream responses in the mid-latitudes for similar warm Arctic patterns in their studies.

4.3. Results

In this paper, we focus on results of CCSM4, HadGEM2-CC, and IPSL-CM5A-LR. They showed different temporal and spatial downstream responses with respect to the initial concurrent composite fields. They showed characteristic atmospheric evolutions in the end. We analyze results from CCSM4 for comparison with Mills et al. (2016) who performed a similar analysis to that presented here, but with sensible heat flux as the SOM training variable. While predicted SIT by CCSM4 and HadGEM2-CC showed good agreement with observations, IPSL-CM5A-LR SIT was overestimated as indicated above. Figure 4.3 shows each model's mean autumn months' SIC and SIT over the study period. Figures 4, 5, and 6 show the initial composite fields and selected weeks after the initial period for near-surface temperature (TAS), sea ice concentration (SIC), sea ice thickness (SIT), total surface energy flux (SFCNF), 1000-500hPa thickness (TTHK), geopotential height at 500 hPa, and sea level pressure (SLP) of

CCSM4, HadGEM2-CC, and IPSL-CM5A-LR, respectively. The different variables are shown in the rows of these figures while the different time lags are shown as columns. Note that different time lags are used for each of the models to best illustrate the individual model's temporal evolution.

4.3.1. CCSM4

Looking at the initial state in CCSM4 (Figure 4.4, column 1), strong positive anomalies of TAS covered the Arctic Basin including the northern part of Eastern Siberia. From the Norwegian Sea to eastern North America, while negative anomalies were present in far eastern Asia. Low-level circulation contributed to this pattern: negative anomalies of SLP were centered near Svalbard and positive anomalies covered Eastern Siberia resulting in warm air advection (WAA) into the Arctic basin. While warm air moved toward the Kara Sea, SFCNF showed weak negative anomalies over the Arctic Ocean, which suggests that the warm TAS anomaly was driven by WAA rather than direct heating from the surface in the Arctic. TTHK showed strong positive anomalies over the Arctic Basin and positive anomalies of temperature at 500Pa (not shown) covers a similar area demonstrating the depth of the temperature signal, which was also consistent with this initial warm anomaly being driven by WAA. Negative anomalies of SIC, largest over the coastal areas of the continents of Eurasia and North America, indicated the open water area was larger than the mean state. Negative anomalies of SIT were present over most of the climatological Arctic sea ice areas with positive anomalies over the Canadian Arctic Archipelago, west side of Greenland, and west side of Novaya Zemlya. Large negative anomalies of SFCNF in the Barents and Kara Seas (BK; Figure 4.1) look counterintuitive, but increased open waters corresponding to less SIC raised air temperatures to the north, and as this warmer air moves over areas of low SIC further south the expected upward flux is reduced

giving a negative SFCNF in the anomaly plotted in Figure 4.4. This is consistent with results shown in Cassano and Cassano (2017).

Negative anomalies of SLP remained dominant over the Arctic Ocean through week 8 (Figure 4.4, row 4), but the center location was not stationary. Unlike the SLP anomalies the negative SIC anomalies in the BK were persistent through all weeks, while those in the Beaufort Sea were weakened by week 10 (Figure 4.4, row 2). As for SIT, areas of negative anomalies began to shrink at week 6, but those in the Beaufort Sea and BK were persistent (Figure 4.4, row 3). Positive anomalies of SFCNF covered the two areas with less sea ice (BK and Beaufort Sea) from week 2 to week 12 (Figure 4.4, row 4). The surface warm signal that appeared across the entire Arctic at the initial composite period was reduced by week 2, with persistent and significant positive anomalies of TAS remaining over the Beaufort Sea through week 8, and those over the BK and northern Russia remaining through week 12 (Figure 4.4, row 1). As a result of the persistent upward SFCNF forcing deep atmospheric warming in the fields of TAS and TTHK from week 4 (not shown) through week 8 resulting in 500 hPa ridging occurring above the BK (Figure 4.4, row 7) starting at week 6. This ridge began to move downstream by week 10. Positive SLP anomalies were formed in northern Russia by week 6 (Figure 4.4, row 8), which was just downstream of the 500 hPa ridge. During week 8, the center of positive SLP anomalies remained downstream of the 500 hPa ridge axis. Strong negative SLP anomalies near Iceland appeared from week 4 to week 8 and that low-level circulation induced WAA into the Eurasian side of the Arctic (Figure 4.4, rows 1 and 5). This WAA and the surface forcing both helped to build the 500 hPa ridge over the BK region. While the positive SFCNF and TAS anomalies coincided with the northern part of the 500 hPa ridge, the rest of the ridge was collocated with positive TAS anomalies and negative SFCNF anomalies consistent with forcing

from WAA. Thus, it is suspected that surface forcing played a dominant role for development of the northern part of the 500 hPa ridge. There were positive SLP anomalies in Russia at weeks 6 and 8 and TAS showed weak anomalies on the downstream side of the high SLP. This could indicate that TAS was less warm on the eastern side of the SLP ridge, consistent with CAA from the Arctic in response to the SLP ridge. From week 10, the surface and upper level features that developed through week 8 had been weakened.

In contrast to the results for the BK region, 500 hPa ridging did not occur in response to the surface warm signals over the Beaufort area. The warm signals in this region were short-lived and limited to a small area compared to those in the BK. Therefore, the corresponding upper-level signals were neither generated nor appeared.

4.3.2. HadGEM2-CC

Positive TAS anomalies initially covered the entire Arctic in HadGEM2-CC (Figure 4.5, column 1), similar to the CCSM4 initial state. Unlike CCSM4 there were no strong negative SLP anomalies located around the periphery of the Arctic in HadGEM2-CC that would suggest WAA into the Arctic. In contrast to the CCSM4 results, positive SFCNF anomalies were found across the entire Arctic Basin initially, suggesting that the anomalous warmth in this model was driven by surface processes rather than circulation.

Negative anomalies of SIC across most of the Arctic were persistent through the entire 12-week period (Figure 4.5, row 2). The negative SIC anomalies were initially largest in the Beaufort, East Siberian, Laptev, and BK Seas. The magnitude of the SIC anomaly decreased by week 10 except in the BK. Strong negative SIT anomalies initially covered the entire Arctic (Figure 4.5, row 3). While the strong negative SIT anomalies gradually weakened in the central Arctic

Ocean, the strong signal propagated to the marginal seas, the Labrador and Bering Seas and Sea of Okhotsk. The largest negative SIC anomalies, collocated with negative SIT anomalies, from week 6 through week 12, occurred in the BK and Bering Seas, with weaker negative anomalies in both fields occurring across the Arctic through week 12. Positive SFCNF anomalies covered the Arctic Basin through all weeks, with the largest positive flux anomalies seen in the BK region from week 6 through week 12.

Positive TAS anomalies were dominant over the Arctic during the entire period, and notable positive anomalies over the coastal Arctic from Europe to Alaska via Russia were especially persistent. This corresponded to the persistent negative anomalies of SIC and SIT and positive SFCNF anomalies. It appeared that the warm signal at the surface in HadGEM2-CC was very strongly driven by anomalies in the sea ice state and associated surface fluxes.

Positive anomalies of 500 hPa geopotential height were persistent over the Arctic for all weeks. The most persistent signal was located over the Greenland and Kara Seas corresponding to the edge of positive SFCNF anomalies with the most pronounced 500 hPa ridging in this region seen at week 10. Positive anomalies of SLP near the Scandinavian Peninsula, which is south of the 500 hPa ridge, were seen for all weeks, but the largest positive SLP anomaly occurred at weeks 10 and 12. Associated with this positive SLP anomaly are cold TAS and TTHK conditions extending from Russia across most of Europe in weeks 2 through 12. The coldest conditions in this region occurred during week 10, when BK 500 hPa ridging and northern Scandinavian SLP ridging was strongest. The cold conditions are consistent with easterly flow from interior of Eurasia on south side of the surface high-pressure area over central and northern Europe.

4.3.3. IPSL-CM5A-LR

In the IPSL-CM5A-LR model the initial state has a deep warm signal over the Arctic Basin extending to Russia as indicated by the anomaly fields of TAS and TTHK (Figure 6, column 1). Negative anomalies of SFCNF at week 0 were dominant over the Arctic and the SLP pattern in the vicinity of the Barents and Kara Seas showed similarities to the initial CCSM4 state: negative SLP anomalies centered near Svalbard and positive SLP anomalies centered in Russia. Thus, low-level circulation and associated WAA was likely the cause of the initial warm signal in this model. In the initial field of SIC and SIT, negative coastal anomalies were similar to the CCSM4, but positive anomalies appeared east of Greenland, consistent with this models over-estimation of SIC (and SIT) in the Greenland Sea (Figure 4.3).

Coastal negative anomalies of SIC over the Beaufort, Chukchi, East Siberian, Laptev, Kara, and Barents Seas are most evident from week 0 through week 6 and weaken beyond week 6. Only a very limited area near the Bering Strait had persistent strong negative SIC anomalies through week 12. Negative SIT anomalies form an annular shaped pattern around the Arctic, with positive SIT anomalies in the central Arctic for all weeks. This mixed pattern of positive and negative SIT anomalies looked unusual and may be related to the representation of sea ice dynamics in this model or related to this model's overly expansive sea ice coverage seen in Figure 4.3.

Only the negative SIC and SIT anomalies near the Bering Strait are associated with persistent positive TAS and SFCNF through all weeks, although these features covered a small area. While these features suggested that there was persistent surface forcing in the Bering Sea, no associated anomalies were observed at the 500 hPa geopotential height, in contrast to the results seen in

CCSM4 and HadGEM2-CC. The size of the forcing area in IPSL-CM5A-LR could be too small to excite signals in the middle and upper levels, or the area was overlapping substantially with the North Pacific storm track and the large variability associated with the storm track in this region could obscure responses to any surface forced signals.

At week 6, large positive anomalies of 500 hPa geopotential height existed in the western and eastern North Pacific and Atlantic Oceans and over the Caucasus mountains. Strong negative SFCNF anomalies coincided with 500 hPa ridges in the eastern Pacific and Atlantic Oceans and moderate negative anomalies appeared in Eastern Europe and Japan and its adjacent waters. Strong positive SLP anomalies were located downstream of the 500 hPa ridges in the eastern Pacific and Atlantic Oceans, and over Russia. Their magnitudes and spatial patterns changed every week but those anomalies at lower latitudes were persistent and the signals were mostly statistically significant. This suggests that the lower-latitude forcing of this model was stronger and possibly overwhelmed any Arctic signal.

4.4. Discussion

We investigated concurrent composites having anomalously warm surface conditions following Mills et al. (2016) and Cassano and Cassano (2017). Similar to their findings, CCSM4, HadGEM2-CC, and IPSL-CM5A-LR showed persistent negative anomalies of SIC and SIT and positive SFCNF anomalies associated with warm surface conditions. However, common temporal and spatial downstream responses were not found across these three models.

While our CCSM4 analysis indicated that 500 hPa ridging originating from sea ice, flux, and surface temperature anomalies existed over the BK, there was no apparent mid-latitude cold anomaly signal associated with the ridge. Only weak positive TAS anomalies on the downwind

side of the surface high pressure system in Asia (Figure 4.4, weeks 6 and 8) were identifiable as a mid-latitude signal to the BK forcing. This looked comparable with CAA into Eurasia found in Cassano and Cassano (2017). It is suspected that the lack of cold mid-latitude temperatures reflected the overall warming trends in this model, which therefore masked the cold signal.

On the other hand, HadGEM2-CC results showed similarity to Mills et al. (2016) and Cassano and Cassano (2017) regarding the downstream response. Positive TAS anomalies were associated with persistent negative SIC and SIT and positive SFCNF anomalies and that built a 500 hPa ridge and positive SLP anomalies on the south side of the ridge. Eventually, the SLP ridging resulted in CAA into Russia and Europe.

IPSL-CM5A-LR also showed a similar result: positive TAS anomalies were associated with persistent negative SIC and SIT and positive SFCNF anomalies in a limited area near the Bering Strait. However, these surface anomalies failed to generate an upper level response and thus no corresponding mid-latitude responses to Arctic forcing were observed in this model. Instead, lower-latitude forcing looked dominant in this model based on the large 500 hPa anomalies seen outside of the Arctic from weeks 6 through 12.

Regarding the lack of mid-latitude responses with respect to persistent positive TAS anomalies in the Arctic, a possible cause was the intensity of the surface forcing. As for IPSL-CM5A-LR, the spatial extent of the forcing area near the Bering Sea was limited even if the warm signals were obvious. Thus, it is reasonable to assume that the surface forcing may need to exceed a temporal and spatial threshold to build ridges in the upper level. Cassano and Cassano (2017) documented that when the surface forcing was not as strong nor persistent, it did not develop a

downstream response. Finding the spatial and temporal conditions that can create responses at 500 hPa from the surface warming signals is an area of future work.

Another important factor causing different downstream evolutions was internal climate variability. While storm tracks could affect the upper level anomalies with respect to local surface forcing as previously mentioned, the cyclone tracks were also possibly influenced by sea ice variability through changes in baroclinicity (Inoue et al. 2012). McCusker et al. (2016) documented that the last few decades cooling over central Europe was probably due to a sea-ice-independent internally generated circulation pattern in the vicinity of the BK. Sun et al. (2016) suggested that observed continental cooling since 1990 was not evidence for a systematic change in winter climate. Instead the cooling reflected a strong articulation of internal atmospheric variability. Further analysis with other CMIP5 output having underestimated SIT using the same framework is advisable to evaluate the response to changing surface conditions.

4.5. Summary

Rapid changes have been observed in the Arctic in recent decades and it is reasonable to assume lower latitude atmospheric conditions are affected by those changes including sea ice loss. Despite the effort of the scientific community, the linkages between Arctic sea ice reduction and mid-latitude weather remain uncertain. In this manuscript we have investigated atmospheric responses to changes in surface state in the Arctic following the framework of Mills et al. (2016) and Cassano and Cassano (2017). Six models having well-simulated and overestimate SIT were selected from CMIP5 and their TAS representing surface forcing were utilized to classify initial states. For autumn months (September – November) from 1979 to 2014, running weekly mean TAS were computed first and the anomalies were created by using the running weekly mean and

the weekly average over the entire period for the particular day. The SOM technique allowed us to create multiple anomaly patterns (nodes), which is referred to as the master SOM from all the selected models. From the six nodes of the master SOM, the one with the largest anomalously warm surface conditions was chosen for further analysis. Each model's TAS anomalies were compared to this node and days showing similar patterns to this warm surface condition were composited. Based on these lists, each model's concurrent composite state at this initial condition and the following 12 weeks were created with variables, TAS, SIC, SIT, SFCNF, TTHK, geopotential height, and SLP.

CCSM4, HadGEM2-CC, and IPSL-CM5A-LR showed different downstream responses while they shared similar TAS anomaly patterns in the beginning. Generally, persistent warm surface signals were induced by persistent negative SIC and SIT anomalies in addition to positive SFCNF anomalies in certain areas. Subsequently, ridging at 500 hPa occurred and positive SLP anomalies were generated downstream of the ridge in two of the three models analyzed in detail here. The positive SLP anomalies occurred in central Russia for CCSM4 at weeks 6 and 8 and in western Russia for HadGEM2-CC at weeks 10 and 12. Accordingly, the corresponding colder TAS was observed in north Asia and over central and northern Europe for CCSM4 and HadGEM2-CC, respectively. Mills et al. (2016) and Cassano and Cassano (2017) found CAA induced by the same mechanism into eastern North America and into central and northern Asia, respectively. On the other hand, ridging at 500 hPa responding to persistent warm surface signals and the positive SLP anomalies and CAA, which were expected to be generated in the area, were not observed for IPSL-CM5A-LR. Instead it appears that lower-latitude forcing was stronger in this model. Similar to Cassano and Cassano (2017), we found that the surface forcing needed to

exceed a temporal and spatial threshold to build ridges in the upper level, which can eventually induce mid-latitude CAA.

Acknowledgements

This study was supported by National Science Foundation grant PLR-1304807 and NASA grant NNX14AH89G.

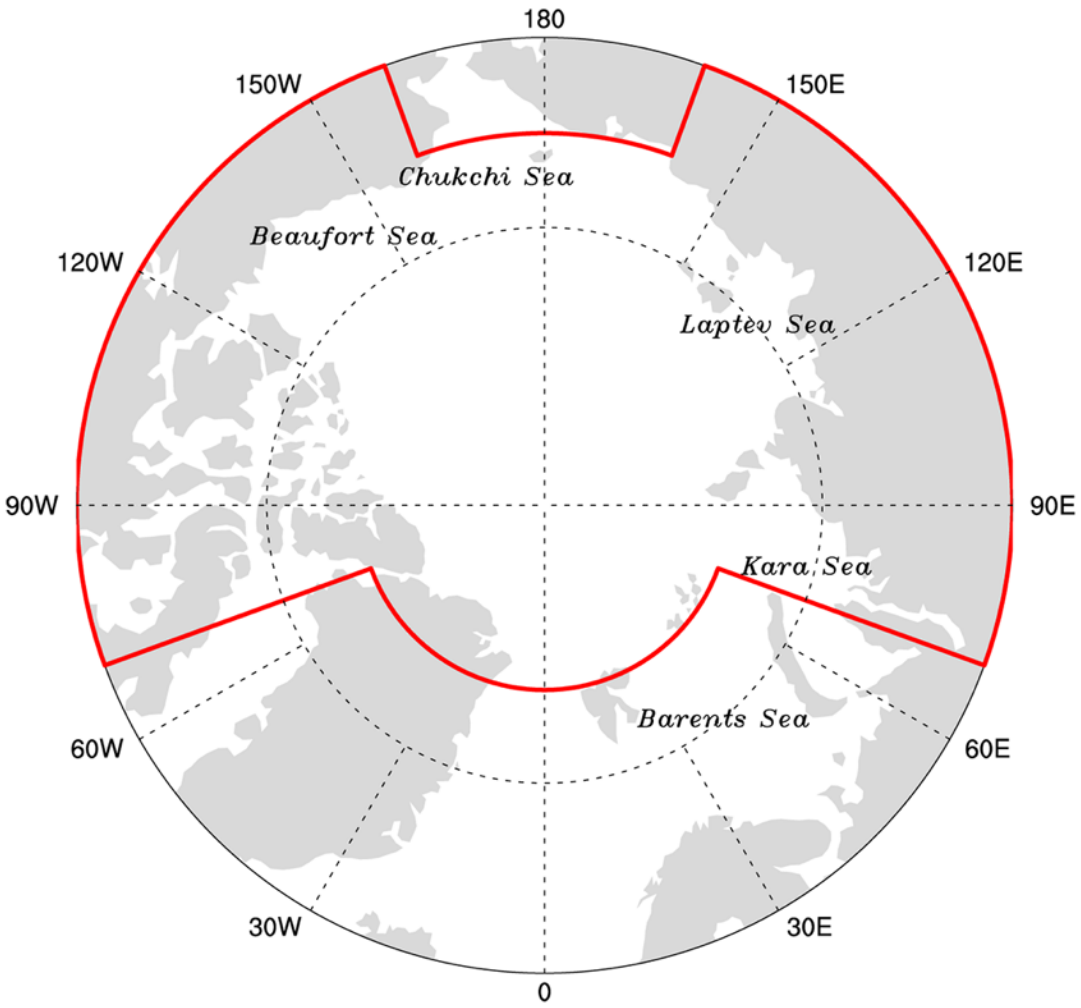

Figure 4.1. Arctic map showing locations of marginal seas. North of the red outline shows the ocean area of near-surface air temperature data that are used to train the SOM [from Cassano and Cassano (2017)].

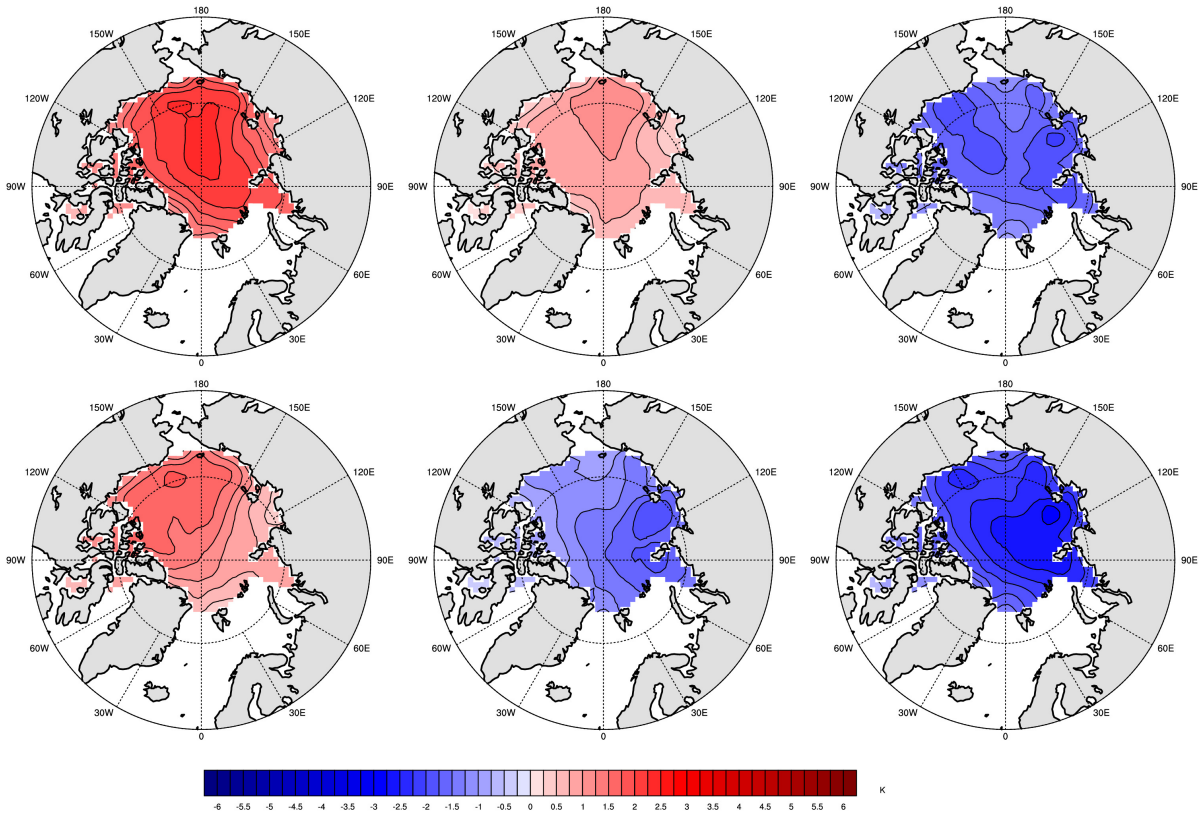

Figure 4.2. Master SOM of near-surface temperature anomaly from six model runs.

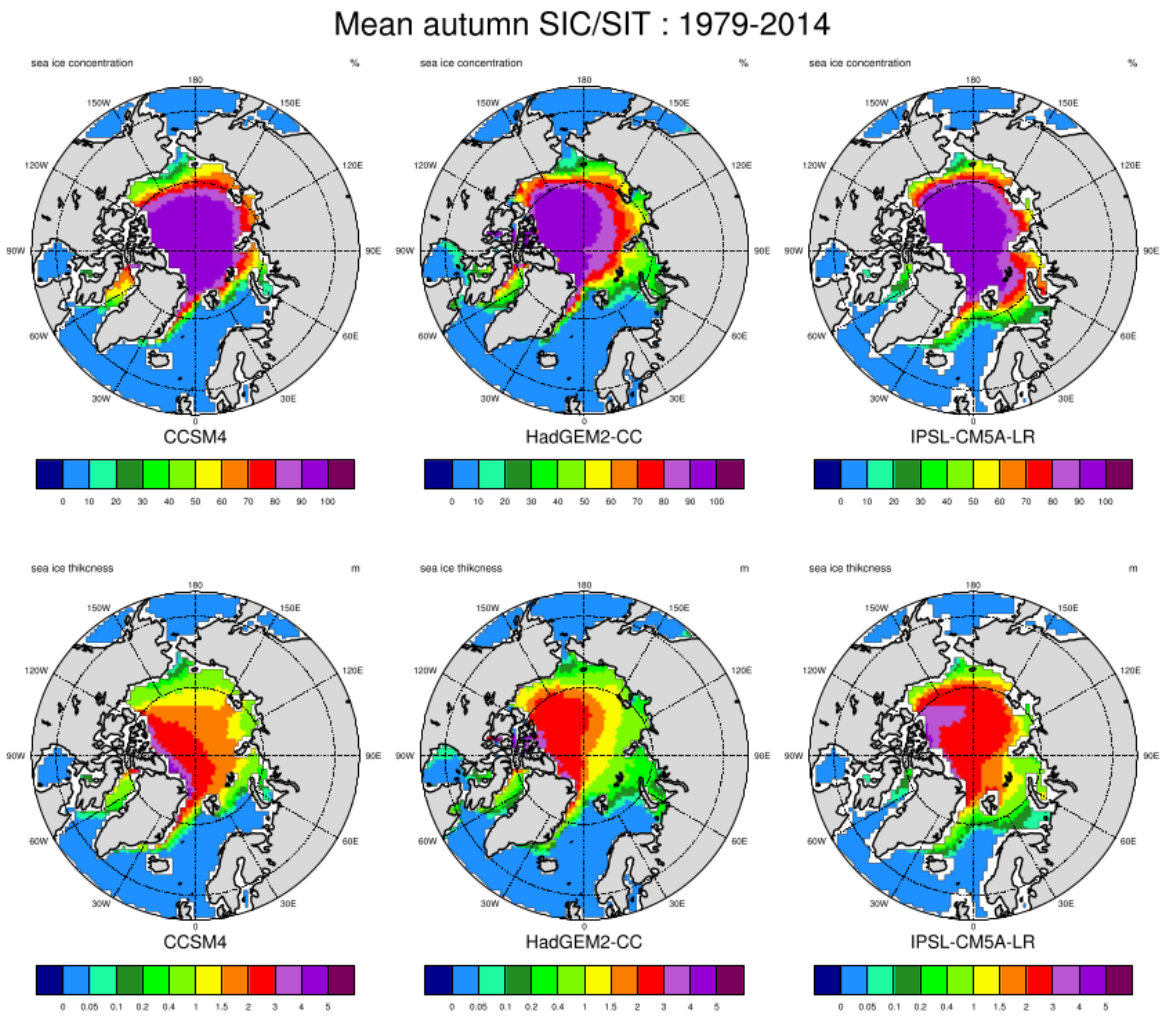

Figure 4.3. Mean sea ice concentration (above) and sea ice thickness (bottom) over autumn months (September – November) from 1979 to 2014 for CCSM4, HadGEM2-CC, and IPSL-CM5A-LR.

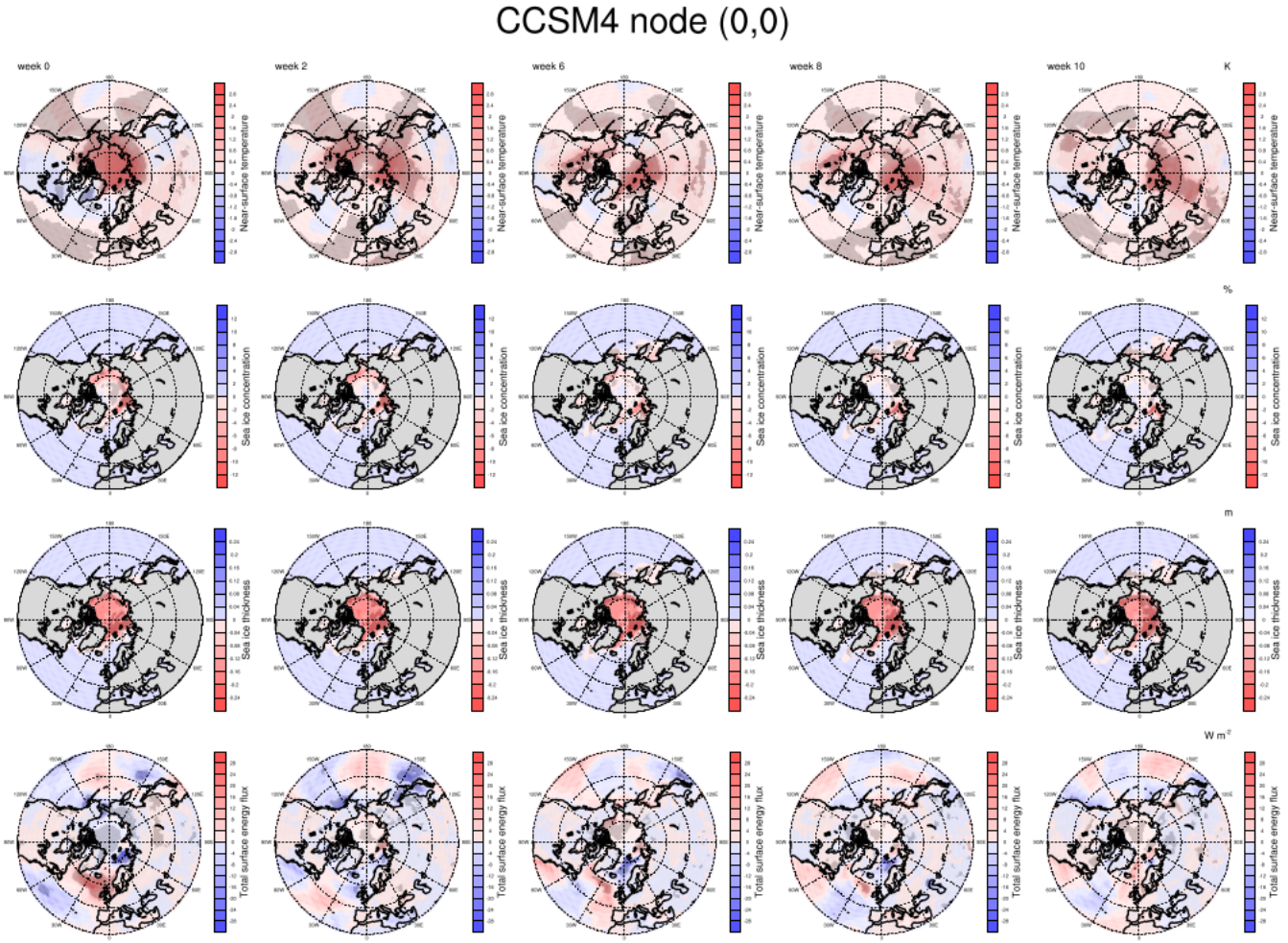

Figure 4.4. Composite atmospheric fields of CCSM4 created by compositing anomaly fields for the days clustered on the top-left SOM pattern shown in Figure 4.2: rows from top to bottom show near-surface temperature, sea ice concentration, sea ice thickness, total surface energy flux, near-surface temperature, 1000 to 500 hPa thickness, geopotential height at 500 hPa, and sea level pressure, respectively. Columns, from left to right show composites at weeks 0, 2, 6, 8, and 10 respectively.

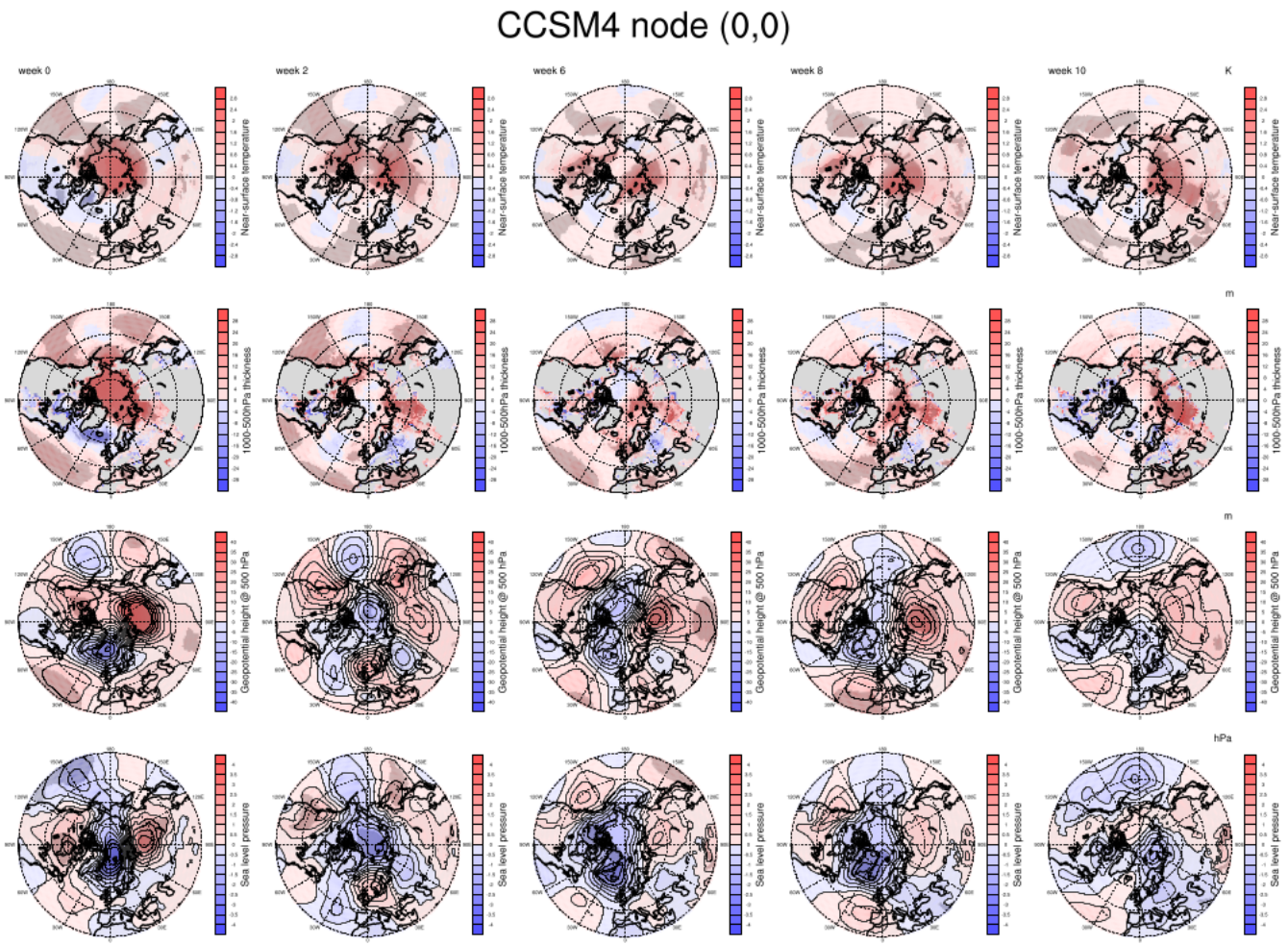

Figure 4.4. (Continued)

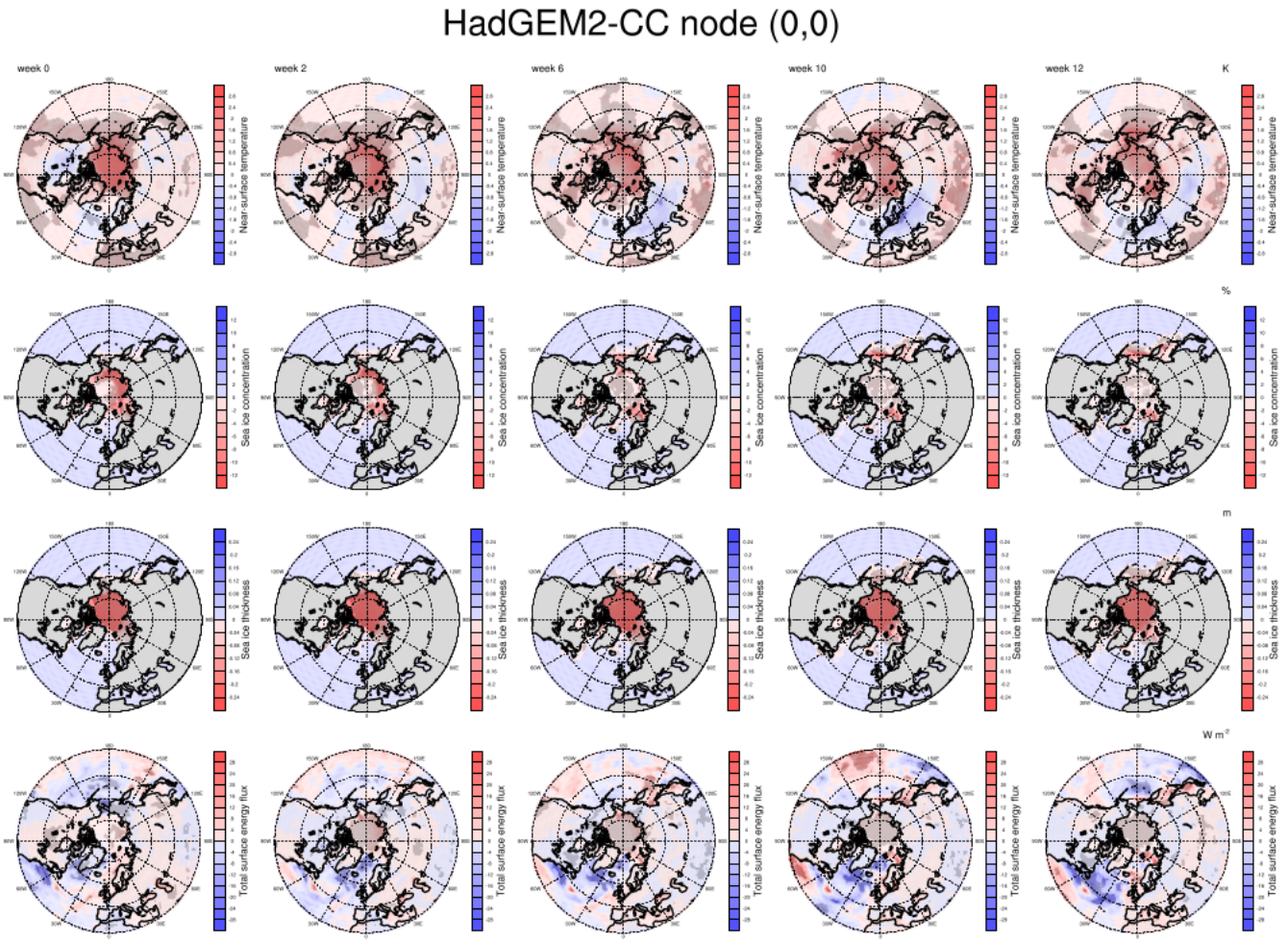

Figure 4.5. As in Figure 4.4 but for HadGEM2-CC with columns, from left to right showing composites at weeks 0, 2, 6, 10, and 12respectively.

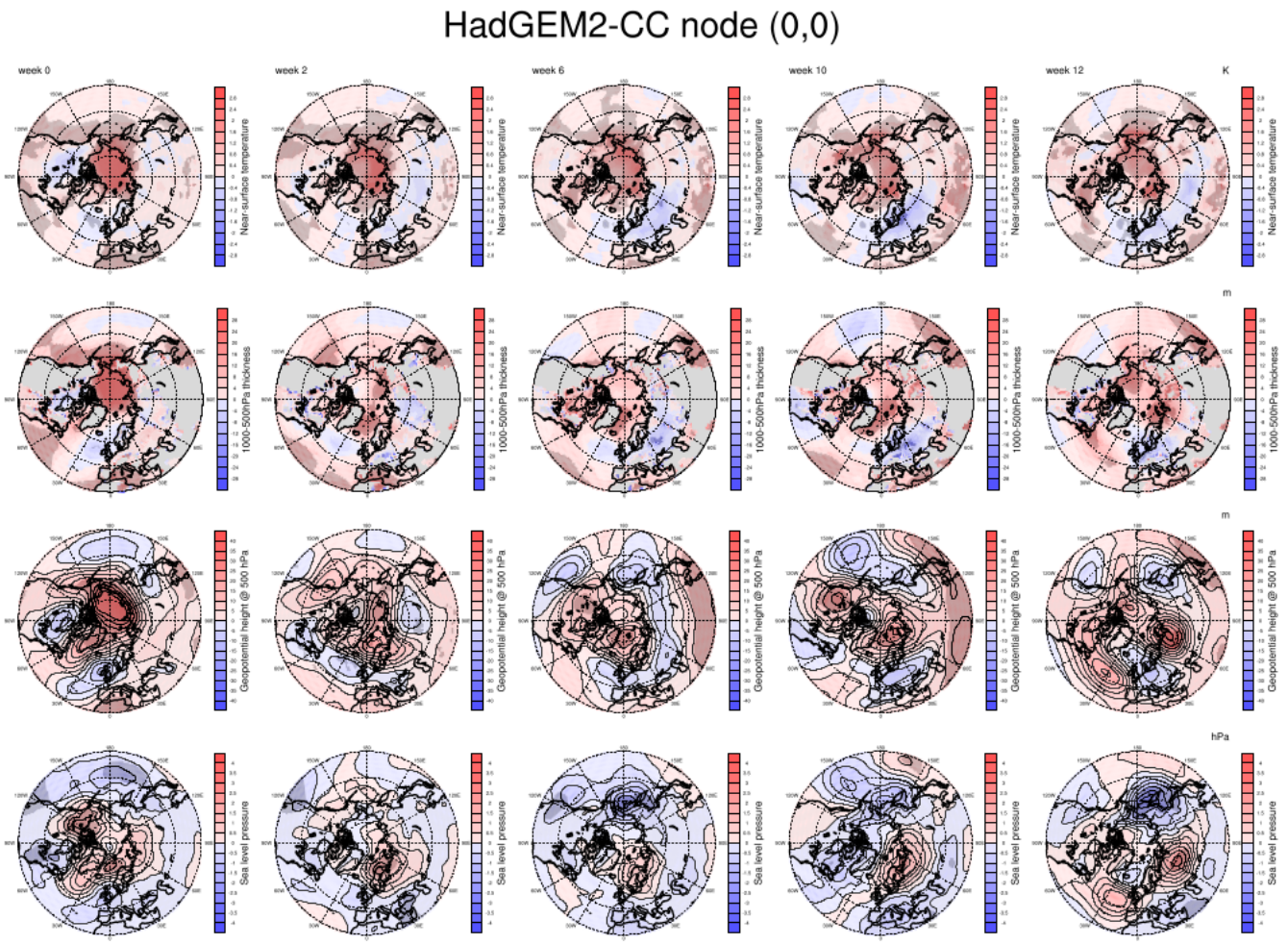

Figure 4.5. (Continued)

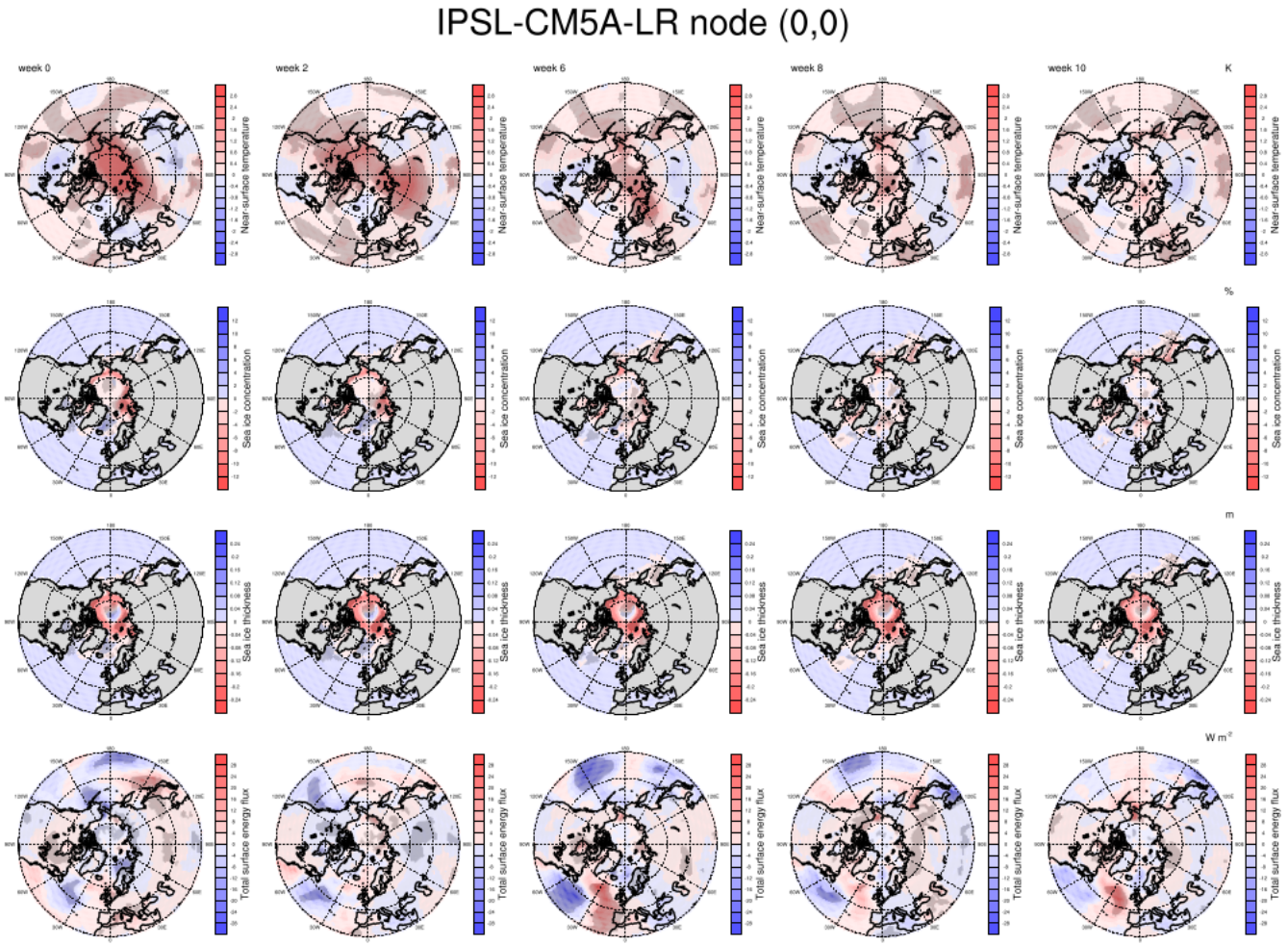

Figure 4.6. As in Figure 4.4 but for IPSL-CM5A-LR.

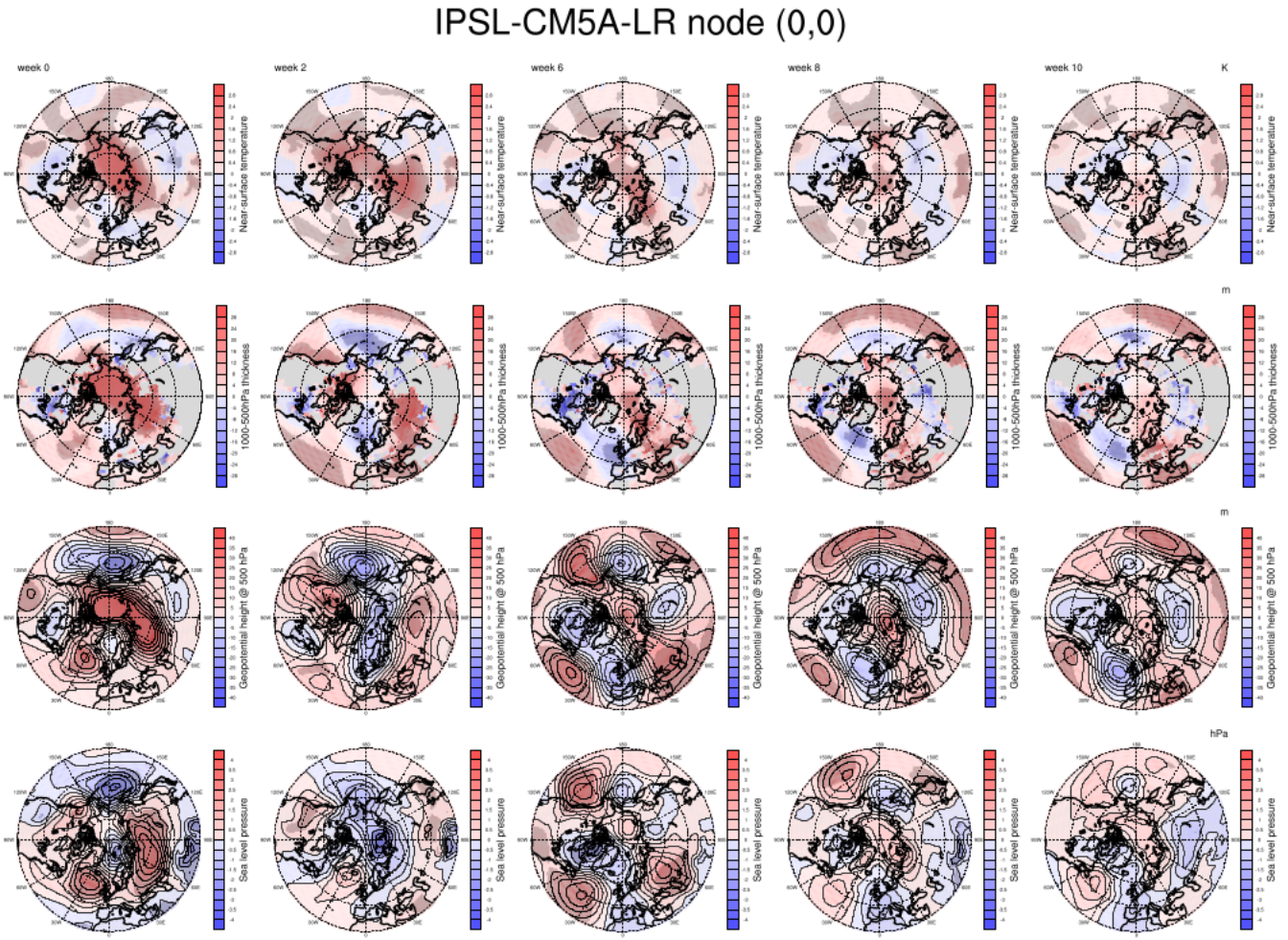

Figure 4.6. (Continued)

CHAPTER 5

SUMMARY

Motivation for the series of investigations presented in this dissertation comes from observations of a rapidly warming lower atmosphere in the Arctic in the post-satellite era. The mass loss from the Greenland ice sheet (GrIS) and the decline in sea ice extent (SIE) are obvious and their significant negative effects on sea ice-dependent species such as polar bears have drawn the attention of the general public. Possible linkages between Arctic sea ice loss and corresponding changes in the mid-latitudes have been investigated by many researchers but still remain uncertain since the atmosphere is very complex and internal climate variability may obscure the influence of the Arctic climate change. The fundamental motivation for the research presented in this dissertation is to provide information to address the overarching research question: how do weather patterns in the Northern Hemisphere respond to the observed rapid changes in the Arctic, especially sea ice loss?

First, precipitation data from a newly developed reanalysis dataset was analyzed over Greenland. Specifically, Arctic System Reanalysis version 1 (ASRv1) forecasts of monthly precipitation over Greenland were compared with gauge-based precipitation measured by the Danish Meteorological Institute (DMI) and precipitation retrieved from the Precipitation Occurrence Sensor System (POSS) at

Summit. The ASRv1 precipitation generally agrees with the corrected DMI gauge-based precipitation measured at coastal or near-coastal stations in Greenland. In contrast, ASRv1 precipitation at Summit, i.e., located in a higher continental environment, is overestimated compared with the POSS observations. Utilizing a boxplot approach, similar seasonal variability in ASRv1 precipitation is found among stations that are geographically close. The interquartile ranges (IQRs) of DMI precipitation show similar variations to those of ASRv1, but the variability of the median values is not always comparable. The North Atlantic Oscillation (NAO) index and ASRv1 precipitation are moderately correlated over northern Greenland, the North Atlantic, and the Greenland Sea regions (0.32-0.49). It is suspected that local wind events have a larger influence on precipitation where smaller correlations occur. Suggested future work to understand discrepancies between ASRv1 and DMI precipitation fields in Greenland coastal regions is to include case studies of local wind events and corresponding precipitation variations utilizing in-situ measurements during both strong positive and negative NAO phases. At high-altitude and inland areas, further observations are needed to confirm the ASRv1 overestimation. The results will be useful for future hydrological cycle research regarding changes in the GrIS and SIE.

The ASRv1 precipitation study confirms that it is still challenging to obtain reliable Arctic precipitation data for climate study. The harsh environment had been preventing to build and maintain monitoring stations with high spatial resolution. It is suspected that the lack of reliable and accurate observations in the

interior of Greenland is closely related to overestimated ASRv1 precipitation at Summit. While the upgraded regional-15 km Arctic System Reanalysis version 2 (ASRv2) provides improved summertime precipitation (Bromwich et al. 2017), their evaluation followed the framework used by Bromwich et al. (2016): the comparison was performed for a year and was not performed at a high-elevation and inland Greenland location such as Summit. As a next research step, comparison of ASRv2 precipitation with the DMI and POSS precipitation is recommended. These results would improve confidence in ASRv2 precipitation data for future Arctic climate study.

Secondly, changes in cyclone activity in the Arctic with respect to sea ice loss was studied. Extensive summer sea ice loss has occurred within the Beaufort, Chukchi, East Siberian, and Laptev Seas over the last decade. Associated anomalies in sensible and latent heat fluxes in autumn have increased Arctic atmospheric precipitable water and air temperatures, with the potential to impact autumn and winter cyclone activity. To examine if a connection exists between recent Arctic sea ice loss and cyclone activity, several cyclone metrics from 60 to 90°N are analyzed. Results show that following years with less September sea ice, there is a subsequent increase in moisture availability, regional baroclinicity and changes in vertical stability that favor cyclogenesis. However, tracking of individual cyclones indicates no coherent increase in cyclone frequency or intensity associated with sea ice loss. Furthermore, no robust northward progression of extreme cyclones is observed. An unexpected finding from this work was that no robust changes in cyclone activity

were observed despite the changes in moisture availability, regional baroclinicity, and vertical stability. This suggest that other factors are also responsible for controlling changes in Arctic cyclone activity, and further research on this topic is needed.

The results presented in chapter 3 differed from the expectation that robust signals showing changes in Arctic cyclone activity with respect to sea ice loss would appear. Substantial sea ice reduction has been observed and the effects on the atmospheric state have been already confirmed (e.g., Serreze et al. 2009, 2012; Ghatak et al. 2010, 2012; Screen and Simmonds 2010a, 2010b; Inoue and Hori 2011; Cohen et al. 2012; Liu et al. 2012; Orsolini et al. 2012; Stroeve et al. 2012; Serreze and Stroeve 2015; Simmonds 2015). However, multiple cyclone metrics, based on atmospheric reanalyses, do not show obvious correspondences to recent Arctic sea ice loss. Based on these results it is concluded that the complexity of the atmosphere, large internal variability in the Arctic, and the difficulty of defining robust cyclone metrics all played a role in the ambiguous and weak responses. I also learned that a preconceived idea, which appeared to be sensible, could occasionally lead to an unexpected detour when conducting research. Those research experiences taught me that a scientist needs to be always humble in the pursuit of truth. I found an inspirational quote by a famous scientist, Carl Sagan, and will try to keep that in my mind:

"Who is more humble? The scientist who looks at the universe with an open mind and accepts whatever the universe has to teach us, or somebody who says everything in this book must be considered the literal truth and never mind the fallibility of all the human beings involved?" (Sagan 2006)

Lastly, possible atmospheric responses to Arctic change were considered in a larger spatial context. Chapter 4 describes atmospheric responses in mid-latitudes to changes in surface state in the Arctic. The self-organizing map technique was utilized to characterize anomalously warm surface air temperature patterns in the Arctic. Seven models having well-simulated or overestimated sea ice thickness were selected from the CMIP5 archive. Their near-surface air temperature, used to represent surface forcing due to changes in sea ice concentration and thickness and surface energy fluxes, were utilized to classify initial states and the atmospheric evolution for the following twelve weeks. In general, persistent warm surface signals, originating from low sea ice conditions, generated a ridge at 500 hPa and a surface high-pressure system downstream of the ridge. These positive sea level pressure (SLP) anomalies induced cold-air advection into the mid-latitudes in some models. However, details of the temporal and spatial downstream responses were not fully consistent among CCSM4, HadGEM2-CC, and IPSL-CM5A-LR. The positive SLP anomalies occurred in central Russia for CCSM4 at weeks 6 and 8 and in western Russia for HadGEM2-CC at weeks 10 and 12. Corresponding colder surface conditions were found in north Asia and over central and northern Europe for CCSM4 and HadGEM2-CC, respectively. On the other hand, the positive SLP

anomalies and cold-air advection were not observed for IPSL-CM5A-LR. Based on these results it appears that Arctic surface anomalies need to have a sufficiently long persistence over a moderately large area to induce mid-latitude cold-air advection. These results support similar previous studies (e.g., Mills et al. (2016) and Cassano and Cassano (2017)) and the validity of the methodology was confirmed.

The results presented in this paper help explain the contradictory results presented in previous studies (Overland et al. 2011; Francis and Vavrus 2012, 2015; Liu et al. 2012; Outten and Esau 2012; Screen and Simmonds 2014; Barnes and Screen 2015). As shown in this paper, whether mid-latitude weather is impacted by changes in Arctic sea ice depends on the size and location of the area of sea ice loss, the persistence of the Arctic surface forcing, and the strength of lower latitude variability. These aspects of the climate system are represented with varying degrees of realism in different models, and even in reanalyses. The result is that different models and reanalysis products show different intensities of mid-latitude forcing from Arctic sea ice loss leading to the contradictory conclusions seen in the literature. This suggests that greater scrutiny be placed on the assessing models' ability to accurately represent changes in sea ice and the associated changes in surface fluxes. One possible avenue for future research would be to analyze the downstream response from different surface initial conditions, such as anomalous cold near-surface temperature anomalies. It is unclear whether an opposite response would be generated with cold Arctic anomalies.

References

References for Chapter 1

ACIA, 2005: *Impacts of a warming Arctic: Arctic Climate Impact Assessment 2005.* Cambridge University Press, 1042 pp.

Alekseev, G. V., O. M. Johannessen, A. A. Korablev, V. V. Ivanov, and D. V. Kovalevsky, 2001: Interannual variability in water masses in the Greenland Sea and adjacent areas. *Polar Res.*, 20(2), 201–208, doi:10.1111/j.1751-8369.2001.tb00057.x.

Anderson, L. G., and S. Kaltin, 2001: Carbon fluxes in the Arctic Ocean-potential impact by climate change. *Polar Res.*, 20(2), 225–232, doi:10.1111/j.1751-8369.2001.tb00060.x.

Beaugrand, G., 2002: Reorganization of North Atlantic Marine Copepod Biodiversity and Climate. *Science*, 296(5573), 1692–1694, doi:10.1126/science.1071329

Broecker, W. S., 1975: Climatic Change: Are We on the Brink of a Pronounced Global Warming? *Science*, 189(4201), 460–463.

Bromwich, D., Y.-H. Kuo, M. Serreze, J. Walsh, L.-S. Bai, M. Barlage, K. Hines, and A. Slater, 2010: Arctic System Reanalysis: Call for Community Involvement. *Eos, Trans. Amer. Geophys. Union*, 91(2), 13, doi:10.1029/2010EO020001.

Bromwich, D. H., A. B. Wilson, L.-S. Bai, G. W. K. Moore, and P. Bauer, 2016: A comparison of the regional Arctic System Reanalysis and the global ERA-Interim Reanalysis for the Arctic. *Quart. J. Roy. Meteor. Soc.*, 142(695), 644-658, doi:10.1002/qj.2527.

Francis, J. A., W. Chan, D. J. Leathers, J. R. Miller, and D. E. Veron, 2009: Winter Northern Hemisphere weather patterns remember summer Arctic sea-ice extent. *Geophys. Res. Lett.*, 36(7), L07503, doi:10.1029/2009GL037274.

Francis, J. A., and S. J. Vavrus, 2012: Evidence linking Arctic amplification to extreme weather in mid-latitudes. *Geophys. Res. Lett.*, 39(6), L06801, doi:10.1029/2012GL051000.

Forsberg, R., L. Sørensen, and S. Simonsen, 2017: Greenland and Antarctica Ice Sheet Mass Changes and Effects on Global Sea Level. *Surv. Geophys.*, 38(1), 89–104.

Hunter, C. M., H. Caswell, M. C. Runge, E. V. Regehr, S. C. Amstrup, and I. Stirling, 2010: Climate change threatens polar bear populations: a stochastic demographic analysis. *Ecology*. 91(10), 2883–2897, doi:10.1890/09-1641.1.

Inoue, J., and M. E. Hori, 2011: Arctic cyclogenesis at the marginal ice zone: A contributory mechanism for the temperature amplification? *Geophys. Res. Lett.*, 38(12), L12502, doi:10.1029/2011GL047696.

IPCC, 2013: Summary for Policymakers. In: *Climate Change 2013: The Physical Science Basis. Contribution of Working Group I to the Fifth Assessment Report of the Intergovernmental Panel on Climate Change*, Stocker, T.F., D. Qin, G.-K. Plattner, M. Tignor, S.K. Allen, J. Boschung, A. Nauels, Y. Xia, V. Bex and P.M. Midgley, Ed., Cambridge University Press. 1-30.

Johannessen, O. M., Bengtsson, L., Miles, M. W., Kuzmina, S. I., Semenov, V. A., Alekseev, G. V., Nagurnyi, A. P., Zakharov, V.F., Bobylev, L.P., Pettersson, L.H., Hasselmann, K., Cattle, H. P., 2004: Arctic climate change: observed and modelled temperature and sea-ice variability. *Tellus A*, 56(4), 328–341, doi:10.1111/j.1600-0870.2004.00060.x

Kim, B.-M., S.-W. Son, S.-K. Min, J.-H. Jeong, S.-J. Kim, X. Zhang, T. Shim, and J.-H. Yoon, 2014: Weakening of the stratospheric polar vortex by Arctic sea-ice loss. *Nat. Commun.*, 5, 4646.

Koyama, T., J. Stroeve, J. Cassano, and A. Crawford, 2017: Sea ice loss and Arctic cyclone activity from 1979 to 2014. *J. Climate*, 30(12), JCLI-D-16-0542.1, doi:10.1175/JCLI-D-16-0542.1.

Overland, J. E., and M. Wang, 2010: Large-scale atmospheric circulation changes are associated with the recent loss of Arctic sea ice. *Tellus, Ser. A Dyn. Meteor. Oceanogr.*, 62(1), 1–9.

Rahmstorf, S., 1999: Shifting seas in the greenhouse? *Nature*, 399(6736), 523–524, doi:10.1038/21066.

Screen, J. A., and I. Simmonds, 2010: The central role of diminishing sea ice in recent Arctic temperature amplification. *Nature*, 464(7293), 1334–1337, doi:10.1038/nature09051.

Screen, J. A., C. Deser, I. Simmonds, and R. Tomas, 2014: Atmospheric impacts of Arctic sea-ice loss, 1979–2009: separating forced change from atmospheric internal variability. *Climate Dyn.*, 43(1–2), 333–344.

Serreze, M. C., A. P. Barrett, J. C. Stroeve, D. N. Kindig, and M. M. Holland, 2009: The emergence of surface-based Arctic amplification. *Cryosph.*, 3(1), 11–19.

Serreze, M. C., A. P. Barrett, and J. J. Cassano, 2011: Circulation and surface controls on the lower tropospheric air temperature field of the Arctic. *J. Geophys. Res.*, 116(D7).

Serreze, M. C., A. P. Barrett, A. G. Slater, R. A. Woodgate, K. Aagaard, R. B. Lammers, M. Steele, R. Moritz, M. Meredith, and C. M. Lee, 2006: The large-scale freshwater cycle of the Arctic. *J. Geophys. Res.*, 111(C11), C11010, doi:10.1029/2005JC003424.

Serreze, M. C., and R. G. Barry, 2011: Processes and impacts of Arctic amplification: A research synthesis. *Glob. Planet. Change*, 77(1–2), 85–96.

Serreze, M. C., M. Holland, and J. C. Stroeve, 2007: Perspectives on the Arctic's shrinking sea-ice cover. *Science*, 315, 1533–1536.

Serreze, M. C., and J. Stroeve, 2015: Arctic sea ice trends, variability and implications for seasonal ice forecasting. *Philos. Trans. Roy. Soc. A Math. Phys. Eng. Sci.*, 373(2045).

Shepherd, A. et al., 2012: A Reconciled Estimate of Ice-Sheet Mass Balance. *Science*, 338(6111), 1183–1189.

Simmonds, I., 2015: Comparing and contrasting the behaviour of Arctic and Antarctic sea ice over the 35 year period 1979–2013. *Ann. Glaciol.*, 56(69), 18–28.

Simmonds, I., and K. Keay, 2009: Extraordinary September Arctic sea ice reductions and their relationships with storm behavior over 1979–2008. *Geophys. Res. Lett.*, 36(19), L19715, doi:10.1029/2009GL039810.

Stroeve, J. C., M. C. Serreze, A. Barrett, and D. N. Kindig, 2011: Attribution of recent changes in autumn cyclone associated precipitation in the Arctic. *Tellus A*, 63(4), 653–663.

Stroeve, J. C., M. C. Serreze, M. M. Holland, J. E. Kay, J. Malanik, and A. P. Barrett, 2012: The Arctic's rapidly shrinking sea ice cover: A research synthesis. *Climate Change*, 110(3–4), 1005–1027.

Trenberth, K., 2011: Changes in precipitation with climate change. *Climate Res.*, 47(1), 123–138, doi:10.3354/cr00953.

Ulbrich, U., G. C. Leckebusch, and J. G. Pinto, 2009: Extra-tropical cyclones in the present and future climate: a review. *Theor. Appl. Climatol.*, 96(1–2), 117–131, doi:10.1007/s00704-008-0083-8.

Wallace, J. M., and P. V Hobbs, 2006: *Atmospheric science: an introductory survey*, Academic press, 467pp.

Watts, N. et al., 2015: Health and climate change: policy responses to protect public

health. *Lancet*, 386(10006), 1861–1914, doi:10.1016/S0140-6736(15)60854-6.

References for Chapter 2

Abe, M., Nozawa, T., Ogura, T., & Takata, K., 2016: Effect of retreating sea ice on arctic cloud cover in simulated recent global warming. *Atmos. Chem. Phys.*, 16, 14343-14356. doi:10.5194/acp-16-14343-2016

Aðalgeirsdóttir, G., M. Stendel, J. H. Christensen, J. Cappelen, F. Vejen, H. A. Kjær, R. Mottram, and P. Lucas-Picher, 2009: Assessment of the temperature, precipitation and snow in the RCM HIRHAM4 at 25 km resolution. Danish Climate Centre Report 09-08, 80pp.

Akperov, M., I. Mokhov, A. Rinke, K. Dethloff, and H. Matthes, 2014: Cyclones and their possible changes in the Arctic by the end of the twenty first century from regional climate model simulations. *Theor. Appl. Climatol.*, 122, 85–96, doi:10.1007/s00704-014-1272-2.

Albert, M., and R. Hawley, 2000: Seasonal differences in surface energy exchange and accumulation at Summit, Greenland. *Ann. Glaciol.*, 31, 387–390, doi:10.3189/172756400781820129.

Appenzeller, C., J. Schwander, S. Sommer, and T. F. Stocker, 1998: The North Atlantic Oscillation and its imprint on precipitation and ice accumulation in Greenland. *Geophys. Res. Lett.*, 25(11), 1939–1942, doi:10.1029/98GL01227.

Bales, R. C., J. R. McConnell, E. Mosley-Thompson, and B. Csatho, 2001: Accumulation over the Greenland ice sheet from historical and recent records. *J. Geophys. Res. Atmos.*, 106, 33813–33825, doi:10.1029/2001JD900153.

Bengtsson, L., K. I. Hodges, and E. Roeckner, 2006: Storm tracks and climate change. *J. Climate*, 19, 3518–3543, doi:10.1175/JCLI3815.1.

Bengtsson, L., K. I. Hodges, and N. Keenlyside, 2009: Will Extratropical Storms Intensify in a Warmer Climate? *J. Climate*, 22, 2276–2301, doi:10.1175/2008JCLI2678.1.

Berkelhammer, M., D. C. Noone, H. C. Steen-Larsen, A. Bailey, C. J. Cox, M. S. ONeill, D. Schneider, K. Steffen, and J. W. C. White, 2016: Surface-atmosphere decoupling limits accumulation at Summit, Greenland. *Sci. Adv.*, 2, e1501704–e1501704, doi:10.1126/sciadv.1501704.

Bintanja, R., and F. M. Selten, 2014: Future increases in Arctic precipitation linked to local evaporation and sea-ice retreat. *Nature*, 509, 479–482, doi:10.1038/nature13259.

Bougamont, M., J. L. Bamber, and W. Greuell, 2005: A surface mass balance model for the Greenland Ice Sheet. *J. Geophys. Res. Earth Surf.*, 110, doi:10.1029/2005JF000348.

Bromwich, D. H., Q. Chen, Y. Li, and R. I. Cullather, 1999: Precipitation over Greenland and its relation to the North Atlantic Oscillation. *J. Geophys. Res.*, 104, 103–115, doi:10.1029/1999JD900373.

Bromwich, D., Y.-H. Kuo, M. Serreze, J. Walsh, L.-S. Bai, M. Barlage, K. Hines, and A. Slater, 2010: Arctic System Reanalysis: Call for Community Involvement. *Eos, Trans. Amer. Geophys. Union*, 91, 13, doi:10.1029/2010EO020001.

Bromwich, D. H., A. B. Wilson, L.-S. Bai, G. W. K. Moore, and P. Bauer, 2016: A comparison of the regional Arctic System Reanalysis and the global ERA-Interim Reanalysis for the Arctic. *QUART. J. Roy. Meteor. Soc.*, 142, 644–658, doi:10.1002/qj.2527.

Calder, C. A., P. F. Craigmile, and E. Mosley-Thompson, 2008: Spatial variation in the influence of the North Atlantic Oscillation on precipitation across Greenland. *J. Geophys. Res.*, 113, D06112, doi:10.1029/2007JD009227.

Cappelen, J., 2014: Weather observations from Greenland 1958-2013 - Observation data with description. Technical Report 14-08, 24 pp.

Castellani, B. B., M. D. Shupe, D. R. Hudak, and B. E. Sheppard, 2015: The annual cycle of snowfall at Summit, Greenland. *J. Geophys. Res. Atmos.*, 120, 6654–6668, doi:10.1002/2015JD023072.

Cavalieri, D. J., C. L. Parkinson, P. Gloersen, J. C. Comiso, and H. J. Zwally, 1999: Deriving long-term time series of sea ice cover from satellite passive-microwave multisensor data sets. *J. Geophys. Res.*, 104, 15803, doi:10.1029/1999JC900081.

Chen, Q., D. H. Bromwich, and L. Bai, 1997: Precipitation over Greenland Retrieved by a Dynamic Method and Its Relation to Cyclonic Activity. *J. Climate*, 10, 839–870, doi:10.1175/1520-0442(1997)010<0839:POGRBA>2.0.CO;2.

Cohen, J. L., J. C. Furtado, M. A. Barlow, V. A. Alexeev, and J. E. Cherry, 2012: Arctic warming, increasing snow cover and widespread boreal winter cooling. *Environ. Res. Lett.*, 7, 14007, doi:10.1088/1748-9326/7/1/014007.

Enderlin, E. M., I. M. Howat, S. Jeong, M.-J. Noh, J. H. van Angelen, and M. R. van den Broeke, 2014: An improved mass budget for the Greenland ice sheet. *Geophys. Res. Lett.*, 41, 866–872, doi:10.1002/2013GL059010.

Ettema, J., M. R. van den Broeke, E. van Meijgaard, W. J. van de Berg, J. L. Bamber, J. E. Box, and R. C. Bales, 2009: Higher surface mass balance of the Greenland ice sheet revealed by high-resolution climate modeling. *Geophys. Res. Lett.*, 36, L12501, doi:10.1029/2009GL038110.

Fitzgerald, P. W., J. L. Bamber, J. K. Ridley, and J. C. Rougier, 2012: Exploration of parametric uncertainty in a surface mass balance model applied to the Greenland ice sheet. *J. Geophys. Res.*, 117, F01021, doi:10.1029/2011JF002067.

Fonseca, R. M., T. Zhang, and K.-T. Yong, 2015: Improved simulation of precipitation in the tropics using a modified BMJ scheme in the WRF model. *Geosci. Model Dev.*, 8, 2915–2928, doi:10.5194/gmd-8-2915-2015.

Forsberg, R., L. Sørensen, and S. Simonsen, 2017: Greenland and Antarctica Ice Sheet Mass Changes and Effects on Global Sea Level. *Surv. Geophys.*, 38, 89–104, doi:10.1007/s10712-016-9398-7.

Francis, J. A., W. Chan, D. J. Leathers, J. R. Miller, and D. E. Veron, 2009: Winter Northern Hemisphere weather patterns remember summer Arctic sea-ice extent. *Geophys. Res. Lett.*, 36, L07503, doi:10.1029/2009GL037274.

Ghatak, D., C. Deser, A. Frei, G. Gong, A. Phillips, D. A. Robinson, and J. Stroeve, 2012: Simulated Siberian snow cover response to observed Arctic sea ice loss, 1979-2008. *J. Geophys. Res.*, 117, D23108, doi:10.1029/2012JD018047.

Hurrell, J. W., 1995: Decadal Trends in the North Atlantic Oscillation: Regional Temperatures and Precipitation. *Science*, 269, 676–9, doi:10.1126/science.269.5224.676.

Inoue, J., M. E. Hori, and K. Takaya, 2012: The Role of Barents Sea Ice in the Wintertime Cyclone Track and Emergence of a Warm-Arctic Cold-Siberian Anomaly. *J. Climate*, 25, 2561–2568, doi:10.1175/JCLI-D-11-00449.1.

Jahn, A., J. E. Kay, M. M. Holland, and D. M. Hall, 2016: How predictable is the timing of a summer ice-free Arctic? *Geophys. Res. Lett.*, 43, 9113–9120, doi:10.1002/2016GL070067.

Jones, P. D., T. Jonsson, and D. Wheeler, 1997: Extension to the North Atlantic oscillation using early instrumental pressure observations from Gibraltar and south-west Iceland. *Int. J. Climatol.*, 17, 1433–1450.

Kattsov, V. M., J. E. Walsh, W. L. Chapman, V. A. Govorkova, T. V. Pavlova, and X. Zhang, 2007: Simulation and Projection of Arctic Freshwater Budget Components by the IPCC AR4 Global Climate Models. *J. Hydrometeorol.*, 8, 571–589, doi:10.1175/JHM575.1.

Kay, J. E., and A. Gettelman, 2009: Cloud influence on and response to seasonal Arctic sea ice loss. *J. Geophys. Res.*, 114, D18204, doi:10.1029/2009JD011773.

Koerner, R., and R. D. Russell, 1979: $\delta^{18}O$ variations in snow on the Devon Island ice cap, Northwest Territories, Canada. *Can. J. Earth Sci.*, 16, 1419–1427, doi:10.1139/e79-126.

Kopec, B. G., X. Feng, F. A. Michel, and E. S. Posmentier, 2016: Influence of sea ice on Arctic precipitation. *Proc. Natl. Acad. Sci.*, 113, 46–51, doi:10.1073/pnas.1504633113.

Koyama, T., J. Stroeve, J. Cassano, and A. Crawford, 2017: Sea ice loss and Arctic cyclone activity from 1979 to 2014. *J. Climate*, 30, 4735–4754, doi:10.1175/JCLI-D-16-0542.1.

Lim, Y.-K., S. D. Schubert, S. M. J. Nowicki, J. N. Lee, A. M. Molod, R. I. Cullather, B. Zhao, and I. Velicogna, 2016: Atmospheric summer teleconnections and Greenland Ice Sheet surface mass variations: insights from MERRA-2. *Environ. Res. Lett.*, 11, 24002, doi:10.1088/1748-9326/11/2/024002.

Liston, G. E., and M. Sturm, 2004: The role of winter sublimation in the Arctic moisture budget. *Nord. Hydrol.*, 35, 325–334.

Liu, J., J. A. Curry, H. Wang, M. Song, and R. M. Horton, 2012: Impact of declining Arctic sea ice on winter snowfall. *Proc. Natl. Acad. Sci.*, 109, 4074–4079, doi:10.1073/pnas.1114910109.

Massonnet, F., T. Fichefet, H. Goosse, C. M. Bitz, G. Philippon-Berthier, M. M. Holland, and P.-Y. Barriat, 2012: Constraining projections of summer Arctic sea ice. *Cryosph.*, 6, 1383–1394, doi:10.5194/tc-6-1383-2012.

Matrosov, S. Y., 2007: Modeling Backscatter Properties of Snowfall at Millimeter Wavelengths. *J. Atmos. Sci.*, 64, 1727–1736, doi:10.1175/JAS3904.1.

Matrosov, S. Y., C. Campbell, D. Kingsmill, and E. Sukovich, 2009: Assessing Snowfall Rates from X-Band Radar Reflectivity Measurements. *J. Atmos. Ocean. Technol.*, 26, 2324–2339, doi:10.1175/2009JTECHA1238.1.

McCabe, G. J., M. P. Clark, and M. C. Serreze, 2001: Trends in Northern Hemisphere Surface Cyclone Frequency and Intensity. *J. Climate*, 14, 2763–2768, doi:10.1175/1520-0442(2001)014<2763:TINHSC>2.0.CO;2.

Mekis, E., and W. D. Hogg, 1999: Rehabilitation and analysis of Canadian daily precipitation time series. *Atmos.-Ocean*, 37, 53–85, doi:10.1080/07055900.1999.9649621.

Mernild, S. H., E. Hanna, J. R. McConnell, M. Sigl, A. P. Beckerman, J. C. Yde, J. Cappelen, J. K. Malmros, and K. Steffen, 2015: Greenland precipitation trends in a long-term instrumental climate context (1890-2012): evaluation of coastal and ice core records. *Int. J. Climatol.*, 35, 303–320, doi:10.1002/joc.3986.

Mishchenko, M. I., 2000: Calculation of the amplitude matrix for a nonspherical particle in a fixed orientation. *Appl. Opt.*, 39, 1026, doi:10.1364/AO.39.001026.

Moore, G. W. K., and I. A. Renfrew, 2005: Tip Jets and Barrier Winds: A QuikSCAT Climatology of High Wind Speed Events around Greenland. *J. Climate*, 18, 3713–3725, doi:10.1175/JCLI3455.1.

Moore, G. W. K., D. H. Bromwich, A. B. Wilson, I. Renfrew, and L. Bai, 2016: Arctic System Reanalysis improvements in topographically forced winds near Greenland. *Quart. J. Roy. Meteor. Soc.*, 142, 2033–2045, doi:10.1002/qj.2798.

Moran, K. P., B. E. Martner, M. J. Post, R. A. Kropfli, D. C. Welsh, and K. B. Widener, 1998: An Unattended Cloud-Profiling Radar for Use in Climate Research. *Bull. Amer. Amer. Soc.*, 79, 443–455, doi:10.1175/1520-0477(1998)079<0443:AUCPRF>2.0.CO;2.

Mosley-Thompson, E., C. R. Readinger, P. Craigmile, L. G. Thompson, and C. A. Calder, 2005: Regional sensitivity of Greenland precipitation to NAO variability. *Geophys. Res. Lett.*, 32, L24707, doi:10.1029/2005GL024776.

Noël, B., W. J. van de Berg, E. van Meijgaard, P. Kuipers Munneke, R. S. W. van de Wal, and M. R. van den Broeke, 2015: Evaluation of the updated regional climate model RACMO2.3: summer snowfall impact on the Greenland Ice Sheet. *Cryosph.*, 9, 1831–1844, doi:10.5194/tc-9-1831-2015.

Notz, D., and J. Stroeve, 2016: Observed Arctic sea-ice loss directly follows anthropogenic CO 2 emission. *Science*, 354, 747–750, doi:10.1126/science.aag2345.

Orsolini, Y. J., R. Senan, G. Balsamo, F. J. Doblas-Reyes, F. Vitart, A. Weisheimer, A. Carrasco, and R. E. Benestad, 2013: Impact of snow initialization on sub-seasonal forecasts. *Climate Dyn.*, 41, 1969–1982, doi:10.1007/s00382-013-1782-0.

Peterson, T. C., and R. S. Vose, 1997: An Overview of the Global Historical Climatology Network Temperature Database. *Bull. Amer. Amer. Soc.*, 78, 2837–2849.

Rasmussen, R. et al., 2012: How Well Are We Measuring Snow: The NOAA/FAA/NCAR Winter Precipitation Test Bed. *Bull. Amer. Amer. Soc.*, 93, 811–829, doi:10.1175/BAMS-D-11-00052.1.

Rogers, J. C., 1984: The Association between the North Atlantic Oscillation and the Southern Oscillation in the Northern Hemisphere. *Mon. Wea. Rev.*, 112, 1999–2015.

Screen, J. A., and I. Simmonds, 2010: The central role of diminishing sea ice in recent Arctic temperature amplification. *Nature*, 464, 1334–1337, doi:10.1038/nature09051.

Screen, J. A., I. Simmonds, C. Deser, and R. Tomas, 2013: The Atmospheric Response to Three Decades of Observed Arctic Sea Ice Loss. *J. Climate*, 26, 1230–1248, doi:10.1175/JCLI-D-12-00063.1

Serreze, M. C., A. P. Barrett, J. C. Stroeve, D. N. Kindig, and M. M. Holland, 2009: The emergence of surface-based Arctic amplification. *Cryosph.*, 3, 11–19, doi:10.5194/tc-3-11-2009.

Serreze, M. C., A. P. Barrett, and J. Stroeve, 2012: Recent changes in tropospheric water vapor over the Arctic as assessed from radiosondes and atmospheric reanalyses. *J. Geophys. Res. Atmos.*, 117, doi:10.1029/2011JD017421.

Serreze, M. C., and R. G. Barry, 2014: *The Arctic Climate System*. Cambridge University Press, Cambridge, 404pp.

Serreze, M. C., A. D. Crawford, and A. P. Barrett, 2015: Extreme daily precipitation events at Spitsbergen, an Arctic Island. *Int. J. Climatol.*, 35, 4574–4588, doi:10.1002/joc.4308.

Serreze, M. C., and J. Stroeve, 2015: Arctic sea ice trends, variability and implications for seasonal ice forecasting. *Philos. Trans. Roy. Soc. A Math. Phys. Eng. Sci.*, 373, 20140159, doi:10.1098/rsta.2014.0159.

Shepherd, A. et al., 2012: A Reconciled Estimate of Ice-Sheet Mass Balance. *Science*, 338, 1183–1189, doi:10.1126/science.1228102.

Sheppard, B. E., and P. I. Joe, 2008: Performance of the Precipitation Occurrence Sensor System as a Precipitation Gauge. *J. Atmos. Ocean. Technol.*, 25, 196–212, doi:10.1175/2007JTECHA957.1.

Sodemann, H., C. Schwierz, and H. Wernli, 2008: Interannual variability of Greenland winter precipitation sources: Lagrangian moisture diagnostic and North Atlantic Oscillation influence. *J. Geophys. Res.*, 113, D03107, doi:10.1029/2007JD008503.

Stroeve, J., 2001: Assessment of Greenland albedo variability from the advanced very high resolution radiometer Polar Pathfinder data set. *J. Geophys. Res. Atmos.*, 106, 33989–34006, doi:10.1029/2001JD900072.

Stroeve, J. C., V. Kattsov, A. Barrett, M. Serreze, T. Pavlova, M. Holland, and W. N. Meier, 2012a: Trends in Arctic sea ice extent from CMIP5, CMIP3 and observations. *Geophys. Res. Lett.*, 39, L16502, doi:10.1029/2012GL052676.

Stroeve, J. C., M. C. Serreze, M. M. Holland, J. E. Kay, J. Malanik, and A. P. Barrett, 2012b: The Arctic's rapidly shrinking sea ice cover: A research synthesis. *Climate Change*, 110, 1005–1027, doi:10.1007/s10584-011-0101-1.

Stroeve, J., and D. Notz, 2015: Insights on past and future sea-ice evolution from combining observations and models. *Glob. Planet. Change*, 135, 119–132, doi:10.1016/j.gloplacha.2015.10.011.

Stroeve, J. C., Mioduszewski, J. R., Rennermalm, A., Boisvert, L. N., Tedesco, M., & Robinson, D., 2017: Investigating the Local Scale Influence of Sea Ice on Greenland Surface Melt. *Cryosph.*, 11, 2363-2381, doi: 10.5194/tc-11-2363-2017

Tedesco, M., X. Fettweis, M. R. van den Broeke, R. S. W. van de Wal, C. J. P. P. Smeets, W. J. van de Berg, M. C. Serreze, and J. E. Box, 2011: The role of albedo and accumulation in the 2010 melting record in Greenland. *Environ. Res. Lett.*, 6, 14005, doi:10.1088/1748-9326/6/1/014005.

Thomas, R., 2000: Mass Balance of the Greenland Ice Sheet at High Elevations. *Science*, 289, 426–428, doi:10.1126/science.289.5478.426.

Ulbrich, U., G. C. Leckebusch, and J. G. Pinto, 2009: Extra-tropical cyclones in the present and future climate: a review. *Theor. Appl. Climatol.*, 96, 117–131, doi:10.1007/s00704-008-0083-8.

van den Broeke, M., J. Bamber, J. Ettema, E. Rignot, E. Schrama, W. J. van de Berg, E. van Meijgaard, I. Velicogna, and B. Wouters, 2009: Partitioning Recent Greenland Mass Loss. *Science.*, 326, 984–986, doi:10.1126/science.1178176.

Vazquez, M., R. Nieto, A. Drumond, and L. Gimeno, 2017: Extreme Sea Ice Loss over the Arctic: An Analysis Based on Anomalous Moisture Transport. *Atmosphere.*, 8, 32, doi:10.3390/atmos8020032.

Vihma, T., 2014: Effects of Arctic Sea Ice Decline on Weather and Climate: A Review. *Surv. Geophys.*, 35, 1175–1214, doi:10.1007/s10712-014-9284-0.

Vizcaíno, M., W. H. Lipscomb, W. J. Sacks, and M. van den Broeke, 2014: Greenland Surface Mass Balance as Simulated by the Community Earth System Model. Part II: Twenty-First-Century Changes. *J. Climate*, 27, 215–226, doi:10.1175/JCLI-D-12-00588.1.

Wong, G. J., E. C. Osterberg, R. L. Hawley, Z. R. Courville, D. G. Ferris, and J. A. Howley, 2015: Coast-to-interior gradient in recent northwest Greenland precipitation trends (1952–2012). *Environ. Res. Lett.*, 10, 114008, doi:10.1088/1748-9326/10/11/114008.

Yang, D., S. Ishida, B. E. Goodison, and T. Gunther, 1999: Bias correction of daily precipitation measurements for Greenland. *J. Geophys. Res.*, 104, 6171, doi:10.1029/1998JD200110.

Yin, J. H., 2005: A consistent poleward shift of the storm tracks in simulations of 21st century climate. *Geophys. Res. Lett.*, 32, L18701, doi:10.1029/2005GL023684.

Zhang, X., J. E. Walsh, J. Zhang, U. S. Bhatt, and M. Ikeda, 2004: Climatology and interannual variability of Arctic cyclone activity: 1948-2002. *J. Climate*, 17, 2300–2317, doi:10.1175/1520-0442(2004)017<2300:CAIVOA>2.0.CO;2.

References for Chapter 3

Bengtsson, L., K. I. Hodges, and E. Roeckner, 2006: Storm tracks and climate change. *J. Climate*, 19 (15), 3518–3543, doi:10.1175/JCLI3815.1.

Boisvert, L. N., 2016: The impact of the extreme winter 2015/16 Arctic cyclone on the Barents-Kara seas. *Mon. Wea. Rev.*, 144, 4279–4287, doi:10.1175/MWR-D-16-0234.1.

Boschat, G., I. Simmonds, A. Purich, T. Cowan, and A. B. Pezza, 2016: On the use of composite analyses to form physical hypotheses: An example from heat wave SST associations. *Sci. Rep.*, 6, 29599, doi:10.1038/srep29599.

Carnell, R. E., C. A. Senior, and J. F. B. Mitchell, 1996: An assessment of measures of storminess: simulated changes in northern hemisphere winter due to increasing C02. *Climate Dyn.*, 12, 475– 496, doi:10.1007/BF02346820.

Cavalieri, D. J., C. L. Parkinson, P. Gloersen, J. C. Comiso, and H. J. Zwally, 1999: Deriving long-term time series of sea ice cover from satellite passive-microwave multisensor data sets. *J. Geophys. Res.*, 104 (C7), 15803–15814, doi:10.1029/1999JC900081.

Chang, E. K. M., 2014: Impacts of background field removal on CMIP5 projected changes in Pacific winter cyclone activity. *J. Geophys. Res.*, 119 (8), 4626–4639, doi:10.1002/2013JD020746.

Chang, E. K. M., Y. Guo, and X. Xia, 2012: CMIP5 multimodel ensemble projection of storm track change under global warming. *J. Geophys. Res.*, 117, D23118, doi:10.1029/2012JD018578.

Charney, J. G., 1947: The Dynamics of Long Waves in a Baroclinic Westerly Current. *J. Meteor.*, 4 (5), 136–162.

Cohen, J. L., J. C. Furtado, M. A. Barlow, V. A. Alexeev, and J. E. Cherry, 2012: Arctic warming, increasing snow cover and widespread boreal winter cooling. *Environ. Res. Lett.*, 7 (1), 014007, doi:10.1088/1748-9326/7/1/014007.

Crawford, A. D., and M. C. Serreze, 2016: Does the Summer Arctic Frontal Zone Influence Arctic Ocean Cyclone Activity? *J. Climate*, 29 (13), 4977–4993, doi:10.1175/JCLI-D-15-0755.1.

de Jong, M. F., and L. de Steur, 2016: Strong winter cooling over the Irminger Sea in winter 2014- 2015, exceptional deep convection, and the emergence of

anomalously low SST. *Geophys. Res. Lett.*, 43 (13), 7106–7113, doi:10.1002/2016GL069596.

Dee, D. P., and Coauthors, 2011: The ERA-Interim reanalysis: configuration and performance of the data assimilation system. *Quart. J. Roy. Meteor. Soc.*, 137 (656), 553–597, doi:10.1002/qj. 828.

Descamps, L., D. Ricard, A. Joly, and P. Arbogast, 2007: Is a Real Cyclogenesis Case Explained by Generalized Linear Baroclinic Instability? *J. Atmos.* Sci., 64 (12), 4287–4308.

Eady, E. T., 1949: Long Waves and Cyclone Waves. *Tellus*, 1 (3), 33–52, doi:10.1111/j.2153-3490. 1949.tb01265.x.

Finnis, J., M. M. Holland, M. C. Serreze, and J. J. Cassano, 2007: Response of Northern Hemisphere extratropical cyclone activity and associated precipitation to climate change, as represented by the Community Climate System Model. *J. Geophys. Res.*, 112 (G4), G04S42, doi: 10.1029/2006JG000286.

Francis, J. A., W. Chan, D. J. Leathers, J. R. Miller, and D. E. Veron, 2009: Winter Northern Hemisphere weather patterns remember summer Arctic sea-ice extent. *Geophys. Res. Lett.*, 36 (7), L07503, doi:10.1029/2009GL037274.

Geng, Q., and M. Sugi, 2003: Possible Change of Extratropical Cyclone Activity due to Enhanced Greenhouse Gases and Sulfate AerosolsStudy with a High-Resolution AGCM. *J. Climate*, 16 (13), 2262–2274.

Ghatak, D., C. Deser, A. Frei, G. Gong, A. Phillips, D. A. Robinson, and J. Stroeve, 2012: Simulated Siberian snow cover response to observed Arctic sea ice loss, 1979-2008. *J. Geophys. Res.*, 117 (D23), D23108, doi:10.1029/2012JD018047.

Ghatak, D., A. Frei, G. Gong, J. Stroeve, and D. Robinson, 2010: On the emergence of an Arctic amplification signal in terrestrial Arctic snow extent. *J. Geophys. Res.*, 115 (D24), D24105, doi:10.1029/2010JD014007.

Gitelman, A. I., J. S. Risbey, R. E. Kass, and R. D. Rosen, 1997: Trends in the surface meridional temperature gradient. *Geophys. Res. Lett.*, 24, 1243.

Gulev, S. K., O. Zolina, and S. Grigoriev, 2001: Extratropical cyclone variability in the Northern Hemisphere winter from the NCEP/NCAR reanalysis data. *Climate Dyn.*, 17 (10), 795–809, doi:10.1007/s003820000145.

Hall, N. M. J., B. J. Hoskins, P. J. Valdes, and C. A. Senior, 1994: Storm tracks in a high-resolution GCM with doubled carbon dioxide. *Quart. J. Roy. Meteor. Soc.*, 120, 1209–1230, doi:10.1002/ qj.49712051905.

Haylock, M. R., P. D. Jones, R. J. Allan, and T. J. Ansell, 2007: Decadal changes in 18702004 Northern Hemisphere winter sea level pressure variability and its relationship with surface temperature. *J. Geophys. Res.*, 112 (D11), D11103, doi:10.1029/2006JD007291.

Hoskins, B. J., and P. J. Valdes, 1990: On the Existence of Storm-Tracks. *J. Atmos. Sci.*, 47 (15), 1854–1864.

Hurrell, J. W., Y. Kushnir, and G. Ottersen, 2003: An overview of the North Atlantic oscillation. *The North Atlantic Oscillation: Climatic Significance and Environmental Impact*, J.W. Hurrell, Y. Kushnir, G. Ottersen, M. Visbeck, and M.H. Visbeck, Eds., Geophys. Monogr. Ser., Amer. Geophys. Union, 1-35 doi:10.1029/134GM01.

Inoue, J., and M. E. Hori, 2011: Arctic cyclogenesis at the marginal ice zone: A contributory mechanism for the temperature amplification? *Geophys. Res. Lett.*, 38 (12), L12502, doi:10. 1029/2011GL047696.

Inoue, J., M. E. Hori, and K. Takaya, 2012: The Role of Barents Sea Ice in the Wintertime Cyclone Track and Emergence of a Warm-Arctic Cold-Siberian Anomaly. *J. Climate*, 25 (7), 2561–2568, doi:10.1175/JCLI-D-11-00449.1.

Jaiser, R., K. Dethloff, D. Handorf, A. Rinke, and J. Cohen, 2012: Impact of sea ice cover changes on the Northern Hemisphere atmospheric winter circulation. *Tellus*, 64, 11595, doi:10.3402/tellusa. v64i0.11595.

Kalnay, E., and Coauthors, 1996: The NCEP/NCAR 40-Year Reanalysis Project. *Bull. Amer. Meteor. Soc.*, 77 (3), 437–471.

Kuo, Y.-H., S. Low-Nam, and R. J. Reed, 1991: Effects of Surface Energy Fluxes during the Early Development and Rapid Intensification Stages of Seven Explosive Cyclones in the Western Atlantic. *Mon. Wea. Rev.*, 119 (2), 457–476.

Lee, W.-J., and M. Mak, 1994: Observed Variability in the Large-Scale Static Stability. *J. Atmos. Sci.*, 51 (14), 2137–2144.

Lehmann, A., K. Getzlaff, and J. Harlaß, 2011: Detailed assessment of climate variability in the Baltic Sea area for the period 1958 to 2009. *Climate Res.*, 46 (2), 185–196, doi:10.3354/cr00876.

Li, M., T. Woollings, K. Hodges, and G. Masato, 2014: Extratropical cyclones in a warmer, moister climate: A recent Atlantic analogue. *Geophys. Res. Lett.*, 41 (23), 8594–8601, doi: 10.1002/2014GL062186.

Lim, E.-P., and I. Simmonds, 2007: Southern Hemisphere Winter Extratropical Cyclone Characteristics and Vertical Organization Observed with the ERA-40 Data in 19792001. *J. Climate*, 20 (11), 2675–2690, doi:10.1175/JCLI4135.1.

Liu, J., J. A. Curry, H. Wang, M. Song, and R. M. Horton, 2012: Impact of declining Arctic sea ice on winter snowfall. *Proc. Natl. Acad. Sci.*, 109 (11), 4074–4079, doi:10.1073/pnas. 1114910109.

McCabe, G. J., M. P. Clark, and M. C. Serreze, 2001: Trends in Northern Hemisphere Surface Cyclone Frequency and Intensity. *J. Climate*, 14 (12), 2763–2768.

Mearns, L. O., R. W. Katz, and S. H. Schneider, 1984: Extreme High-Temperature Events: Changes in their probabilities with Changes in Mean Temperature. *J. Climate Appl. Meteor.*, 23 (12), 1601–1613, doi:10.1175/1520-0450(1984)023⟨1601:EHTECI⟩2.0.CO;2.

Neu, U., and Coauthors, 2013: IMILAST: A Community Effort to Intercompare Extratropical Cyclone Detection and Tracking Algorithms. *Bull. Amer. Meteor. Soc.*, 94 (4), 529–547, doi: 10.1175/BAMS-D-11-00154.1.

Noer, G., and M. Ovhed, 2003: Forecasting of polar lows in the Norwegian and the Barents Sea. Paper presented at the *9th Meeting of the EGS Polar Lows working Group*, Eur. Geophys. Soc., Cambridge, UK.

Orsolini, Y. J., R. Senan, R. E. Benestad, and A. Melsom, 2012: Autumn atmospheric response to the 2007 low Arctic sea ice extent in coupled ocean-atmosphere hindcasts. *Climate Dyn.*, 38 (11-12), 2437–2448, doi:10.1007/s00382-011-1169-z.

Overland, J. E., and M. Wang, 2010: Large-scale atmospheric circulation changes are associated with the recent loss of Arctic sea ice. *Tellus*, 62 (1), 1–9, doi:10.1111/j.1600-0870.2009.00421. x.

Paciorek, C. J., J. S. Risbey, V. Ventura, and R. D. Rosen, 2002: Multiple Indices of Northern Hemisphere Cyclone Activity, Winters 1949-99. *J. Climate*, 15 (13), 1573–1590, doi:10.1175/ 1520-0442(2002)015⟨1573:MIONHC⟩2.0.CO;2.

Parkinson, C. L., and J. C. Comiso, 2013: On the 2012 record low Arctic sea ice cover: Combined impact of preconditioning and an August storm. *Geophys. Res. Lett.*, 40 (7), 1356–1361, doi: 10.1002/grl.50349.

Polyakova, E. I., A. G. Journel, I. V. Polyakov, and U. S. Bhatt, 2006: Changing relationship between the North Atlantic Oscillation and key North Atlantic climate parameters. *Geophys. Res. Lett.*, 33 (3), L03 711, doi:10.1029/2005GL024573.

Raible, C. C., P. M. Della-Marta, C. Schwierz, H. Wernli, and R. Blender, 2008: Northern Hemisphere Extratropical Cyclones: A Comparison of Detection and Tracking Methods and Different Reanalyses. *Mon. Wea. Rev.*, 136 (3), 880–897, doi:10.1175/2007MWR2143.1.

Rasmussen, E., and J. Turner, 2003: Polar Lows: mesoscale weather systems at high latitudes.

Rienecker, M. M., and Coauthors, 2011: MERRA: NASAs Modern-Era Retrospective Analysis for Research and Applications. *J. Climate*, 24 (14), 3624–3648, doi:10.1175/JCLI-D-11-00015. 1.

Rigor, I. G., J. M. Wallace, and R. L. Colony, 2002: Response of Sea Ice to the Arctic Oscillation. *J. Climate*, 15 (18), 2648–2663, doi:10.1175/1520-0442(2002)015⟨2648:ROSITT⟩2.0.CO;2.

Rogers, J. C., 1997: North Atlantic Storm Track Variability and Its Association to the North Atlantic Oscillation and Climate Variability of Northern Europe. *J. Climate*, 10 (7), 1635–1647, doi:10.1175/1520-0442(1997)010⟨1635:NASTVA⟩2.0.CO;2.

Rogers, R. R., 1978: Short course in cloud physics. Pergamon press.

Romero, R., and K. Emanuel, 2017: Climate Change and Hurricane-Like Extratropical Cyclones: Projections for North Atlantic Polar Lows and Medicanes Based on CMIP5 Models. *J. Climate*, 30 (1), 279–299, doi:10.1175/JCLI-D-16-0255.1.

Rudeva, I., S. K. Gulev, I. Simmonds, and N. Tilinina, 2014: The sensitivity of characteristics of cyclone activity to identification procedures in tracking algorithms. *Tellus*, 66A, 24 961, doi: 10.3402/tellusa.v66.24961.

Screen, J. A., and I. Simmonds, 2010a: Increasing fall-winter energy loss from the Arctic Ocean and its role in Arctic temperature amplification. *Geophys. Res. Lett.*, 37, doi: 10.1029/2010GL044136.

Screen, J. A., and I. Simmonds, 2010b: The central role of diminishing sea ice in recent Arctic temperature amplification. *Nature*, 464 (7293), 1334–1337, doi:10.1038/nature09051.

Serreze, M. C., and A. P. Barrett, 2008: The Summer Cyclone Maximum over the Central Arctic Ocean. *J. Climate*, 21 (5), 1048–1065, doi:10.1175/2007JCLI1810.1.

Serreze, M. C., A. P. Barrett, and J. Stroeve, 2012: Recent changes in tropospheric water vapor over the Arctic as assessed from radiosondes and atmospheric reanalyses. *J. Geophys. Res.*, 117 (10), doi:10.1029/2011JD017421.

Serreze, M. C., A. P. Barrett, J. C. Stroeve, D. N. Kindig, and M. M. Holland, 2009: The emergence of surface-based Arctic amplification. *Cryosph.*, 3 (1), 11–19.

Serreze, M. C., and R. G. Barry, 2014: *The Arctic Climate System*. Cambridge University Press, Cambridge, 404pp.

Serreze, M. C., F. Carse, R. G. Barry, and J. C. Rogers, 1997: Icelandic Low Cyclone Activity: Climatological Features, Linkages with the NAO, and Relationships with Recent Changes in the Northern Hemisphere Circulation. *J. Climate*, 10 (3), 453–464.

Serreze, M. C., and A. J. Etringer, 2003: Precipitation characteristics of the Eurasian Arctic drainage system. *Int. J. Climatol.*, 23 (11), 1267–1291, doi:10.1002/joc.941.

Serreze, M. C., A. H. Lynch, and M. P. Clark, 2001: The arctic frontal zone as seen in the NCEP- NCAR reanalysis. *J. Climate*, 14 (7), 1550–1567, doi:10.1175/1520-0442(2001)014⟨1550: TAFZAS⟩2.0.CO;2.

Serreze, M. C., and J. Stroeve, 2015: Arctic sea ice trends, variability and implications for seasonal ice forecasting. Philos. Trans. Roy. Soc. A Math. Phys. Eng. Sci., 373(2045), 20140159, doi:10.1098/rsta.2014.0159.

Simmonds, I., 2015: Comparing and contrasting the behaviour of Arctic and Antarctic sea ice over the 35 year period 1979-2013. *Ann. Glaciol.*, 56 (69), 18–28, doi:10.3189/2015AoG69A909.

Simmonds, I., C. Burke, and K. Keay, 2008: Arctic Climate Change as Manifest in Cyclone Behavior. *J. Climate*, 21 (22), 5777–5796, doi:10.1175/2008JCLI2366.1.

Simmonds, I., and K. Keay, 2009: Extraordinary September Arctic sea ice reductions and their relationships with storm behavior over 1979-2008. *Geophys. Res. Lett.*, 36 (19), L19 715, doi: 10.1029/2009GL039810.

Simmonds, I., K. Keay, and E.-P. Lim, 2003: Synoptic Activity in the Seas around Antarctica. *Mon. Wea. Rev.*, 131 (2), 272–288, doi:10.1175/1520-0493(2003)131⟨0272:SAITSA⟩2.0.CO;2.

Simmonds, I., and E.-P. Lim, 2009: Biases in the calculation of Southern Hemisphere mean baroclinic eddy growth rate. *Geophys. Res. Lett.*, 36 (1), L01707, doi:10.1029/2008GL036320.

Simmonds, I., and I. Rudeva, 2012: The great Arctic cyclone of August 2012. *Geophys. Res. Lett.*, 39 (23), L23709, doi:10.1029/2012GL054259.

Simmonds, I., and I. Rudeva, 2014: A comparison of tracking methods for extreme cyclones in the Arctic basin. *Tellus A*, 66, 25252, doi:10.3402/tellusa.v66.25252.

Sorokina, S. A., C. Li, J. J. Wettstein, and N. G. Kvamstø, 2016: Observed Atmospheric Coupling between Barents Sea Ice and the Warm-Arctic Cold-Siberian Anomaly Pattern. *J. Climate*, 29 (2), 495–511, doi:10.1175/JCLI-D-15-0046.1.

Sorteberg, A., and J. E. Walsh, 2008: Seasonal cyclone variability at 70N and its impact on moisture transport into the Arctic. *Tellus A*, 60 (3), 570–586, doi:10.1111/j.1600-0870.2008.00314.x.

Stramler, K., A. D. Del Genio, and W. B. Rossow, 2011: Synoptically Driven Arctic Winter States. *J. Climate*, 24 (6), 1747–1762, doi:10.1175/2010JCLI3817.1.

Stroeve, J. C., M. C. Serreze, A. Barrett, and D. N. Kindig, 2011: Attribution of recent changes in autumn cyclone associated precipitation in the Arctic. *Tellus A*, 63 (4), 653–663, doi:10.1111/j. 1600-0870.2011.00515.x.

Stroeve, J. C., M. C. Serreze, M. M. Holland, J. E. Kay, J. Malanik, and A. P. Barrett, 2012: The Arctic's rapidly shrinking sea ice cover: A research synthesis. *Climatic Change*, 110, 1005– 1027, doi:10.1007/s10584-011-0101-1.

Sun, L., J. Perlwitz, and M. Hoerling, 2016: What caused the recent Warm Arctic, Cold Continents trend pattern in winter temperatures? *Geophys. Res. Lett.*, 43 (10), 5345–5352, doi:10.1002/ 2016GL069024.

Tang, Q., X. Zhang, X. Yang, and J. a. Francis, 2013: Cold winter extremes in northern continents linked to Arctic sea ice loss. *Environ. Res. Lett.*, 8, 014036, doi:10.1088/1748-9326/8/1/014036.

Thompson, D. W. J., and J. M. Wallace, 1998: The Arctic oscillation signature in the wintertime geopotential height and temperature fields. *Geophys. Res. Lett.*, 25 (9), 1297-1300, doi:10.1029/98GL00950.

Tsukernik, M., D. N. Kindig, and M. C. Serreze, 2007: Characteristics of winter cyclone activity in the northern North Atlantic: Insights from observations and regional modeling. *J. Geophys. Res.*, 112 (D3), D03101, doi:10.1029/2006JD007184.

Ulbrich, U., G. C. Leckebusch, and J. G. Pinto, 2009: Extra-tropical cyclones in the present and future climate: a review. *Theor. Appl. Climatol.*, 96 (1-2), 117–131, doi:10.1007/ s00704-008-0083-8.

Vallis, G. K., 2006: *Atmospheric and Oceanic Fluid Dynamics.* Cambridge University Press, Cambridge, U.K., 745 pp.

Vavrus, S. J., 2013: Extreme Arctic cyclones in CMIP5 historical simulations. *Geophys. Res. Lett.*, 40 (23), 6208–6212, doi:10.1002/2013GL058161.

Wallace, J. M., and P. V. Hobbs, 2006: *Atmospheric science: an introductory survey,* Academic press, 467pp.

Wang, X. L., V. R. Swail, and F. W. Zwiers, 2006: Climatology and Changes of Extratropical Cyclone Activity: Comparison of ERA-40 with NCEPNCAR Reanalysis for 19582001. *J. Climate*, 19 (13), 3145–3166, doi:10.1175/JCLI3781.1.

Willison, J., W. A. Robinson, and G. M. Lackmann, 2013: The Importance of Resolving Mesoscale Latent Heating in the North Atlantic Storm Track. *J. Atmos. Sci.*, 70 (7), 2234–2250, doi:10.1175/JAS-D-12-0226.1.

Woods, C., and R. Caballero, 2016: The Role of Moist Intrusions in Winter Arctic Warming and Sea Ice Decline. *J. Climate*, 29 (12), 4473–4485, doi:10.1175/JCLI-D-15-0773.1.

Woollings, T., B. Harvey, M. Zahn, and L. Shaffrey, 2012: On the role of the ocean in projected atmospheric stability changes in the Atlantic polar low region. *Geophys. Res. Lett.*, 39 (24), L24802, doi:10.1029/2012GL054016.

Yamazaki, A., J. Inoue, K. Dethloff, M. Maturilli, and G. Konig-Langlo, 2015: Impact of radiosonde observations on forecasting summertime Arctic cyclone formation. *J. Geophys. Res.*, 120 (8), 3249–3273, doi:10.1002/2014JD022925.

Zahn, M., and H. von Storch, 2010: Decreased frequency of North Atlantic polar lows associated with future climate warming. *Nature*, 467 (7313), 309–312, doi:10.1038/nature09388.

Zhang, J., R. Lindsay, A. Schweiger, and M. Steele, 2013: The impact of an intense summer cyclone on 2012 Arctic sea ice retreat. *Geophys. Res. Lett.*, 40 (4), 720–726, doi:10.1002/grl. 50190.

Zhang, X., J. E. Walsh, J. Zhang, U. S. Bhatt, and M. Ikeda, 2004: Climatology and interannual variability of Arctic cyclone activity: 1948-2002. *J. Climate*, 17 (12), 2300–2317, doi:10.1175/ 1520-0442(2004)017⟨2300:CAIVOA⟩2.0.CO;2.

Zveryaev, I. I., 1999: Decadal and longer changes of the winter sea level pressure fields and related synoptic activity over the North Atlantic. *Int. J. Climatol.*, 19 (11), 1177–1185, doi:10.1002/(SICI)1097-0088(199909)19:11⟨1177::AID-JOC424⟩3.0.CO;2-4.

References for Chapter 4

Barnes, E. A., and J. A. Screen, 2015: The impact of Arctic warming on the midlatitude jet-stream: Can it? Has it? Will it? *Wiley Interdiscip. Rev. Climate Chang.*, 6(3), 277–286, doi:10.1002/wcc.337.

Bentsen, M. et al., 2013: The Norwegian Earth System Model, NorESM1-M – Part 1: Description and basic evaluation of the physical climate. *Geosci. Model Dev.*, 6(3), 687–720, doi:10.5194/gmd-6-687-2013.

Bokhorst, S. et al., 2016: Changing Arctic snow cover: A review of recent developments and assessment of future needs for observations, modelling, and impacts. *Ambio*, 45(5), 516–537, doi:10.1007/s13280-016-0770-0.

Brodzik, M. J., B. Billingsley, T. Haran, B. Raup, and M. H. Savoie, 2012: EASE-Grid 2.0: Incremental but Significant Improvements for Earth-Gridded Data Sets. *ISPRS Int. J. Geo-Information*, 1(3), 32–45, doi:10.3390/ijgi1010032.

Callaghan, T. V. et al., 2011: The Changing Face of Arctic Snow Cover: A Synthesis of Observed and Projected Changes. *Ambio*, 40(S1), 17–31, doi:10.1007/s13280-011-0212-y.

Cassano, E. N., and J. J. Cassano, 2017: Atmospheric response to anomalous autumn surface forcing in the Arctic Basin. *J. Geophys. Res. Atmos.*, 122(17), 9011–9023, doi:10.1002/2017JD026765.

Cassano, E., J. Glisan, J. Cassano, W. Gutowski, and M. Seefeldt, 2015: Self-organizing map analysis of widespread temperature extremes in Alaska and Canada. *Climate Res.*, 62(3), 199–218, doi:10.3354/cr01274.

Cohen, J. et al., 2014: Recent Arctic amplification and extreme mid-latitude weather. *Nat. Geosci.*, 7(9), 627–637, doi:10.1038/ngeo2234.

Comiso, J. C., C. L. Parkinson, R. Gersten, and L. Stock, 2008: Accelerated decline in the Arctic sea ice cover. *Geophys. Res. Lett.*, 35 (1), L01703, doi:10.1029/2007GL031972.

de Boer, G., W. Chapman, J. E. Kay, B. Medeiros, M. D. Shupe, S. Vavrus, and J. Walsh, 2012: A Characterization of the Present-Day Arctic Atmosphere in CCSM4. *J. Climate*, 25(8), 2676–2695, doi:10.1175/JCLI-D-11-00228.1.

Dufresne, J.-L. et al., 2013: Climate change projections using the IPSL-CM5 Earth System Model: from CMIP3 to CMIP5. *Climate Dyn.*, 40(9–10), 2123–2165, doi:10.1007/s00382-012-1636-1.

Francis, J. A., and S. J. Vavrus, 2012: Evidence linking Arctic amplification to extreme weather in mid-latitudes. *Geophys. Res. Lett.*, 39 (6), L06801, doi:10.1029/2012GL051000.

Francis, J. A., and S. J. Vavrus, 2015: Evidence for a wavier jet stream in response to rapid Arctic warming. *Environ. Res. Lett.*, 10(1), 14005, doi:10.1088/1748-9326/10/1/014005.

The HadGEM2 Development Team: G. M. Martin, Bellouin, N., Collins, W. J., Culverwell, I. D., Halloran, P. R., Hardiman, S. C., Hinton, T. J., Jones, C. D., McDonald, R. E., McLaren, A. J., O'Connor, F. M., Roberts, M. J., Rodriguez, J. M., Woodward, S., Best, M. J., Brooks, M. E., Brown, A. R., Butchart, N., Dearden, C., Derbyshire, S. H., Dharssi, I., Doutriaux-Boucher, M., Edwards, J. M., Falloon, P. D., Gedney, N., Gray, L. J., Hewitt, H. T., Hobson, M., Huddleston, M. R., Hughes, J., Ineson, S., Ingram, W. J., James, P. M., Johns, T. C., Johnson, C. E., Jones, A., Jones, C. P., Joshi, M. M., Keen, A. B., Liddicoat, S., Lock, A. P., Maidens, A. V., Manners, J. C., Milton, S. F., Rae, J. G. L., Ridley, J. K., Sellar, A., Senior, C. A., Totterdell, I. J., Verhoef, A., Vidale, P. L., and Wiltshire, A., 2011: The HadGEM2 family of Met Office Unified Model climate configurations. *Geosci. Model Dev.*, 4(3), 723-757, doi:10.5194/gmd-4-723-2011.

Hasselmann, K., 1976: Stochastic climate models Part I. Theory. *Tellus*, 28(6), 473–485, doi:10.3402/tellusa.v28i6.11316.

Hewitson, B. and R. Crane, 2002: Self-organizing maps: Applications to synoptic climatology. *Climate Res.*, 22(1), 13-26.

Inoue, J., and M. E. Hori, 2011: Arctic cyclogenesis at the marginal ice zone: A contributory mechanism for the temperature amplification? *Geophys. Res. Lett.*, 38 (12), L12502, doi:10.1029/2011GL047696.

Inoue, J., M. E. Hori, and K. Takaya, 2012: The role of barents sea ice in the wintertime cyclone track and emergence of a warm-Arctic cold-Siberian anomaly. *J. Climate*, 25(7), 2561–2568, doi:10.1175/JCLI-D-11-00449.1.

Kalnay, E., 2003: *Atmospheric modeling, data assimilation, and predictability*. Cambridge University Press, 341pp.

Knutti, R., and J. Sedláček, 2012: Robustness and uncertainties in the new CMIP5 climate model projections. *Nat. Climate Chang.*, 3(4), 369–373, doi:10.1038/nclimate1716.

Kohonen, T., 1997: *Self-Organizing Maps*. Springer Berlin Heidelberg, 443pp.

Kwok, R., and D. A. Rothrock, 2009: Decline in Arctic sea ice thickness from submarine and ICESat records: 1958-2008. *Geophys. Res. Lett.*, 36 (15), L15501, doi:10.1029/2009GL039035.

Laxon, S. W. et al., 2013: CryoSat-2 estimates of Arctic sea ice thickness and volume. *Geophys. Res. Lett.*, 40 (4), 732–737, doi:10.1002/grl.50193.

Lindsay, R., and A. Schweiger, 2015: Arctic sea ice thickness loss determined using subsurface, aircraft, and satellite observations. *Cryosph.*, 9(1), 269–283, doi:10.5194/tc-9-269-2015.

Liu, J., J. A. Curry, H. Wang, M. Song, and R. M. Horton, 2012: Impact of declining Arctic sea ice on winter snowfall. *Proc. Natl. Acad. Sci.*, 109(11), 4074–4079, doi:10.1073/pnas.1114910109.

Maykut, G. A., 1978: Energy exchange over young sea ice in the central Arctic. *J. Geophys. Res.*, 83(C7), 3646, doi:10.1029/JC083iC07p03646.

McCusker, K. E., J. C. Fyfe, and M. Sigmond, 2016: Twenty-five winters of unexpected Eurasian cooling unlikely due to Arctic sea-ice loss. Nat. Geosci., 9(11), 838–842, doi:10.1038/ngeo2820. Outten, S. D., and I. Esau, 2012), A link between Arctic sea ice and recent cooling trends over Eurasia, *Climate Change*, 110(3–4), 1069–1075, doi:10.1007/s10584-011-0334-z.

Mills, C. M., J. J. Cassano, and E. N. Cassano, 2016: Midlatitude atmospheric responses to Arctic sensible heat flux anomalies in Community Climate Model, Version 4. *Geophys. Res. Lett.*, 43 (23), 12270-12277, doi:10.1002/2016GL071356.

Outten, S. D., & Esau, I., 2012: A link between Arctic sea ice and recent cooling trends over Eurasia. *Climate Change*, 110(3–4), 1069–1075, doi:10.1007/s10584-011-0334-z

Overland, J. E., K. Dethloff, J. A. Francis, R. J. Hall, E. Hanna, S.-J. Kim, J. A. Screen, T. G. Shepherd, and T. Vihma, 2016: Nonlinear response of mid-latitude weather to the changing Arctic. *Nat. Climate Chang.*, 6(11), 992–999, doi:10.1038/nclimate3121.

Overland, J. E., K. R. Wood, and M. Wang, 2011: Warm Arctic—cold continents: climate impacts of the newly open Arctic Sea. *Polar Res.*, 30(1), 15787, doi:10.3402/polar.v30i0.15787.

Parkinson, C. L., 2014: Global Sea Ice Coverage from Satellite Data: Annual Cycle and 35-Yr Trends. *J. Climate*, 27(24), 9377–9382, doi:10.1175/JCLI-D-14-00605.1.

Screen, J. A., and I. Simmonds, 2010a: Increasing fall-winter energy loss from the Arctic Ocean and its role in Arctic temperature amplification. *Geophys. Res. Lett.*, 37, L16707, doi:10.1029/2010GL044136.

Screen, J. A., and I. Simmonds, 2010b: The central role of diminishing sea ice in recent Arctic temperature amplification. *Nature*, 464(7293), 1334–1337, doi:10.1038/nature09051.

Screen, J. A., and I. Simmonds, 2014: Amplified mid-latitude planetary waves favour particular regional weather extremes. *Nat. Climate Chang.*, 4(8), 704–709, doi:10.1038/nclimate2271.

Serreze, M. C., A. P. Barrett, and J. J. Cassano, 2011: Circulation and surface controls on the lower tropospheric air temperature field of the Arctic. *J. Geophys. Res.*, 116(D7), D07104, doi:10.1029/2010JD015127.

Serreze, M. C., A. P. Barrett, J. C. Stroeve, D. N. Kindig, and M. M. Holland, 2009: The emergence of surface-based Arctic amplification. *Cryosph.*, 3(1), 11–19, doi:10.5194/tc-3-11-2009.

Serreze, M. C., and J. Stroeve, 2015: Arctic sea ice trends, variability and implications for seasonal ice forecasting. *Philos. Trans. Roy. Soc. A Math. Phys. Eng. Sci.*, 373(2045), 20140159, doi:10.1098/rsta.2014.0159.

Sheridan, S. C., and C. C. Lee, 2011: The self-organizing map in synoptic climatological research. *Prog. Phys. Geogr.*, 35(1), 109–119, doi:10.1177/0309133310397582.

Simmonds, I., 2015: Comparing and contrasting the behaviour of Arctic and Antarctic sea ice over the 35 year period 1979-2013. *Ann. Glaciol.*, 56(69), 18–28, doi:10.3189/2015AoG69A909.

Stroeve, J., A. Barrett, M. Serreze, and A. Schweiger, 2014: Using records from submarine, aircraft and satellites to evaluate climate model simulations of Arctic sea ice thickness. *Cryosph.*, 8(5), 1839–1854, doi:10.5194/tc-8-1839-2014.

Stroeve, J., M. Serreze, S. Drobot, S. Gearheard, M. Holland, J. Maslanik, W. Meier, and T. Scambos, 2008: Arctic Sea Ice Extent Plummets in 2007. *Eos, Trans. Amer. Geophys. Union*, 89(2), 13, doi:10.1029/2008EO020001.

Stroeve, J. C., M. C. Serreze, M. M. Holland, J. E. Kay, J. Malanik, and A. P. Barrett, 2012: The Arctic's rapidly shrinking sea ice cover: A research synthesis. *Climate Change*, 110(3–4), 1005–1027, doi:10.1007/s10584-011-0101-1.

Sun, L., J. Perlwitz, and M. Hoerling, 2016: What caused the recent "Warm Arctic, Cold Continents" trend pattern in winter temperatures? *Geophys. Res. Lett.*, 43 (10), 5345–5352, doi:10.1002/2016GL069024.

Taylor, K. E., R. J. Stouffer, and G. A. Meehl, 2012), An Overview of CMIP5 and the Experiment Design. *Bull. Amer. Amer. Soc.*, 93(4), 485–498, doi:10.1175/BAMS-D-11-00094.1.

Wang, M., and J. E. Overland, 2009: A sea ice free summer Arctic within 30 years? *Geophys. Res. Lett.*, 36 (7), L07502, doi:10.1029/2009GL037820.

Watanabe, M. et al., 2010: Improved Climate Simulation by MIROC5: Mean States, Variability, and Climate Sensitivity. *J. Climate*, 23, 6312–6335, doi:10.1175/2010JCLI3679.1.

Watanabe, S. et al., 2011). MIROC-ESM 2010: model description and basic results of CMIP5-20c3m experiments. *Geosci. Model Dev.*, 4, 845–872, doi:10.5194/gmd-4-845-2011

Zhang, J., and D. A. Rothrock, 2003: Modeling Global Sea Ice with a Thickness and Enthalpy Distribution Model in Generalized Curvilinear Coordinates. Mon. Wea. Rev.*, 131(5), 845–861, doi:10.1175/1520-0493(2003)131<0845:MGSIWA>2.0.CO;2.*

References for Chapter 5

Barnes, E. A., and J. A. Screen, 2015: The impact of Arctic warming on the midlatitude jet-stream: Can it? Has it? Will it? *Wiley Interdiscip. Rev. Climate Chang.*, 6(3), 277–286, doi:10.1002/wcc.337.

Bromwich, D. H., Wilson, A. B., Bai, L., Liu, Z., Barlage, M., Shih, C.-F., … Walsh, J. E., 2017: The Arctic System Reanalysis Version 2. *Bull. Amer. Amer. Soc.*, BAMS-D-16-0215.1. doi:10.1175/BAMS-D-16-0215.1

Cassano, E. N., and J. J. Cassano, 2017: Atmospheric response to anomalous autumn surface forcing in the Arctic Basin. *J. Geophys. Res. Atmos.*, 122(17), 9011–9023, doi:10.1002/2017JD026765.

Cohen, J. L., J. C. Furtado, M. A. Barlow, V. A. Alexeev, and J. E. Cherry, 2012: Arctic warming, increasing snow cover and widespread boreal winter cooling. *Environ. Res. Lett.*, 7, 14007, doi:10.1088/1748-9326/7/1/014007.

Francis, J. A., and S. J. Vavrus, 2012: Evidence linking Arctic amplification to extreme weather in mid-latitudes. *Geophys. Res. Lett.*, 39(6), L06801, doi:10.1029/2012GL051000.

Ghatak, D., C. Deser, A. Frei, G. Gong, A. Phillips, D. A. Robinson, and J. Stroeve, 2012: Simulated Siberian snow cover response to observed Arctic sea ice loss, 1979-2008. *J. Geophys. Res.*, 117 (D23), D23108, doi:10.1029/2012JD018047.

Ghatak, D., A. Frei, G. Gong, J. Stroeve, and D. Robinson, 2010: On the emergence of an Arctic amplification signal in terrestrial Arctic snow extent. *J. Geophys. Res.*, 115 (D24), D24105, doi:10.1029/2010JD014007.

Inoue, J., and M. E. Hori, 2011: Arctic cyclogenesis at the marginal ice zone: A contributory mechanism for the temperature amplification? *Geophys. Res. Lett.*, 38(12), L12502, doi:10.1029/2011GL047696.

Liu, J., J. A. Curry, H. Wang, M. Song, and R. M. Horton, 2012: Impact of declining Arctic sea ice on winter snowfall. *Proc. Natl. Acad. Sci.*, 109, 4074–4079, doi:10.1073/pnas.1114910109.

Mills, C. M., J. J. Cassano, and E. N. Cassano, 2016: Midlatitude atmospheric responses to Arctic sensible heat flux anomalies in Community Climate Model. Version 4, *Geophys. Res. Lett.*, 43(23), 12270-12277, doi:10.1002/2016GL071356.

Orsolini, Y. J., R. Senan, R. E. Benestad, and A. Melsom, 2012: Autumn atmospheric response to the 2007 low Arctic sea ice extent in coupled ocean-atmosphere hindcasts. *Climate Dyn.*, 38 (11-12), 2437–2448, doi:10.1007/s00382-011-1169-z.

Outten, S. D., & Esau, I., 2012: A link between Arctic sea ice and recent cooling trends over Eurasia. *Climate Change*, 110(3–4), 1069–1075, doi:10.1007/s10584-011-0334-z

Overland, J. E., K. R. Wood, and M. Wang, 2011: Warm Arctic—cold continents: climate impacts of the newly open Arctic Sea. *Polar Res.*, 30(1), 15787, doi:10.3402/polar.v30i0.15787.

Screen, J. A., and I. Simmonds, 2010a: Increasing fall-winter energy loss from the Arctic Ocean and its role in Arctic temperature amplification. *Geophys. Res. Lett.*, 37, doi: 10.1029/2010GL044136.

Screen, J. A., and I. Simmonds, 2010b: The central role of diminishing sea ice in recent Arctic temperature amplification. *Nature*, 464 (7293), 1334–1337, doi:10.1038/nature09051.

Sagan, C., 2006: *Conversations with Carl Sagan.* (T. Head, Ed.). University of Press Mississippi, 194pp

Screen, J. A., and I. Simmonds, 2014: Amplified mid-latitude planetary waves favour particular regional weather extremes. *Nat. Climate Chang.*, 4(8), 704–709, doi:10.1038/nclimate2271.

Serreze, M. C., A. P. Barrett, J. C. Stroeve, D. N. Kindig, and M. M. Holland, 2009: The emergence of surface-based Arctic amplification. *Cryosph.*, 3(1), 11–19, doi:10.5194/tc-3-11-2009.

Serreze, M. C., and J. Stroeve, 2015: Arctic sea ice trends, variability and implications for seasonal ice forecasting. *Philos. Trans. Roy. Soc. A Math. Phys. Eng. Sci.*, 373(2045), 20140159, doi:10.1098/rsta.2014.0159.

Simmonds, I., 2015: Comparing and contrasting the behaviour of Arctic and Antarctic sea ice over the 35 year period 1979–2013. *Ann. Glaciol.*, 56(69), 18–28.

Stroeve, J. C., M. C. Serreze, M. M. Holland, J. E. Kay, J. Malanik, and A. P. Barrett, 2012: The Arctic's rapidly shrinking sea ice cover: A research synthesis. *Climate Change*, 110(3–4), 1005–1027.